



UCGE Reports
Number 20251

Department of Geomatics Engineering

**RF Interference Impact on GPS L5 Reception
Performance**

(URL: <http://www.geomatics.ucalgary.ca/research/publications/GradTheses.html>)

by

Jianning Qiu

January 2007



UNIVERSITY OF CALGARY

RF Interference Impact on GPS L5 Reception Performance

by

Jianning Qiu

A THESIS

SUBMITTED TO THE FACULTY OF GRADUATE STUDIES
IN PARTIAL FULFILMENT OF THE REQUIREMENTS FOR THE
DEGREE OF MASTER OF SCIENCE

DEPARTMENT OF GEOMATICS ENGINEERING

CALGARY, ALBERTA

JANUARY, 2007

© Jianning Qiu 2007

Abstract

As a part of the Global Navigation System (GPS) modernization plan in support of improved navigation services, initial transmission of a new L5 signal is planned for 2008, with a full operational availability around 2012. GPS is a radio-navigation system which is vulnerable to RF interference, especially at low signal power levels. In this research, the RF interference of interest includes cross-correlation and broadband random noise. Researchers have conducted statistical analyses of and mitigation methods of multiuser interference (the counterpart of cross-correlation in the field of mobile communication) and achieved significant progress.

In light of the aforementioned research work and the similarity of GPS and mobile communication in their system and signal structure, the theoretical study of the L5 behaviour presented herein manages to quantify interference effects in terms of several important receiver parameters, such as average SNR, tracking jitter, symbol estimation error rate, and so forth. The theoretical component of this thesis includes some background on GPS receiver fundamentals, signal and interference models, and the L5 receiver's response (parameters listed above) to the interference or noise. The investigation concentrates on the performance of the correlator and phase tracking loops. Numerical evaluations and their analyses including the experimental design, as well as the presentation and comparison of results with theoretically inferred outcomes, are presented in order to verify the theoretical results.

Acknowledgement

I would like to express my sincere appreciation to my supervisors Professor Gérard Lachapelle and Professor Richard Klukas for their constant guidance and support throughout this research.

Further gratitude extends to my parents Daren Qiu and Daoping Wang for their love and unconditional encouragement and support to my career.

Special thanks to my friend Natalya Nicolson for her valuable suggestions and proofreading my thesis.

I would like to thank my friend and colleague Wei Yu for many constructive discussions during this research.

Last but not least, acknowledgement to my friends and colleagues Ning Luo, Gang Mao, Donghua Yao, Moncton Gao, Minmin Lin and Tao Wu for sharing a memorable experience in Calgary.

I acknowledge the financial support received from iCORE and the GEOIDE Network of Centres of Excellence.

Table of Contents

Abstract.....	iii
Acknowledgement	iv
Table of Contents.....	v
List of Figures and Illustrations	vii
List of Symbols, Abbreviations and Nomenclature.....	ix
List of Tables	xi
CHAPTER ONE: INTRODUCTION.....	1
1.1 Background	1
1.2 Relevant Research.....	2
1.3 Research Motivation and Objectives.....	7
1.4 Thesis outline	9
CHAPTER TWO: INTERFERENCE EFFECTS ON ACQUISITION	11
2.1 GPS L5 Signal Features	11
2.2 Acquisition Algorithm	16
2.3 Broadband Noise Impact on Detection Performance.....	20
2.4 Cross-Correlation Impact on Detection Performance	23
2.5 Mean Acquisition Time Computation.....	26
CHAPTER THREE: RFI IMPACT ON RECEIVED SNR.....	27
3.1 Theory of Matched Filters.....	27
3.1.1 Development of a Detector.....	28
3.1.2 Performance of Matched Filter.....	33
3.2 Correlator Output SNR Analysis in the Presence of Broadband Noise and Cross-Correlation	35
3.2.1 Theoretical Estimation.....	36
3.2.2 Numerical Evaluation.....	46
3.2.2.1 Simulation Scheme	46
3.2.2.2 Results and Analysis.....	48
3.3 Conclusions	53

CHAPTER FOUR: RFI IMPACT ON L5 TRACKING LOOPS.....	55
4.1 Theory of PLL Tracking Loops	55
4.1.1 Elementary Tracking Theory.....	55
4.1.2 The Effect of Additive Noise and Other Disturbances.....	61
4.2 L5 Decision-Directed PLL Tracking Error in the Presence of Broadband Noise and Cross-Correlation	64
4.2.1 Theoretical Investigation	64
4.2.2 Numerical Evaluation.....	75
4.2.2.1 Simulation Scheme	75
4.2.2.2 Results and Analysis.....	78
4.3 L5 Decision-Directed PLL Symbol Estimation Error in the Presence of Broadband Noise and Cross-Correlation	85
4.3.1 Theoretical Investigation.....	85
4.3.2 Numerical Evaluation.....	92
4.3.2.1 Simulation Scheme	92
4.3.2.2 Results and Analysis.....	94
4.4 Conclusions	96
 CHAPTER FIVE: CONCLUSIONS AND RECOMMENDATIONS	 99
5.1 Conclusions	99
5.2 Recommendations for Future Research	101
 REFERENCES	 103

List of Figures and Illustrations

Figure 2.1: Standard Acquisition Scheme	17
Figure 2.2: Probability of Detection ($1e^{-3}$) for Total (I+Q) C/N_0 at the Antenna Output Ranging from 25 to 40 dB-Hz.	23
Figure 2.3: Probability of Detection versus total (I+Q) C/N_0 at the Antenna Output, for the Worst Case Cross-Correlation	25
Figure 3.1: Detection Performance of Matched Filter (Kay 1998).....	35
Figure 3.2: Auto-Correlation Function of NH Code.....	43
Figure 3.3: Simulation Scheme for Average SNR.....	47
Figure 3.4: The Average SNR of the I5 Correlator Output under Broadband Noise	49
Figure 3.5: SNR of the I5 Correlator Output under Cross-Correlation Only	49
Figure 3.6: I5 Correlation SNR under Broadband Noise and Cross-Correlation	51
Figure 3.7: Partial Correlation between Satellite 1 Data Channel and Satellite 2 Data Channel	52
Figure 4.1: Phase-Locked Loop (Viterbi 1966).....	56
Figure 4.2: Non-linear Model of Phase-Locked Loop (Viterbi 1966).....	58
Figure 4.3: Linear Model of Phase-Locked Loop (Viterbi 1966).....	61
Figure 4.4: Linear Model (S Domain) of Phase-Locked Loop (Viterbi 1966).....	61
Figure 4.5: Non-linear Model of a Phase-Locked Loop with Additive Noise.....	63
Figure 4.6: Linear Model of a Phase-Locked Loop with Additive Noise	63
Figure 4.7: Baseband Satellite Signal Simulation	76
Figure 4.8: Decision-Directed PLL Simulation	77
Figure 4.9: L5 Receiver PLL Error in the Presence of Broadband Noise only	78

Figure 4.10: L5 Receiver PLL Error in the Presence of Broadband Noise only	80
Figure 4.11: L5 PLL Error under Cross-Correlation only	80
Figure 4.12: The PLL Tracking Error under Broadband Noise and Cross-Correlation ...	82
Figure 4.13: The PLL Tracking Error for an Indoor Scenario.....	83
Figure 4.14: Search for the Maximum Cross-Correlation	93
Figure 4.15: Symbol Estimation Error.....	94
Figure 4.16: Symbol Estimation Error Rate for Broadband Noise only.....	95
Figure 4.17: Symbol Estimation Error Rate under Broadband Noise and Cross- Correlations.....	96

List of Symbols, Abbreviations and Nomenclature

AGC	Automatic Gain Control
AWGN	Additive White Gaussian Noise
BPSK	Bi-Phase Shift Keying
C/A	Coarse Acquisition
CDF	Cumulative Probability Function
C/N ₀	Carrier-to-Noise density ratio
CDMA	Code Division Multiple Access
dB	Decibel
dBW	Decibel Watt
DLL	Delay Lock Loop
DS	Direct Sequence
E-911	Enhanced-911
ENR	Energy-to-Noise Ratio
FIR	Finite Impulse Response
GPS	Global Positioning System
<i>J/N</i>	Jamming-to-Noise Power Ratio
I&D	Integration and Dump
IF	Intermediate Frequency
LOS	Line of sight
NCO	Numerically Controlled Oscillator
NH	Neumann-Hoffman
PLAN	Position Location And Navigation Group
PLL	Phase Locked Loop
PN (PRN)	Pseudo-Random Noise
PSD	Power Spectral Density
QPSK	Quadrature Phase Shift Keying
RFI	Radio Frequency Interference
RMS	Root Mean Square

SIC	Successive Interference Cancellation
SNR	Signal-to-Noise power Ratio
SSMA	Spread-Spectrum Multiple Access
UWB	Ultra WideBand
VCO	Voltage Controlled Oscillator
WN	White Noise
P_k	L5 Signal Power (Data plus Pilot) for Satellite k
P_{FA}	Probability of false alarm
P_D	Probability of detection
ω_0	Receiver IF
N_0	One-Sided PSD
$\Phi(x)$	CDF for Normalized Gaussian Variable
τ_k	Code Delay of Satellite k
ϕ_k	Phase Offset of Satellite k
α_k	Power Ratio of Satellite k to the Desired Satellite

List of Tables

Table 4.1 the Maximum Cross-Correlation and Associated Combination of Parameters.....	92
--	----

Chapter One: INTRODUCTION

1.1 Background

The need to deliver positioning and location services in harsh environments has stimulated extensive research in the area of wireless Enhanced 911 (E911) applications of the Global Positioning System (GPS). Such settings include indoors, under heavy foliage and urban canyons. Signal strength under these conditions normally ranges between 10 dB and 30 dB lower than that of comparable line-of-sight (LOS) signals. In general, standard GPS receivers are ideally suited to LOS operation, while high sensitivity receivers are designed for weak signal circumstances (Tsui & Bao 2000). Moreover, GPS is a radionavigation system which is vulnerable to radio frequency interference (RFI), especially at low signal power levels. The carrier to noise density ratio (C/N_0) of all of the GPS signals is reduced by the effects of radio frequency interference on code correlation and loop filtering (Ward 1996a). Thus, overall receiver performance is degraded with large tracking errors and loss of lock associated with the tracking loops.

To satisfy increasing demands from the civil community for improved navigation services, implementation of a new signal called L5 (Spilker & Dierendonck 1999) is planned, with the first satellite with L5 capability to be launched in 2008. The L5 signal is mainly designed to support safety-of-life applications including navigation for aviation (Macabiau *et al* 2003). Its enhanced signal strength and improved cross-correlation properties, as compared to the corresponding L1 and L2C characteristics, deliver superior support to positioning services indoor. The L5 signal provides improved multipath

resistance and protection against narrow-band interference. To increase the spectral diversity, L5 must be an independent signal, which can be acquired directly, without any aid from other GPS signals.

Deshpande (2004) evaluated the impact of RF interference on GPS L1 reception performance based on a software receiver. In concept, software-based GPS receivers, associated with the concept of software radio, have numerous advantages over hardware receivers. For example, they offer more parameters for monitoring the inner state of the receiver; flexibility, which is desirable both for the adjustment of controlling parameters, and the implementation of new algorithms. A software radio allows a single hardware configuration to serve as multiple radios (Akos 1997). Operating with a suitable antenna and front-end, a software receiver can be used to conveniently acquire and track the new L5 signal.

Because of potential differences in GPS L5 receiver operation as compared to L1, there is also a real need to evaluate the RFI effects on L5 receivers. The aim of this research is to gain a deep understanding of wideband interference, including cross-correlation and broadband random noise. The study will be implemented by the quantification of some vital reception parameters theoretically, and the verification by or comparison to numerical evaluation / simulation results.

1.2 Relevant Research

As a navigation system intended for both civil and military applications, GPS is designed to tolerate a considerable amount of interference and jamming. The RF interference may be friendly or intentional; it may be present as wideband Gaussian noise from intentional

jammers, wideband pulses from radar transmitters, or narrowband or wideband modulation resulting from harmonics due to out-of-band transmitters' non-linear effects. A certain level of interference from the signals of other GPS satellites (cross-correlation) or pseudolites is considered to be the most common type of wideband interference (Ward 1996a). Although a spread spectrum signal is much less susceptible to interference than a narrow band signal, the operation of any navigation system, including GPS, can be severely disrupted, e.g., in the presence of an interference source of sufficiently high power (Spilker & Natali 1996). GPS signals transmitted by satellites far away from the earth surface have especially weak power levels (-160 dBW or so) upon reaching the user, due to geometric spreading effects. Most of the relevant research work was implemented on the GPS L1 and Bi-Phase Shift Keying (BPSK) signals used in mobile communication systems, due to their long history and wide application. As a Quadrature Phase Shift Keying (QPSK) signal, L5 differs from L1 and other BPSK signals in terms of its signal structure – two channels versus one. However, the insights gained into the operation of the latter two signals remains instrumental to the investigation of RF interference effects on L5.

In the literature, the contributions of thermal noise and interference signals have been referred to as equivalent to the noise floor at which the performance was evaluated (Kaplan 1996). A receiver is unable to keep track of signals if the C/N_0 decreases below the tracking threshold and, thus, loses the ability to navigate (Ward 1996b) since reacquisition is impossible under these circumstances. This is because the threshold of C/N_0 for acquisition (as a rule of thumb) is set 6 dB above that employed for tracking.

The unjammed C/N_0 and the tracking threshold are determined so as to produce that value of C/N_0 that can be effectively tolerated pursuant to jamming.

The impact of cross-correlation between different satellites on GPS receiver performance has been a topic of interest in recent research, because of the demand for GPS indoor use, where the power of signals from various satellites may differ by 20 dB or more. The origin of this phenomenon, that is similar to the near-far problem in mobile communication, is the different signal strength attenuation due to different propagation paths. The combination of strong and weak signals in the receiver input may present higher cross-correlations between a strong signal and a local replica of the weak signal than would the weak signal autocorrelation peak. Bastide *et al* (2004) conducted a theoretical analysis of L5 acquisition performance, including the probability of detection (P_d) and false alarm (P_{fa}), and the variation of P_d at a specific P_{fa} while varying C/N_0 . On this basis, they determined the threshold for the acquisition of the GPS L5 signal in the presence of cross-correlation and receiver thermal noise.

Cross-correlation not only generates “false alarms” in acquisition, but also results in large pseudorange errors at the metre level (Van Dierendonck *et al* 2002), and code tracking errors similar to those due to multipath interference (Van Nee 1992). The rationale of the phase-locked loop (PLL) and its behaviour under interference and noise conditions were analyzed and described in depth in (Viterbi 1963), which is also the theoretical basis for predicting the behaviour of the delay-locked loop (DLL).

Based on the system model in the presence of noise, a statistical analysis of multi-user interference on the phase estimator of the PLL for coherent DS-CDMA reception was implemented (Huang *et al* 1998) on a BPSK signal, and a one-sided power spectral

density (PSD) was derived. The steady state (stationary) probability density of the first-order-loop phase error resulting from interference and noise can be determined through a partial differential equation called the Fokker-Planck equation (Viterbi 1966). The performance of high order loops could be evaluated through a linear time-invariant model, which would allow accurate deduction of the tracking error at high signal to noise ratio (SNR) levels.

The Fokker-Planck equation was also employed in the investigation of the variance of the code tracking error of a first-order DLL, in a multi-user interference and additive noise environment (Huang & Andonovic 1998). The steady-state probability density function (PDF) at a high SNR was theoretically shown to conform to a Gaussian distribution.

The foregoing investigation of RF impact on the CDMA system, including SNR quantification, PLL and DLL jitter estimation, is aimed at the BPSK signal for a mobile communication system. Its conclusions and outcomes are not necessarily applicable to the L5 QPSK signal with a dataless channel and two layers of spreading codes. Moreover, due to the complexity in mathematics, the methodology based on the Fokker-Planck equation has not been applied to the evaluation of GPS receivers, where the second or third order loop dominates the receiver design. The conceptual approach and methodology, however, give some indication of and guidance to the evaluation of research on L5 reception performance.

As a type of intentional interference signal, broadband random noise is Gaussian in nature and similar to GPS correlation noise. Broadband noise increases the amount of noise in the GPS spectrum without distorting the signal spectrum (Heppel & Ward 2003). Actually, broadband random noise is used to model the receiver thermal noise (which is

the most significant interference source in the receiver), sky noise and some other wideband interference sources. Recently, some investigations intended to “quantify the degree of equivalence in RFI impact of UWB (ultra wideband) signals relative to broadband random noise” (RTCA 2000), since this noise model was deeply studied and well understood for any communication or electronic system. Progress has been made, for instance, in the quantization of the self-interference effect on BPSK signals. A broadband RF interference averages the spectral lines and causes an asymptotic effect similar to a Sinc function (Kaplan 1996). Generally speaking, a broadband signal (for example, the GPS signal itself) is very difficult to detect and isolate using filters or to nullify with the use of an antenna (Spilker & Natali 1996).

The various RF interference monitoring and mitigation algorithms that have been proposed to minimize the effects on receiver performance will be described briefly below. It is of no use to prolong the predetection period against cross-correlation. By reconstructing the strong signal from its parameters, as obtained from tracking programs, that signal can be subtracted from the input (Psiaki 2001). The successive interference cancellation (SIC) technique, originating from CDMA communication, was successfully applied to the near-far problem encountered by a GPS L1 system augmented by ground-based pseudolites (Madhani *et al* 2003).

A jamming-to-noise power ratio (J/N) meter was devised to detect the presence of RF interference, via detection of abnormality of automatic gain control's (AGC) control voltage level (Bastide *et al* 2003). The J/N meter is capable of ascertaining the existence of a jamming signal independently, whether the receiver is tracking the GPS satellite or not. Out-of-band interference is suppressed by the receiver front end, whose passive filter

has a sharp cutoff with deep stop-band characteristics. Greater filtering at increasingly narrow bandwidths can be obtained by means of a multi-stage filter set before and after each local oscillator mixing stage (Ward 1996b). In order to protect the receiver front end from high power pulsed interference, a pulse blanking technique (Hegarty *et al* 2000) has been proposed to zero out the signal when its power exceeds a predetermined threshold (Grabowski & Hegarty 2002). Because the interference signal must be incident from some specific direction, space-time or space-frequency adaptive processing methods based on antenna array structure were proposed and proved to be effective against both narrowband and wideband interference forms (Gupta & Moore 2001).

1.3 Research Motivation and Objectives

Continuous investigation of GPS performance degradation due to RF interference is the major motivation for this research. Another motivation is to test and validate the new L5 signal's reception performance in a controlled signal environment associated with GPS indoor applications. To satisfy the requirement of GPS indoor use, L5 signal structure and strength are more robust against cross-correlation and broadband noise. Therefore, this research is confined to the L5 receiving quality under cross-correlation and broadband noise.

The objective is to deepen the understanding of RF interference effects on the GPS L5 receiver from both theoretical and practical perspectives. The theoretical study of the behavior of L5 under various types of interference endeavours to quantify the interference effects in terms of several important receiver parameters, such as SNR, tracking jitters, symbol estimation error rate, and so forth. The theoretical component

covers some background on GPS receiver structure, signal and interference models, and the L5 receiver's response (parameters mentioned above) to the interference or noise, which will be discussed in Chapters 3 and 4. The empirical measurements and their analyses consist of the experimental design, data processing, result presentation and comparison with theoretically inferred outcomes. To achieve this end, the tasks can be appropriately divided into five parts:

1. Investigation of a GPS L5 receiver architecture, including acquisition and tracking schemes that are closely related to the satellite signal pattern;
2. Discussion of the core component of the receiver – the matched filters or correlators – and the associated key parameter (SNR) under broadband random noise and cross-correlation interference;
3. Investigation of cross-correlation interference and broadband random noise effects on carrier phase tracking in terms of a linear model;
4. Experimental design based on theoretical considerations;
5. Result analyses and comparison with the expected theoretically deduced outcome.

Novel contributions include the development of a theoretical assessment (average SNR, PLL tracking error and symbol estimation error rate) according to the investigation of Pursley (1977a) and Huang et al (1998) on BPSK signal due to the similarity of the signal structure to that L5, and some novel approaches necessary because of the difference in signal structure. The analytical geometry method is proposed for the derivation of the maximum cross-correlation since L5 has two channels (inphase and quadrature) whereas the BPSK signal has one channel only. This difference also results in crossing terms

between the two channels that must be dealt with. Finally, some additional work is introduced by the two-layer pseudo-random code structure of L5.

It is hoped that an improved understanding of the impact of RF interference on the GPS L5 receiver will provide some useful indications of signal and receiver design for L5 signal acquisition and tracking. Although the theoretical analysis will not match the empirical result perfectly in every aspect, due to unavoidable simplifications or approximations existing in both the signal and system models, theoretical considerations should expose some general characteristics of GPS receiver behavior under various RF interference conditions.

1.4 Thesis outline

The thesis is organized into five chapters. Chapter 2 discusses the mechanisms by which various types of interference and noise affect the operation of an L5 receiver, and introduces previous research, which analysed the cross-correlation and broadband random noise effects on L5 acquisition. Chapter 2 begins with a description of the L5 signal, coupled with some necessary comparisons with L1 and L2C and an exploration of a basic receiver architecture, including general strategies for L5 acquisition and tracking. Then, it describes detection ability evaluation under the aforementioned interferences achieved already by previous researchers.

Chapters 3 and 4 present the progress obtained in the estimation of cross-correlation and broadband random noise effects on L5 reception performance. The measurement errors and performance degradation are analyzed in accordance with the signal and system models established upon those strategies. Chapter 3 describes the theory of the matched

filter and its performance as background knowledge, then derives the matched filter or correlator output SNR in the presence of cross-correlation and broadband noise. The configuration of a numerical evaluation is presented – for the verification of speculations proposed in theory – coupled with the results and conclusions. Chapter 4 introduces the general theory of PLL and tracking loops used in GPS receivers. The interference impact on L5 phase tracking loops is evaluated in terms of tracking error (RMS) and symbol estimation error rate, followed by simulations and conclusions. Chapter 5 deals with conclusions and recommendations for future work.

Chapter Two: INTERFERENCE EFFECTS ON ACQUISITION

The GPS signal is transmitted as a continuous wave modulated by a specific direct sequence (DS) also known as code division multiple-access (CDMA). The advantages of CDMA signals include a preferred strong resistance to radio frequency (RF) and multipath interference, however, GPS receivers are still vulnerable to interference (intentional or unintentional) due to the weak GPS signal strength near the earth's surface. This problem is more acute for indoor positioning. This chapter intends to investigate and quantify the impact of unintentional self-interference within the GPS system as well as the broadband random noise on an L5 receiver.

2.1 GPS L5 Signal Features

The L5 civil signal differs from the current L1 and L2C signals because it uses the in-phase and quadrature channels, I5 and Q5, while L1 and L2C use only the in-phase channel and reserve the quadrature channel for military use. The I5 and Q5 channels on L5 are bi-phase modulated by a pair of pseudo-random noise (PN) codes, which are deliberately designed and chosen because of their low cross-correlation properties. At zero time offset, the two PN codes selected for one satellite are nearly uncorrelated. Correlation is less than -74 dB for the first 32 satellites and -62 dB for the last 5. The cross-correlation statistics for the L5 signal indicate a 10 dB improvement over current

L1 C/A code. The cross-correlation characteristics within the L5 signal allows receivers to operate with a minimum of self-interference while improving operational performance. The PN codes are generated at a 10.23 Mc/s rate, which spreads the L5 signal spectrum to ten times that of L1 or L2C that have chipping rates of 1.023 Mc/s. L5 PN codes have a length of 10230 chips so their period (1 ms) is the same as that of the L1 C/A code and is ten times longer than that of C/A code in the number of chips.

A Neumann-Hoffman (NH) code with a chip width of 1 ms is multiplied by the PN code. Only L5 has the additional NH code, giving it a unique two-layer spreading code structure. This process makes it possible to leave the PN code cycle unchanged or to invert it. PN codes and NH codes of the I5 channel are further modulated by the GPS navigation message. The navigation message has a bit width of 10 ms which is the same as the I5 NH code period. This makes the synchronization of these three codes possible and allows successful and easier demodulation inside receivers, which is necessary for pseudorange measurement and positioning.

The pilot (Q5) channel carries no navigation message and is therefore called a dataless channel. The period of the NH code on the pilot channel is 20 ms. The introduction of the NH code to the data channel allows more efficient data synchronization. This means that the boundary of a cycle of NH code is aligned with that of a data bit. Adding NH codes to the L5 signal, including the dataless component, makes it more robust against narrowband interference. It does this by reducing the 1 kHz spectral line power by over 10 dB, while suppressing cross-correlation interference between space vehicles.

The following section provides a more in-depth description of the L5 signal structure.

The transmitted signal from satellite m is the mixture of an in-phase (data) channel and a quadrature data free (pilot) channel of equal amplitude:

$$S_m(t) = \sqrt{P_m} NH_{20}(t) XQ_m(t) \sin(2\pi f_5 t + \phi) + \sqrt{P_m} D_m(t) NH_{10}(t) XI_m(t) \cos(2\pi f_5 t + \phi) \quad (2.1)$$

where:

- L5 is the carrier frequency ($f_5 = 1176.45$ MHz);
- D_m is the 100 bps encoded data stream of satellite m ;
- P_m is the L5 signal power (data plus pilot);
- NH_{20} and NH_{10} are Neumann-Hoffman codes of length 20 for the pilot channel and length 10 for the data channel, respectively.

The pseudorandom code sequence is denoted by:

$$\begin{aligned} XQ_m(t) &= \sum_{l=-\infty}^{\infty} XQ_{m,l} p_{T_C}(t - lT_C) \\ XI_m(t) &= \sum_{l=-\infty}^{\infty} XI_{m,l} p_{T_C}(t - lT_C) \end{aligned} \quad (2.2)$$

where $p_\tau = 1$ for $0 \leq t < \tau$ and $p_\tau = 0$ otherwise, and the elements XI_m and XQ_m are the PN code pairs of length 10230. These are carefully chosen and can be thought of as a unique identifier for each satellite.

The careful selection and realization of these codes improves their cross-correlation properties significantly in comparison to the L1 C/A codes. L1 C/A codes belong to the Gold code family which is generated by summing the outputs of two spread-spectrum code sequence generators via a modulo-two addition (Weik 1989). L5 PN codes do not belong to the Gold code family, since their period of 10230 chips is incompatible with the Gold code period 2^n-1 . However, these selected codes perform as well as Gold codes from the perspective of cross-correlation statistics (Spilker & Van Dierendonck 2001).

The code streams NH_{10} , added to the data component, and NH_{20} , added to the pilot channel, are the same for all satellites. A cycle of NH_{10} and NH_{20} code sequences is defined as:

$$NH_{10} = \{+1, +1, +1, +1, -1, -1, +1, -1, +1, -1\} \text{ and}$$

$$NH_{20} = \{+1, +1, +1, +1, +1, -1, +1, +1, -1, -1, +1, -1, +1, -1, +1, +1, -1, -1, -1, +1, \}.$$

The autocorrelation function of the NH code, at zero offset, is an impulse function. It is used to determine SNR degradation and PLL jitter in the following sections. The navigation data and all of the codes mentioned above are referenced to the 10.23 MHz clock in each GPS receiver.

The term broadband random noise refers to the continuous noise whose power spectral density (PSD) is much broader than the RF/intermediate frequency (IF) bandwidth of the GPS receiver. Broadband random noise is used to model receiver thermal noise as follows:

$$n(t) = n_1(t) \sin \omega_0 t + n_2(t) \cos \omega_0 t + \bar{n} \quad (2.3)$$

where:

- ω_0 is the receiver IF frequency;
- $n_1(t)$ and $n_2(t)$ are sample functions of the stationary zero-mean Gaussian processes whose spectral densities $S_1(\omega)$ and $S_2(\omega)$ are negligible for $|\omega| > \omega_0$.

Viterbi (1966) proved that the processes $n_1(t)$ and $n_2(t)$ are linearly independent and Gaussian and therefore also statistically independent. A stationary Gaussian process, $n(t)$, with a mean, \bar{n} , normally considered to be zero, has the following spectral density (S):

$$S_n(\omega) = |H(i\omega)|^2 \quad (2.4)$$

where $H(i\omega)$ is the filter transfer function.

This random process can be generated as the steady state output of a time-invariant linear filter whose input is a zero-mean white Gaussian process with spectral density $S_w(\omega) = 1$.

In this case, the term narrowband does not indicate that the spectral density of $n(t)$ is confined to frequencies near ω_0 . It only imposes a condition that $S_n(\omega)$ be negligible for $|\omega| > 2\omega_0$.

Broadband random noise is considered to be the combined effect of sky noise, receiver thermal noise and other wideband noise. Sky noise refers to fluctuations of the total

power or phase of a detector due to the variation of atmospheric emissivity. All of these noise sources are modeled as white Gaussian noise, since their PSD is nearly a constant within the band of interest. In the analysis of a GPS receiver design and performance, there is no pre-whitening filter implemented to deal with coloured noise. In reality, the correlator or coherent integrator inside the receiver digital channels is an optimum filter (matched filter) based on the white Gaussian noise assumption.

2.2 Acquisition Algorithm

The acquisition process is a two-dimensional search in both the time and frequency domains. Figure 2.1 shows a schematic diagram of the synchronization of the incoming signal with a locally generated replica signal which includes the local code and local carrier. The first summation indicates coherent integration and is followed by non-coherent integration. Maximum correlation occurs when the replica code phase matches the incoming signal. The code phase synchronization at the acquisition stage is not as fine as that of the tracking stage as only the prompt correlator is generally used for acquisition.

The correlation process can be expressed as:

$$\begin{aligned} I_m &= \int_0^{T_p} r(t)S_{Im}(t)dt \\ Q_m &= \int_0^{T_p} r(t)S_{Qm}(t)dt \end{aligned} \tag{2.5}$$

where T_p is the coherent integration time and

$$r(t) = S_\alpha(t) + n(t) \quad (2.6)$$

where $S_\alpha(t)$ is the signal from satellite α .

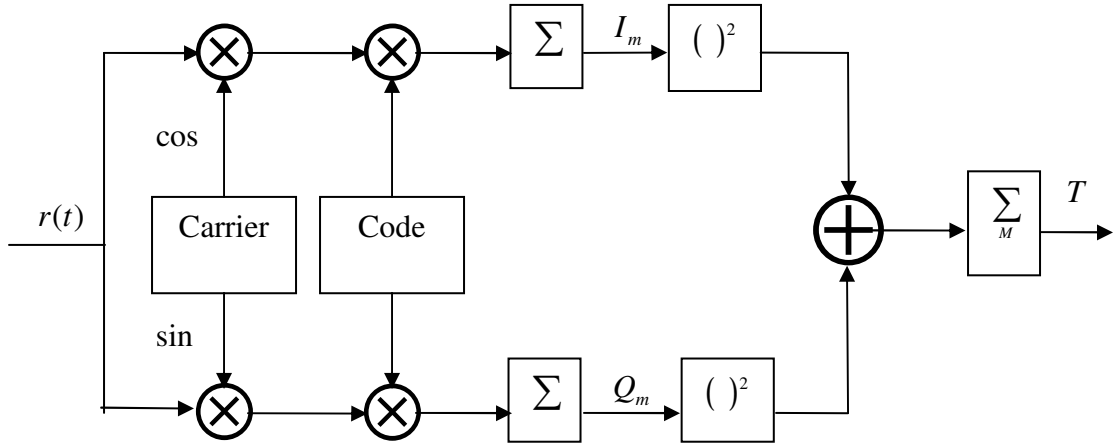


Figure 2.1: Standard Acquisition Scheme

The parameters S_{I_m} and S_{Q_m} are defined as:

$$\begin{aligned} S_{I_m} &= XI_m(t - \hat{\tau}_0) \cos(\hat{\omega}_0 t + \hat{\gamma}_0) \\ S_{Q_m} &= XI_m(t - \hat{\tau}_0) \sin(\hat{\omega}_0 t + \hat{\gamma}_0) \end{aligned} \quad (2.7)$$

The resultant correlator output is:

$$\begin{aligned} I_m(k) &= \sqrt{\frac{P_m}{4}} b(k) R_{\alpha,m}(\epsilon_\tau) \cos(\epsilon_\theta) \frac{\sin(\pi \Delta f T_p)}{\pi \Delta f T_p} + n_I(k) \\ Q_m(k) &= \sqrt{\frac{P_m}{4}} b(k) R_{\alpha,m}(\epsilon_\tau) \sin(\epsilon_\theta) \frac{\sin(\pi \Delta f T_p)}{\pi \Delta f T_p} + n_Q(k) \end{aligned} \quad (2.8)$$

where:

- $R_{\alpha,m}$ is the cross-correlation between the in-phase channel of expected satellite m and either channel of satellite α ;
- ε_θ is the estimated carrier phase error;
- ε_τ is the difference between the incoming signal code delay and the local replica;
- b is the data symbol as the multiplication of navigation message and NH code or NH code only;
- n_I and n_Q are centred Gaussian correlator output noise with power $\sigma_n^2 = \frac{N_0}{4f_p}$ where N_0 is the one-sided spectral density originating from the receiver thermal noise and other external broadband noise; and
- Δf is the frequency offset.

The local code is either the PN code only or a combination of the PN and NH codes for joint acquisition. Normally the PN code is detected first since NH code acquisition is susceptible to a frequency offset. The offset is fairly large at the acquisition stage making the computational load unnecessarily heavy due to the large number of frequency bins.

The traditional GPS signal acquisition algorithm consists of coherent integration followed by non-coherent integration. Coherent integration is the correlation of the incoming GPS signal and the local replica signal. This integration can efficiently enhance the SNR since matching the incoming signal and local replica in the code phase and frequency offset presents a signal peak. This peak can accumulate with respect to the coherent integration

time, while the noise will cancel out due to the assumption that it is characterized by a white Gaussian distribution. In general, the longer the coherent integration time, the higher the resulting SNR. However, the coherent integration period is limited by the change of frequency offset in the presence of receiver dynamics and receiver clock instability. In addition, the data/symbol transition may cause the signal to cancel out. The coherent integration time or predetection period, T_p , will affect the sinc function term in Equation (2.8). Longer coherent integration will result in a narrower null-to-null bandwidth and consequently a smaller frequency search bin size and heavier computational load. The coherent integration time of the L5 signal acquisition is constrained to 1 ms, which is the width of the Neumann-Hoffman code. The NH code is viewed as data symbols due to the unknown boundary of the NH code at the acquisition stage. The use of a 1 ms coherent integration allows the non-coherent combination of the prompt correlator sums for both I5 and Q5 components of L5. The wipe off of the NH code is not necessary since the integration is carried out over the duration of only one NH code symbol.

The purpose of using non-coherent integration is to improve the SNR to a detectable level in the event that coherent integration alone can not accomplish this. Since the frequency bin size is determined solely by the predetection period, the increase of the non-coherent integration time will not increase the number of frequency search bins. Non-coherent integration is not affected by symbol or data transitions, as phase information associated with the data is lost during squaring. Since the noise is not reduced by squaring, the squaring loss results in additional SNR degradation not present in coherent integration.

Signal detection is defined by two hypothesis tests where hypothesis H1 assumes that a satellite is in view and the signal is present, while the hypothesis H0 declares that the signal is not present. The estimator output (T) is compared with a threshold which corresponds to the probability of detection P_d and probability of false alarm P_{fa} .

There are two strategies implemented for L5 signal detection that take advantage of the signal structure improvements of the L5 signal over the current L1 civil signal. Since the data channel and pilot channel components on L5 are synchronized with each other, acquisition can be executed on only one channel (I/Q) or on both. The latter strategy outperforms the former by utilizing more available signal power. However, as a consequence, the computation load is doubled for software based implementation. This research investigates the first strategy.

The detector for the single channel acquisition strategy is:

$$T = \sum_{m=1}^M (I_m^2 + Q_m^2) \quad (2.9)$$

where M is the non-coherent integration time.

2.3 Broadband Noise Impact on Detection Performance

Hypothesis H0: the desired signal is not present

The test statistic for H0, T_o , is based on the following white Gaussian noise assumption:

$$T_0 = \sum_{k=1}^M [n_I^2(k) + n_Q^2(k)] \quad (2.10)$$

where n_I and n_Q are the in-phase and quadrature correlator outputs. The normalized test

statistic, $T_0' = \frac{T_0}{\sigma_n^2}$, has a central chi-square distribution with $2M$ degrees of freedom.

The equations (2.10) to (2.18) are taken from (Bastide *et al* 2002). The false alarm probability is:

$$P_{fa} = \Pr\{T_0' > Th\} = \int_{Th}^{\infty} P_{T_0'}(t) dt = f(Th) \quad (2.11)$$

where $P_{T_0'}(t)$ is the probability density function of the detector (central chi-square), and

Th is the detection threshold. Given that the classical false alarm probability is $P_{fa} = 10^{-3}$,

the detection threshold $Th = 59.7$ (for $M=15$) can be easily (and numerically with some software) determined by inverting the function $f(Th)$.

Hypothesis H1: a useful signal is present

Using the white Gaussian noise assumption, namely the H1 test statistic, T_1 is expressed

as:

$$T_1 = \sum_{k=1}^M \left\{ \begin{aligned} & \left[\sqrt{\frac{P_m}{4}} b_m(k) R_{m,m}(\tilde{\tau}) \frac{\sin(\pi \Delta f T_p)}{\pi \Delta f T_p} \cos(\mathbf{\epsilon}_{\theta}) + n_I(k) \right]^2 + \\ & \left[\sqrt{\frac{P_m}{4}} b_m(k) R_{m,m}(\tilde{\tau}) \frac{\sin(\pi \Delta f T_p)}{\pi \Delta f T_p} \sin(\mathbf{\epsilon}_{\theta}) + n_Q(k) \right]^2 \end{aligned} \right\}. \quad (2.12)$$

The normalized detection criterion, $\frac{T_1}{\sigma_n^2}$, is a non-central chi-square distribution with

$2M$ degrees of freedom and a non-centrality parameter, λ :

$$\lambda = \frac{MP_m}{f_p N_0} R_{m,m}^2(\tilde{\tau}) \left(\frac{\sin(\pi \Delta f T_p)}{\pi \Delta f T_p} \right)^2. \quad (2.13)$$

The probability of detection is determined by the detection threshold and the non-central chi-square distribution. It is associated with the carrier noise density ratio (C/N_0) through the non-centrality parameter.

Figure 2.2 illustrates how the probability of detection at a fixed probability of false alarm ($1e^{-3}$) is related to the carrier noise density ratio. The coherent integration time, T_p , is 1 ms. The blue, green and red curves show the probability of detection for non-coherent integration times of $M = 15, 40$ and 60 , respectively. Front-end filter effects are neglected and uncertainties ($\tilde{\tau}, \Delta f$) are assumed to be zero. Figure 2.2 shows that the desired signal is detected more efficiently at a lower broadband noise power level (higher C/N_0). Normally, robust signal acquisition is achieved if the C/N_0 is above 40 dB-Hz. It is clear that the lengthening of the non-coherent integration time can effectively increase the output SNR to a detectable level. For C/N_0 values in the range of 28 to 35 dB-Hz, 60 ms of non-coherent integration presents the same detection performance (detection probability) as 15 ms of coherent integration, but with a C/N_0 that is 2 to 3 dB-Hz lower. The detection probability of the former differs greatly from that of the latter at the same C/N_0 level.

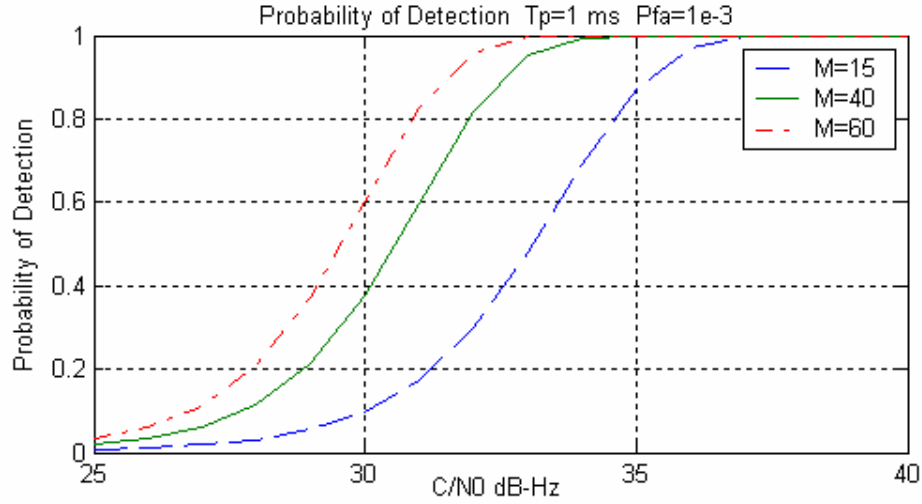


Figure 2.2: Probability of Detection ($1e^{-3}$) for Total (I+Q) C/N_0 at the Antenna Output Ranging from 25 to 40 dB-Hz.

2.4 Cross-Correlation Impact on Detection Performance

Hypothesis H0: The desired signal is not present

If a minor cross-correlation peak is taken into consideration the test statistic, $T_{0,J}$, becomes:

$$T_{0,J} = \sum_{k=1}^M \left\{ \left[\sqrt{\frac{P_J}{4}} b_J(k) R_{J,m}(\tilde{\tau}) \frac{\sin(\pi \Delta f_J T_p)}{\pi \Delta f_J T_p} \cos(\mathbf{e}_{\theta_{0,J}}) + n_I(k) \right]^2 + \left[\sqrt{\frac{P_J}{4}} b_J(k) R_{J,m}(\tilde{\tau}) \frac{\sin(\pi \Delta f_J T_p)}{\pi \Delta f_J T_p} \sin(\mathbf{e}_{\theta_{0,J}}) + n_Q(k) \right]^2 \right\}. \quad (2.14)$$

The normalized detection criterion, $\frac{T_{0,J}}{\sigma_n^2}$ conforms to a non-central chi-square distribution

with $2M$ degrees of freedom, and non-centrality parameter (BASTIDE *et al* 2002):

$$\lambda = \frac{MP_J}{f_p N_0} R_{J,m}^2(\tilde{\tau}) \left(\frac{\sin(\pi\Delta f T_p)}{\pi\Delta f T_p} \right)^2. \quad (2.15)$$

The false alarm probability is determined from the precise cross-correlation, R , between the in-phase channel of the expected satellite J and either channel of satellite m . The acceptable worst case for the cross-correlation term, $\frac{P_J}{N_0} R_{J,m}^2(\tilde{\tau})$, is 19 dB-Hz (Dierendonck 1999).

Hypothesis H1: The desired signal is present

The test statistic, $T_{1,J}$, has the following expression:

$$T_{1,J} = \sum_{k=1}^M \left\{ \begin{aligned} & \left[\sqrt{\frac{P_m}{4}} b_m(k) R_{m,m}(\tilde{\tau}) \frac{\sin(\pi\Delta f T_p)}{\pi\Delta f T_p} \cos(\varepsilon_\theta) + \right. \\ & \left. \sqrt{\frac{P_J}{4}} b_J(k) R_{J,m}(\tilde{\tau}) \frac{\sin(\pi\Delta f_J T_p)}{\pi\Delta f_J T_p} \cos(\varepsilon_{\theta,J}) + n_I(k) \right]^2 + \\ & \left[\sqrt{\frac{P_m}{4}} b_m(k) R_{m,m}(\tilde{\tau}) \frac{\sin(\pi\Delta f T_p)}{\pi\Delta f T_p} \sin(\varepsilon_\theta) + \right. \\ & \left. \sqrt{\frac{P_J}{4}} b_J(k) R_{J,m}(\tilde{\tau}) \frac{\sin(\pi\Delta f_J T_p)}{\pi\Delta f_J T_p} \sin(\varepsilon_{\theta,J}) + n_Q(k) \right]^2 \end{aligned} \right\}. \quad (2.16)$$

The detection criterion $\frac{T_{1,J}}{\sigma_n^2}$ is also a non-central chi-square distribution (BASTIDE *et al* 2002) with $2M$ degrees of freedom and the expected value of the noncentrality parameter λ , is:

$$\lambda = \frac{MP_m}{f_p N_0} R_{m,m}^2(\tilde{\tau}) \left(\frac{\sin(\pi\Delta f T_p)}{\pi\Delta f T_p} \right)^2 + \frac{MP_J}{f_p N_0} R_{J,m}^2(\tilde{\tau}) \left(\frac{\sin(\pi\Delta f_J T_p)}{\pi\Delta f_J T_p} \right)^2. \quad (2.17)$$

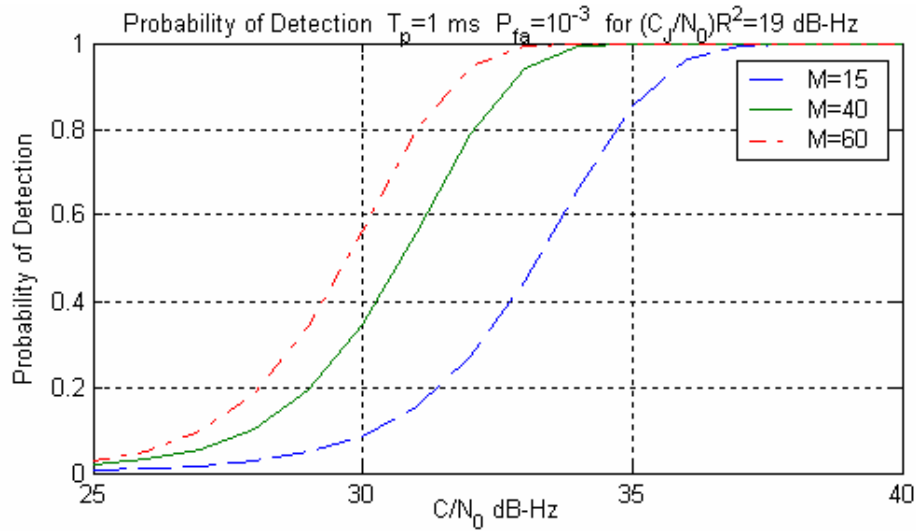


Figure 2.3: Probability of Detection versus total (I+Q) C/N_0 at the Antenna Output, for the Worst Case Cross-Correlation

Figure 2.3 shows the variation of the probability of detection in accordance with various C/N_0 values at a fixed false alarm probability of 10^{-3} and the worst case self-interference condition $\frac{P_J}{N_0} R_{J,m}^2(\tilde{\tau}) = 19$ dB-Hz. The coherent integration time T_p is 1 ms. The blue, green and red curves show the probability of detection for non-coherent integration times M of 15, 40 and 60, respectively. The front-end filter effects and uncertainty $(\tilde{\tau}, \Delta f)$ are again neglected. Figure 2.3 shows approximately the same features as those of Figure 2.2. Due to the presence of self-interference, the overall detection performance is degraded. When averaged across all C/N_0 , the detection probability decreased by 0.08 for the 15 ms non-coherent integration case, 0.11 for 40 ms, and 0.08 for 60 ms.

2.5 Mean Acquisition Time Computation

When using the single dwell time search process, the mean acquisition time is expressed as (Holmes 1990):

$$\bar{T} = \frac{2 + (2 - P_d)(q - 1)(1 + KP_{fa})}{2P_d} \tau_d \quad (2.18)$$

where:

- q is the uncertainty region size,
- τ_d is the dwell time equal to MT_p ,
- K is the penalty factor. It stands for the time lost due to the occurrence of a false alarm, and is chosen so that $K\tau_d = 1$ s.

The uncertainty region size amounts to the total number of cells in the two dimensional code delay and frequency search process. If a half-chip rate is used in the code delay search, there are $10230 \times 2 = 20460$ code bins. The number of frequency search cells is 40 ($2 \times 5000 / 250$) if the search is carried out within a $-5/+5$ KHz Doppler range at a 250 Hz search rate. The uncertainty size is therefore 818400 (20460×40) for this cold start scenario. In the case of aided acquisition where the frequency search is not necessary, this size could be reduced to 20460.

Chapter Three: RFI IMPACT ON RECEIVED SNR

Detection theory is the area of study that deals with electrical signal processing systems for decision making and information extraction. The main function of these systems is to decide when an event of interest happens and to extract useful information about that event. As Chapter 2 discusses, the issue of decision making or hypothesis testing has been investigated in depth by researchers. This chapter will study another important topic, the matched filter or correlator, since the replica correlator is a key component in any GPS receiver that is used in acquisition, code tracking (DLL), and phase tracking (PLL). Elementary knowledge of matched filters will be introduced first according to the description in (Kay 1998), then the GPS L5 correlator performance will be evaluated according to correlator output SNR.

3.1 Theory of Matched Filters

Applications of matched filters are found in many areas, such as communications and radar systems. At the receiving end, it is not usually possible to determine with absolute certainty whether or not a signal is present, because of electrical receiver noise, interference, and other signal distortions. In the face of this limitation, detection theory provides a means for choosing a good technique to infer from the distorted observations the presence or absence of a signal. The matched filter is a widely used tool for the detection of signals embedded in noise.

3.1.1 Development of a Detector

The optimal detector under discussion uses the approach of identifying a known deterministic signal in the presence of white Gaussian noise (WGN), according to the Neyman-Pearson (NP) criterion.

Referred to as the null hypothesis, H_0 stands for the absence of the signal of interest, and H_1 , for the alternative hypothesis. The goal of a detector is to decide between two hypotheses (H_0 or H_1) on the basis of a set of observations $\{x[0], x[1], \dots, x[N-1]\}$, referred to as X . Such a problem is termed a binary hypothesis test. The probability density function (PDF) under each hypothesis is expressed as $p(X; H_0)$ and $p(X; H_1)$. A decision (critical) region is defined as a mapping from a set of values in \mathbb{R}^N to the decision H_0 or H_1 ,

$$R_0 = \{X : \text{decide } H_0 \text{ or reject } H_1\} \quad (3.1)$$

$$R_1 = \{X : \text{decide } H_1 \text{ or reject } H_0\} \quad (3.2)$$

The detector will base the choice between the two hypotheses on the observed data and a pre-determined threshold. Because of noise interference, the detector suffers from two error types. It may select H_1 , while H_0 is true, in which case a Type I error is committed. Or it may select H_0 while H_1 is true, in which case a Type II error is committed. The effects of these two error types are evaluated by the probability of deciding H_1 (H_0) when H_0 (H_1) is true, $P(H_1; H_0)$ and $P(H_0; H_1)$, respectively. It is preferable to reduce both error probabilities as much as possible. Unfortunately, a decrease in one probability is obtained at the expense of an increase in the other. Therefore, an optimal detector can

only minimize one error probability while constraining the other at a predetermined and acceptable level. $P(H_1; H_0)$ is called the probability of a false alarm, and is denoted by (Kay 1998)

$$P_{FA} = \int_{R_1} p(X; H_0) dX = \alpha \quad (3.3)$$

where α is the significance level, or size of the test in statistics.

The Neyman-Pearson approach to signal detection is to maximize the probability of detection $P(H_1; H_1)$ or P_D subject to a chosen value for $P_{FA} = \alpha$, where

$$P_D = \int_{R_1} p(X; H_1) dX . \quad (3.4)$$

Neyman-Pearson Theorem

To maximize P_D for a given $P_{FA} = \alpha$, select H_1 if

$$L(X) = \frac{p(X; H_1)}{p(X; H_0)} > \gamma, \quad (3.5)$$

where the threshold γ is inferred from

$$P_{FA} = \int_{X: L(X) > \gamma_1} p(X; H_0) dX = \alpha . \quad (3.6)$$

The hypotheses of the detection problem under consideration are expressed as

$$\begin{aligned} H_0 : & \quad x[n] = w[n] & \quad n = 0, 1, \dots, N-1 \\ H_1 : & \quad x[n] = s[n] + w[n] & \quad n = 0, 1, \dots, N-1 \end{aligned} , \quad (3.7)$$

where the signal $s[n]$ is considered as known and $w[n]$ is WGN with variance σ^2 . WGN is assumed to be a Gaussian noise process with zero mean and autocorrelation function

$$r_{ww}[k] = E(w[n]w[n+k]) = \sigma^2 \delta[k], \quad (3.8)$$

where $\delta[k]$ is the discrete-time delta function

$$\delta[k] = \begin{cases} 1 & k = 0 \\ 0 & k \neq 0 \end{cases}. \quad (3.9)$$

The NP detector decides, based on the comparison of the likelihood ratio and a threshold aforementioned in Equation (3.5):

$$L(X) = \exp\left[-\frac{1}{2\sigma^2}\left(\sum_{n=0}^{N-1}(x[n]-s[n])^2 - \sum_{n=0}^{N-1}x^2[n]\right)\right] > \gamma, \quad (3.10)$$

because

$$\begin{aligned} p(X; H_1) &= \frac{1}{(2\pi\sigma^2)^{\frac{N}{2}}} \exp\left[-\frac{1}{2\sigma^2}\sum_{n=0}^{N-1}(x[n]-s[n])^2\right] \\ p(X; H_0) &= \frac{1}{(2\pi\sigma^2)^{\frac{N}{2}}} \exp\left[-\frac{1}{2\sigma^2}\sum_{n=0}^{N-1}x^2[n]\right] \end{aligned}. \quad (3.11)$$

Since the logarithm conversion does not change the relationship of the equation on the two sides of the inequality, the NP detector can be expressed as:

$$l(X) = \ln L(X) = -\frac{1}{2\sigma^2}\left(\sum_{n=0}^{N-1}(x[n]-s[n])^2 - \sum_{n=0}^{N-1}x^2[n]\right) > \ln \gamma. \quad (3.12)$$

Because the incoming signal $s[n]$ is known, the inequality can be converted into a more meaningful format by shifting and incorporating terms on both sides:

$$\begin{aligned} T(X) &= \sum_{n=0}^{N-1} x[n]s[n] > \gamma' \\ \gamma' &= \sigma^2 \ln \gamma + \frac{1}{2} \sum_{n=0}^{N-1} s^2[n] \end{aligned}. \quad (3.13)$$

This is the NP detector, made of a test statistic $T(X)$ and a threshold γ' , that ensures a predetermined P_{FA} . The detector is referred to as a correlator or replica correlator, since the incoming signal $x[n]$ is correlated with a local replica of the desired signal $s[n]$. The correlator can be interpreted as a finite impulse (FIR) filter with impulse response

$$h[n] = s[N-1-n] \quad n = 0, 1, \dots, N-1. \quad (3.14)$$

Then, the output at time n is

$$y[n] = \sum_{k=0}^n h[n-k]x[k] = \sum_{k=0}^n s[N-1-(n-k)]x[k]. \quad (3.15)$$

The output of the filter at epoch $N-1$

$$y[N-1] = \sum_{k=0}^{N-1} s[k]x[k] \quad (3.16)$$

is equivalent to the test statistic presented by the replica correlator, and the filter is called a matched filter since the filter impulse response is matched to the desired signal.

An important and advantageous feature of the matched filter is the maximized SNR at its output. Consider all detectors with an arbitrary $h[n]$ over $[0, N-1]$, and zero otherwise. If the SNR output is defined as (Kay 1998)

$$\eta = \frac{E^2(y[N-1]; H_1)}{\text{var}(y[N-1]; H_1)} = \frac{\left(\sum_{k=0}^{N-1} h[N-1-k]s[k] \right)^2}{E \left[\left(\sum_{k=0}^{N-1} h[N-1-k]w[k] \right)^2 \right]}, \quad (3.17)$$

the matched filter maximizes its value. This can be verified by converting the expressions into vectors and manipulating them as follows. Let $S=[s[0] s[1] \dots s[N-1]]^T$, $H=[h[N-1] h[N-2] \dots h[0]]^T$, and $W=[w[0] w[1] \dots w[N-1]]^T$, then

$$\eta = \frac{(H^T S)^2}{E[(H^T W)^2]} = \frac{(H^T S)^2}{H^T E(WW^T)H} = \frac{1}{\sigma^2} \frac{(H^T S)^2}{H^T H}. \quad (3.18)$$

According to the Cauchy-Schwarz inequality

$$(H^T S)^2 \leq (H^T H)(S^T S), \quad (3.19)$$

the equality is achieved if and only if $H=cS$, where c is any constant. Thus,

$$\eta \leq \frac{1}{\sigma^2} S^T S. \quad (3.20)$$

with equality if and only if $H=cS$. Therefore, the maximum output SNR is achieved given that

$$h[n] = s[N-1-n] \quad n = 0, 1, \dots, N-1, \quad (3.21)$$

the definition of the matched filter. The matched filter is considered an energy detector since the maximum SNR, $\eta_{\max} = S^T S / \sigma^2 = \varepsilon / \sigma^2$, is solely dependent on the signal energy, ε , if the noise power is fixed. The matched filter detector is the optimal detector from the viewpoint of both the NP criterion and the maximum SNR criterion if the detection problem is constrained to a known deterministic signal in WGN. Its performance is closely associated with the maximum SNR, and discussed in the next section.

3.1.2 Performance of Matched Filter

The following derivations follow (Kay 1998) closely. The performance of the matched filter will be determined in this section by expressing the probability of detection (P_D) for a given probability of false alarm (P_{FA}). The detection of the desired signal is affirmed if

$$T(X) = \sum_{n=0}^{N-1} x[n]s[n] > \gamma' . \quad (3.22)$$

The following discussion will be centered on $T(X)$, a Gaussian variable since it is a weighted sum of Gaussian random variables $x[n]$ with a different mathematical expectation for each hypothesis. Note that $E(T;H_i)$ and $\text{var}(T;H_i)$ stand for the expected value and variance of the test statistic $T(X)$ in the case of H_i , and that

$$\begin{aligned} E(T; H_0) &= E\left(\sum_{n=0}^{N-1} w[n]s[n]\right) = 0 \\ E(T; H_1) &= E\left(\sum_{n=0}^{N-1} (s[n] + w[n])s[n]\right) = \varepsilon \end{aligned} \quad (3.23)$$

$$\text{var}(T; H_0) = \text{var}\left(\sum_{n=0}^{N-1} w[n]s[n]\right) = \sum_{n=0}^{N-1} \text{var}(w[n])s^2[n] = \sigma^2 \varepsilon \quad (3.24)$$

under the assumption that the noise sequence $w[n]$ is uncorrelated. The distribution of the test statistic is

$$T \sim \begin{cases} N(0, \sigma^2 \varepsilon) & \text{under } H_0 \\ N(\varepsilon, \sigma^2 \varepsilon) & \text{under } H_1 \end{cases} . \quad (3.25)$$

Accordingly, the key indicators of detection performance are

$$\begin{aligned} P_{FA} &= P_r\{T > \gamma'; H_0\} = Q\left(\frac{\gamma'}{\sqrt{\sigma^2 \varepsilon}}\right) \\ P_D &= P_r\{T > \gamma'; H_1\} = Q\left(\frac{\gamma' - \varepsilon}{\sqrt{\sigma^2 \varepsilon}}\right), \end{aligned} \quad (3.26)$$

where

$$\gamma' = \sqrt{\sigma^2 \varepsilon} Q^{-1}(P_{FA}). \quad (3.27)$$

and

$$Q(x) = \int_x^{\infty} \frac{1}{\sqrt{2\pi}} \exp\left(-\frac{1}{2}t^2\right) dt = 1 - \Phi(x), \quad (3.28)$$

where $\Phi(x)$ denotes the cumulative probability function (CDF) for a normalized Gaussian variable, and $Q(x)$ is its complementary function. Since any CDF function increases monotonically, $Q(x)$ is bound to decrease monotonically, and its inverse function $Q^{-1}(x)$ must exist. It follows that the probability of detection can be expressed as a function of the probability of false alarm (Kay 1998):

$$P_D = Q\left(\frac{\sqrt{\sigma^2 \varepsilon} Q^{-1}(P_{FA})}{\sqrt{\sigma^2 \varepsilon}} - \sqrt{\frac{\varepsilon}{\sigma^2}}\right) = Q\left(Q^{-1}(P_{FA}) - \sqrt{\frac{\varepsilon}{\sigma^2}}\right), \quad (3.29)$$

An increase in $\eta = \varepsilon / \sigma^2$, the argument of $Q(\cdot)$, results in the enhancement of P_D if P_{FA} is held at a constant level, as Figure 3.1 shows. Thus, the improvement of detection performance relies on the matched filter output SNR – termed the energy-to-noise ratio

(ENR), since ENR is promoted by the enlargement of signal energy. Under the WGN assumption, the detection probability is solely a function of the ENR and has nothing to do with the shape of the signal. However, the design of the signal shape is an important issue for coloured noise.

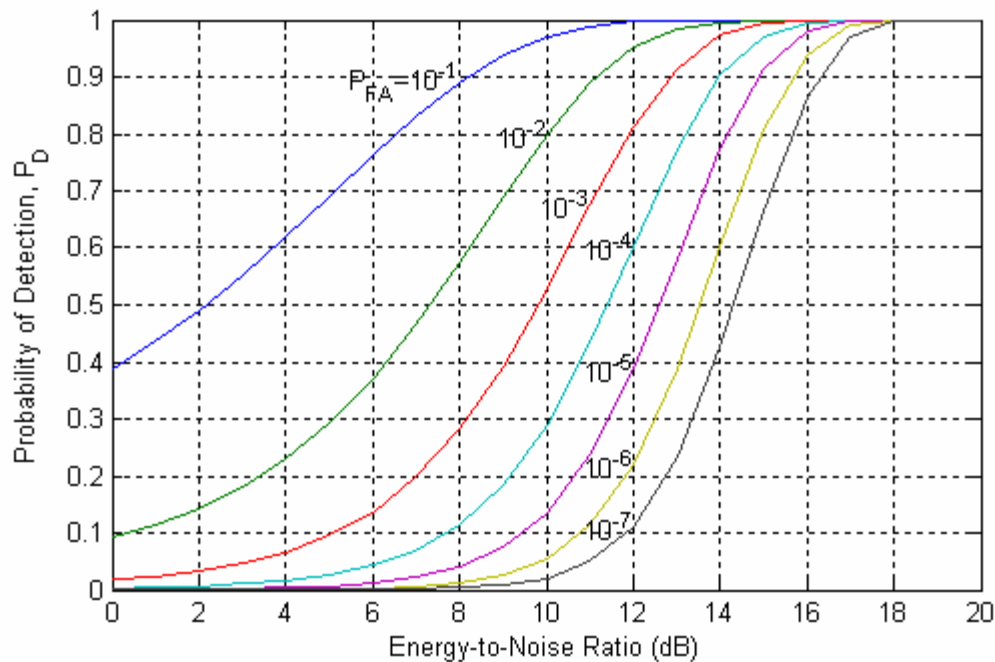


Figure 3.1: Detection Performance of Matched Filter (Kay 1998)

3.2 Correlator Output SNR Analysis in the Presence of Broadband Noise and Cross-Correlation

The replica correlator plays a vital role in the signal processing system of any GPS receiver, because its output is fed into the acquisition unit, code-tracking loop, and phase-tracking loop. In theory, the detection performance depends directly on the correlator

output SNR, so most GPS receivers periodically provide a measurement of SNR as an indicator of the signal quality and receiver performance. The following section will present an average SNR theoretically based on statistics, and verify this theoretical estimate with simulations.

3.2.1 Theoretical Estimation

SNR is one of the most important measurements available for the assessment of receiver performance. A minimum SNR value of approximately 14 dB is required for robust GPS signal acquisition and tracking. Due to propagation path differences, GPS signals from different satellites are temporally misaligned upon their arrival time at the receiver antenna. Thus, the GPS receiver is also an asynchronous phase-coded spread-spectrum multiple access (SSMA) system. Anderson and Wintz (1969) investigated the aperiodic cross-correlation effects on asynchronous phase-coded SSMA systems and presented results and implications for a Bi-Phase Shift Keying (BPSK) signal. Pursley (1977a) presented an approach to analyze the BPSK SSMA system by the average SNR. Due to the similarity of a mobile communication system to a GPS L5 system in terms of signal structure and receiver design, the evaluation of L5 reception is implemented using the same methodology.

If the expected L5 signal of satellite m ($m < K$), broadband random noise, and cross correlation interference from the other ($K - 1$) satellites are taken into account, the received IF signal (Bastide *et al* 2003a) is assumed to be:

$$r(t) = n(t) + \sqrt{P_m} \sum_{k=1}^K \sqrt{\alpha_k} [a_{2k-1}(t-\tau_k)D_k(t-\tau_k)NH_{10}(t-\tau_k)\cos(\omega_0 t + \phi_k) + a_{2k}(t-\tau_k)NH_{20}(t-\tau_k)\sin(\omega_0 t + \phi_k)] \quad (3.30)$$

where:

- a_{2k-1} and a_{2k} are satellite k 's PN codes on the in-phase and quadrature components, respectively, $a_{2k-1} = XI_k$, $a_{2k} = XQ_k$,
- $n(t)$ is the channel noise assumed to be a white Gaussian process with two-sided spectral density $\frac{N_0}{2}$ and zero mean,
- $\alpha_k = P_k / P_m$, P_k is the L5 signal power of satellite k .

The input phase, including phase noise and frequency uncertainty, is investigated as time dependent additive noise. Since only relative phase shifts (ϕ_k) modulo 2π and relative time delays modulo T_p (1 ms, both the coherent integration time and L5 PRN code period) are of interest, one can assume that $\tau_m = 0$, $\phi_m = 0$, and to consider the following bounds: $0 \leq \tau_k < T_p$ and $0 \leq \phi_k < 2\pi$. If the local replica code and carrier phase matches the expected signal from the space vehicle (SV) m , the correlator output is expressed as:

$$Z_{2m-1} = \int_0^{T_p} r(t)a_{2m-1}(t)\cos(\omega_0 t)dt. \quad (3.31)$$

The following derivation is based on the assumption of a receiver IF bandwidth $\omega_0 \gg T_p^{-1}$, where T_p^{-1} is approximately the receiver's baseband width. In this case the

double frequency component, $r(t)\cos(\omega_0 t)$, can be ignored. Practically, this condition is always satisfied in any CDMA communication system. T_p is limited to 1 ms as discussed in section 2.2. This investigation focuses on the in-phase channel of the expected signal, so that the corresponding quadrature channel is a cross-correlation source. Fortunately its impact is negligible due to the L5 cross-correlation suppression (over 74 dB). The expression for the data bit $D_n(t)$ is:

$$D_n(t) = \sum_{l=-\infty}^{\infty} d_{n,l} p_{10T_p}(t - l \times 10T_p) \quad (3.32)$$

where:

- $T_p = NT_C$;
- $d_{k,l}$ is the navigation message on satellite k , which is assumed to take on values of +1 or -1 with equal probability;

In the same way, the NH symbol can be expressed as:

$$NH_{\alpha}(t) = \sum_{l=-\infty}^{\infty} NH_{\alpha,l} p_{T_p}(t - lT_p \alpha / 10) \quad \alpha \in \{10, 20\} \quad (3.33)$$

where $NH_{20,l}$ and $NH_{10,l}$ are periodic sequences for L5 in-phase and quadra-phase channels respectively. The PN code waveform, $a_k(t)$, consists of a periodic sequence with cycle $N = T_p / T_C$, and is defined as:

$$a_k(t) = \sum_{j=-\infty}^{\infty} a_{k,j} p_{T_C}(t - jT_C) \quad (3.34)$$

where T_C is the chip width of the PN code.

It follows that the correlator output is represented as:

$$\begin{aligned} Z_{2m-1} = & \sqrt{\frac{P_m}{4}} \{ b_{2m-1,0} T_P + \sum_{\substack{k=1 \\ k \neq m}}^K \sqrt{\alpha_k} [d_{k,n} NH_{10,-1} R_{2k-1,2m-1}(\tau_k) + d_{k,n} NH_{10,0} \hat{R}_{2k-1,2m-1}(\tau_k)] \cos \phi_k \\ & + \sum_{\substack{k=1 \\ k \neq m}}^K \sqrt{\alpha_k} [NH_{20,-1} R_{2k,2m-1}(\tau_k) + NH_{20,0} \hat{R}_{2k,2m-1}(\tau_k)] \sin \phi_k \} + \int_0^{T_P} n(t) a_{2m-1}(t) \cos \omega_0 t dt \end{aligned} \quad (3.35)$$

where $n \leq n'$, and the definitions of the continuous-time partial cross-correlation functions $R_{j,i}$ and $\hat{R}_{j,i}$ (Pursley 1977a) are:

$$R_{j,i}(\tau) = \int_0^{\tau} a_j(t - \tau) a_i(t) dt \quad (3.36)$$

$$\hat{R}_{j,i}(\tau) = \int_{\tau}^{T_P} a_j(t - \tau) a_i(t) dt \quad (3.37)$$

for $0 \leq \tau \leq T_P$.

It follows that for $0 \leq lT_C \leq \tau \leq (l+1)T_C \leq T_P$, these two functions can be rewritten as

(Pursley 1977a):

$$R_{j,i}(\tau) = C_{j,i}(l-N)T_C + [C_{j,i}(l+1-N) - C_{j,i}(l-N)](\tau - lT_C) \quad (3.38)$$

$$\hat{R}_{j,i}(\tau) = C_{j,i}(l)T_C + [C_{j,i}(l+1) - C_{j,i}(l)](\tau - lT_C). \quad (3.39)$$

Assuming that $\tau = lT_C + \Delta\tau$ for $0 \leq \Delta\tau < T_C$, $R_{j,i}$ becomes:

$$\begin{aligned}
R_{j,i}(\tau) &= \int_0^{lT_C + \Delta\tau} \sum_{k=-\infty}^{\infty} \sum_{m=-\infty}^{\infty} a_{j,k} a_{i,m} P_{T_C}[t - kT_C - lT_C - \Delta\tau] P_{T_C}[t - mT_C] dt \\
&= \sum_{n=0}^{l-1} \int_{nT_C}^{(n+1)T_C} \sum_{k=-\infty}^{\infty} \sum_{m=-\infty}^{\infty} a_{j,k} a_{i,m} P_{T_C}[t - kT_C - lT_C - \Delta\tau] P_{T_C}[t - mT_C] dt + \\
&\quad \int_{lT_C}^{lT_C + \Delta\tau} \sum_{k=-\infty}^{\infty} \sum_{m=-\infty}^{\infty} a_{j,k} a_{i,m} P_{T_C}[t - kT_C - lT_C - \Delta\tau] P_{T_C}[t - mT_C] dt \quad . \quad (3.40) \\
&= \sum_{n=0}^{l-1} a_{i,n} \int_{nT_C}^{(n+1)T_C} \sum_{k=-\infty}^{\infty} a_{j,k} P_{T_C}[t - kT_C - lT_C - \Delta\tau] dt + \\
&\quad a_{i,l} \int_{lT_C}^{lT_C + \Delta\tau} \sum_{k=-\infty}^{\infty} a_{j,k} P_{T_C}[t - kT_C - lT_C - \Delta\tau] dt
\end{aligned}$$

Since $t = nT_C + \delta$ where $0 \leq \delta < T_C$, the unit pulse term $P_{T_C}[t - kT_C - lT_C - \Delta\tau]$ takes on a non-zero value (+1) only if the following condition is met:

$$\begin{aligned}
0 &\leq (nT_C + \delta) - kT_C - lT_C - \Delta\tau < T_C \\
n - l - 1 + \frac{\delta - \Delta\tau}{T_C} &< k \leq n - l + \frac{\delta - \Delta\tau}{T_C} . \quad (3.41)
\end{aligned}$$

The cross-correlation term becomes:

$$\begin{aligned}
R_{j,i}(\tau) &= \sum_{n=0}^{l-1} a_{i,n} \left\{ \int_{nT_C}^{nT_C+\Delta\tau} \sum_{k=-\infty}^{\infty} a_{j,k} P_{T_C} [t - kT_C - lT_C - \Delta\tau] dt + \right. \\
&\quad \left. \int_{nT_C+\Delta\tau}^{(n+1)T_C} \sum_{k=-\infty}^{\infty} a_{j,k} P_{T_C} [t - kT_C - lT_C - \Delta\tau] dt \right\} + a_{j,-1} a_{i,l} \int_{lT_C}^{lT_C+\Delta\tau} dt \\
&= \sum_{n=0}^{l-1} a_{j,n-l-1} a_{i,n} \int_{nT_C}^{nT_C+\Delta\tau} dt + \sum_{n=0}^{l-1} a_{j,n-l} a_{i,n} \int_{nT_C+\Delta\tau}^{(n+1)T_C} dt + a_{j,-1} a_{i,l} \Delta\tau \\
&= \sum_{n=0}^l a_{j,n-l-1} a_{i,n} \Delta\tau + \sum_{n=0}^{l-1} a_{j,n-l} a_{i,n} (T_C - \Delta\tau) \\
&= \sum_{n=0}^{N-1+(l+1-N)} a_{j,n-(l+1-N)} a_{i,n} \Delta\tau + \sum_{n=0}^{N-1+(l-N)} a_{j,n-(l-N)} a_{i,n} (T_C - \Delta\tau) \\
&= C_{j,i}(l+1-N) \Delta\tau + C_{j,i}(l-N) (T_C - \Delta\tau) \\
&= C_{j,i}(l-N) T_C + [C_{j,i}(l+1-N) - C_{j,i}(l-N)] (\tau - lT_C).
\end{aligned} \tag{3.42}$$

The discrete aperiodic cross-correlation function, $C_{j,i}$, for the sequences $(a_{j,n})$ and $(a_{i,n})$

is defined by Pursley (1977b) as:

$$C_{j,i}(l) = \begin{cases} \sum_{n=0}^{N-1-l} a_{j,n} a_{i,n+l}, & 0 \leq l \leq N-1 \\ \sum_{n=0}^{N-1+l} a_{j,n-l} a_{i,n}, & 1-N \leq l \leq 0 \\ 0, & |l| \geq N. \end{cases} \tag{3.43}$$

In Equation (3.35), for the cases where $k > 1$ and $k \neq m$, $b_{2k-1,l}$, τ_k , ϕ_k and $b_{2k,l}$ can be referred to as mutually independent random variables. It is reasonable to assume that τ_k and ϕ_k are uniformly distributed over the intervals $[0, T_p]$ and $[0, 2\pi]$, respectively.

There is no loss of generality in the assumption of $b_{2m-1,0} = +1$ due to the symmetry involved. Therefore, $\sqrt{P_m/4T_p}$ is the desired signal component. The computation of the SNR ratio is achieved through probabilistic averages (expectations) with respect to the

phase shifts, time delays, and data symbols. The expected value of the correlator output is:

$$\begin{aligned}
E(Z_{2m-1}) = & \sqrt{\frac{P_m}{4}} \left\{ T_p + \sum_{\substack{k=1 \\ k \neq m}}^K \sqrt{\alpha_k} [E(NH_{20,-1})R_{2k,2m-1}(\tau_k) + E(NH_{20,0})\hat{R}_{2k,2m-1}(\tau_k)]E(\sin \phi_k) \right. \\
& \left. + \sum_{\substack{k=1 \\ k \neq m}}^K \sqrt{\alpha_k} [E(d_{k,n})E(NH_{10,-1})R_{2k-1,2m-1}(\tau_k) + E(d_{k,n'})E(NH_{10,0})\hat{R}_{2k-1,2m-1}(\tau_k)]E(\cos \phi_k) \right\} \\
& + \int_0^{T_p} E[n(t)]a_m(t) \cos \omega_0 t dt
\end{aligned} \tag{3.44}$$

Because

$$E(\cos \phi_k) = E(\sin \phi_k) = 0 \quad E[n(t)] = 0, \tag{3.45}$$

the expected value of the correlator output can be simplified to $E(Z_{2m-1}) = \sqrt{P_m / 4} T_p$, which is actually the square root of the signal power of the correlator output and will be used in the computation of PLL jitter.

The variance of the correlator output is expressed as:

$$\begin{aligned}
\text{Var}(Z_{2m-1}) = & E(Z_{2m-1}^2) - E^2(Z_{2m-1}) \\
= & P_m / 4 \left\{ \sum_{\substack{k=1 \\ k \neq m}}^K \alpha_k [E(R_{2k-1,2m-1}^2(\tau_k)) + E(\hat{R}_{2k-1,2m-1}^2(\tau_k))]E(\cos^2 \phi_k) \right. \\
& \left. + \sum_{\substack{k=1 \\ k \neq m}}^K \alpha_k [E(R_{2k,2m-1}^2(\tau_k)) + E(\hat{R}_{2k,2m-1}^2(\tau_k))]E(\sin^2 \phi_k) \right\} \\
& + E \left\{ \left[\int_0^{T_p} E[n(t)]a_m(t) \cos \omega_0 t dt \right]^2 \right\}
\end{aligned} \tag{3.46}$$

The cross terms in $E(Z_{2m-1}^2)$, such as

$$\begin{aligned}
 & P_m / 4b_{2m-1,0} T_P \sqrt{\alpha_k} E[d_{k,n} NH_{10,-1} R_{2k-1,2m-1}(\tau_k)] E[\cos \phi_k], \\
 & \alpha_k E[d_{k,n} d_{k,n'}] E[NH_{10,-1} NH_{10,0}] E[R_{2k-1,2m-1}(\tau_k) \hat{R}_{2k-1,2m-1}(\tau_k)] E[\cos^2 \phi_k], \\
 & \alpha_k E[NH_{20,-1} NH_{20,0}] E[R_{2k,2m-1}(\tau_k) \hat{R}_{2k,2m-1}(\tau_k)] E[\sin^2 \phi_k], \\
 & \alpha_k E[d_{k,n}] E[NH_{10,-1} NH_{20,0}] E[R_{2k-1,2m-1}(\tau_k) \hat{R}_{2k,2m-1}(\tau_k)] E[\sin \phi_k \cos \phi_k],
 \end{aligned}$$

are all zero, due to features described previously in Equation (3.44) and

$$\begin{aligned}
 E(NH_{20,-1} NH_{20,0}) &= 0 & E(NH_{10,-1} NH_{10,0}) &= 0 \\
 E(\cos^2 \phi_k) &= E(\sin^2 \phi_k) = 1/2 & E(d_{k,n}) &= 0
 \end{aligned} \tag{3.47}$$

The difference from Pursley's work is that there are more crossing terms to deal with.

The auto-correlation function of the NH code is shown below.

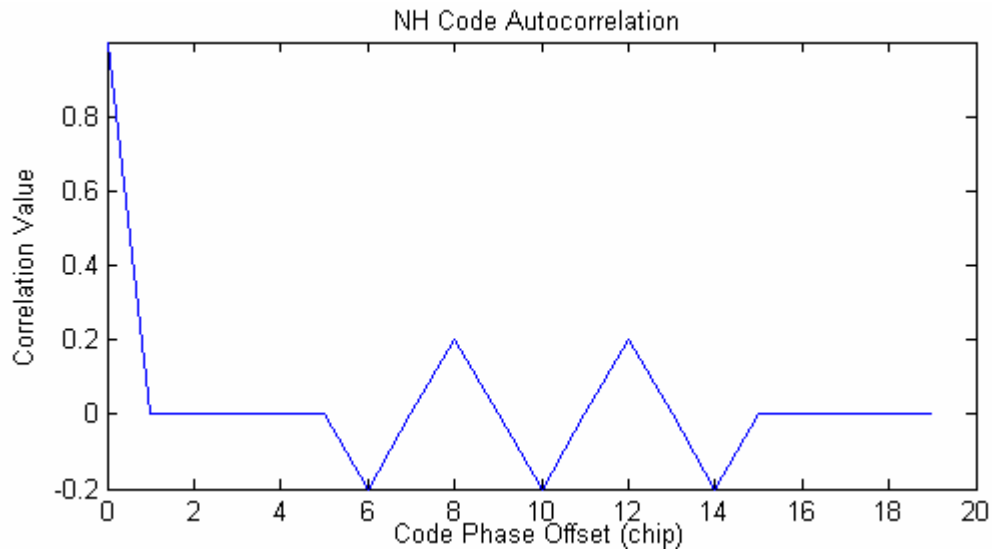


Figure 3.2: Auto-Correlation Function of NH Code

The expected value of the noise term is (Pursley 1977a):

$$\begin{aligned}
& E \left\{ \left[\int_0^{T_P} E[n(t)] a_m(t) \cos \omega_0 t dt \right]^2 \right\} \\
&= \int_0^{T_P} \int_0^{T_P} E[n(t)n(s)] a_m(t) \cos \omega_0 t a_m(s) \cos \omega_0 s dt ds \\
&= \int_0^{T_P} \int_0^{T_P} \frac{N_0}{2} \delta(s-t) a_m(t) \cos \omega_0 t a_m(s) \cos \omega_0 s dt ds \\
&= \frac{N_0}{4} \left(T_P + \frac{\sin 2\omega_0 T_P}{2\omega_0} \right) = \frac{N_0 T_P}{4} \left(1 + \frac{\sin 2\omega_0 T_P}{2\omega_0 T_P} \right) = \frac{N_0 T_P}{4},
\end{aligned} \tag{3.48}$$

if the following condition holds:

$$\omega_0 T_P \gg 1 \quad (\omega_0 T_P > 1000). \tag{3.49}$$

Finally, the variance becomes:

$$\begin{aligned}
\text{Var}(Z_{2m-1}) &= \frac{P_m}{8} \left\{ \sum_{\substack{k=1 \\ k \neq m}}^K \alpha_k [E(R_{2k-1,2m-1}^2(\boldsymbol{\tau}_k)) + E(\hat{R}_{2k-1,2m-1}^2(\boldsymbol{\tau}_k))] + \right. \\
&\quad \left. \sum_{\substack{k=1 \\ k \neq m}}^K \alpha_k [E(R_{2k,2m-1}^2(\boldsymbol{\tau}_k)) + E(\hat{R}_{2k,2m-1}^2(\boldsymbol{\tau}_k))] \right\} + \frac{N_0 T_P}{4} \\
&= \frac{P_m}{8} \left\{ \sum_{\substack{k=1 \\ k \neq m}}^K \alpha_k \left[\int_0^{T_P} R_{2k-1,2m-1}^2(\boldsymbol{\tau}_k) \frac{1}{T_P} d\boldsymbol{\tau}_k + \int_0^{T_P} \hat{R}_{2k-1,2m-1}^2(\boldsymbol{\tau}_k) \frac{1}{T_P} d\boldsymbol{\tau}_k \right] + \right. \\
&\quad \left. \sum_{\substack{k=1 \\ k \neq m}}^K \alpha_k \left[\int_0^{T_P} R_{2k,2m-1}^2(\boldsymbol{\tau}_k) \frac{1}{T_P} d\boldsymbol{\tau}_k + \int_0^{T_P} \hat{R}_{2k,2m-1}^2(\boldsymbol{\tau}_k) \frac{1}{T_P} d\boldsymbol{\tau}_k \right] \right\} + \frac{N_0 T_P}{4}.
\end{aligned} \tag{3.50}$$

Modifying the integration limits, $T_P = NT_C$, the variance is expressed as:

$$\begin{aligned}
\text{Var}(Z_{2m-1}) = & \frac{P_m}{8T_P} \left\{ \sum_{k=1}^K \sum_{l=0}^{N-1} \alpha_k \left[\int_{lT_C}^{(l+1)T_C} R_{2k-1,2m-1}^2(\tau) d\tau + \int_{lT_C}^{(l+1)T_C} \hat{R}_{2k-1,2m-1}^2(\tau) d\tau \right] + \right. \\
& \left. \sum_{k=1}^K \sum_{l=0}^{N-1} \alpha_k \left[\int_{lT_C}^{(l+1)T_C} R_{2k,2m-1}^2(\tau) d\tau + \int_{lT_C}^{(l+1)T_C} \hat{R}_{2k,2m-1}^2(\tau) d\tau \right] \right\} + \frac{N_0 T_P}{4} \quad (3.51)
\end{aligned}$$

Expanding and simplifying Equation (3.51):

$$\begin{aligned}
\int_{lT_C}^{(l+1)T_C} R_{i,j}^2(\tau) d\tau &= \frac{T_C^3}{3} [C_{i,j}^2(l+1-N) + C_{i,j}^2(l-N) + C_{i,j}(l-N)C_{i,j}(l+1-N)] \\
\int_{lT_C}^{(l+1)T_C} \hat{R}_{i,j}^2(\tau) d\tau &= \frac{T_C^3}{3} [C_{i,j}^2(l+1) + C_{i,j}^2(l) + C_{i,j}(l+1)C_{i,j}(l)],
\end{aligned} \quad (3.52)$$

the variance can be simplified to:

$$\text{Var}(Z_{2m-1}) = \frac{P_m T_P^2}{24N^3} \sum_{k=1}^K \sum_{k \neq m} \{ \alpha_k r_{2k-1,2m-1} + \alpha_k r_{2k,2m-1} \} + \frac{N_0 T_P}{4} \quad (3.53)$$

where (Pursley 1977a):

$$\begin{aligned}
r_{i,j} = & \sum_{l=0}^{N-1} \{ C_{i,j}^2(l+1-N) + C_{i,j}^2(l-N) + C_{i,j}(l-N)C_{i,j}(l+1-N) + \\
& C_{i,j}^2(l+1) + C_{i,j}^2(l) + C_{i,j}(l+1)C_{i,j}(l) \}
\end{aligned} \quad (3.54)$$

The SNR is:

$$\text{SNR}_{2m-1} = \frac{\sqrt{P_m / 4T_P}}{\sqrt{\text{Var}(Z_{2m-1})}} = \left[\frac{\sum_{k=1}^K \sum_{k \neq m} \alpha_k (r_{2k-1,2m-1} + r_{2k,2m-1})}{6N^3} + \frac{N_0}{E} \right]^{-\frac{1}{2}} \quad (3.55)$$

where $E = P_m T_p = (P_{mI} + P_{mQ}) T_p = 2P_{mI} T_p$ is the total L5 signal energy of satellite m within period T_p , including both the in-phase and quadrature channels.

If $K=1$ (i.e. there is no cross-correlation), the above equation simplifies to:

$$SNR_1 = \sqrt{\frac{E}{N_0}} = \sqrt{\frac{2E_{1I}}{N_0}} \quad (3.56)$$

which is associated with the error probability $P_e = 1 - \Phi\left(\sqrt{\frac{2E_{1I}}{N_0}}\right)$ for the coherent receiver (matched filter) under the condition of white Gaussian noise.

The assessment of the combined effect of broadband noise and cross-correlation culminates in the Equation (3.55) that will be validated in the section 3.2.2 through simulations.

3.2.2 Numerical Evaluation

3.2.2.1 Simulation Scheme

To verify the theoretical results attained in the previous section, simulations of the replica correlator output will be implemented, based on the same scenario and assumptions made in the above theory. At the acquisition stage, SNR is normally calculated on the basis of a two-dimensional search. Most GPS receivers output a temporary SNR estimate associated with other measurements, such as pseudorange, phase, Doppler and so forth.

However, the SNR of interest here is termed average SNR, a probabilistic average value over all possible situations in accordance with some statistical models.

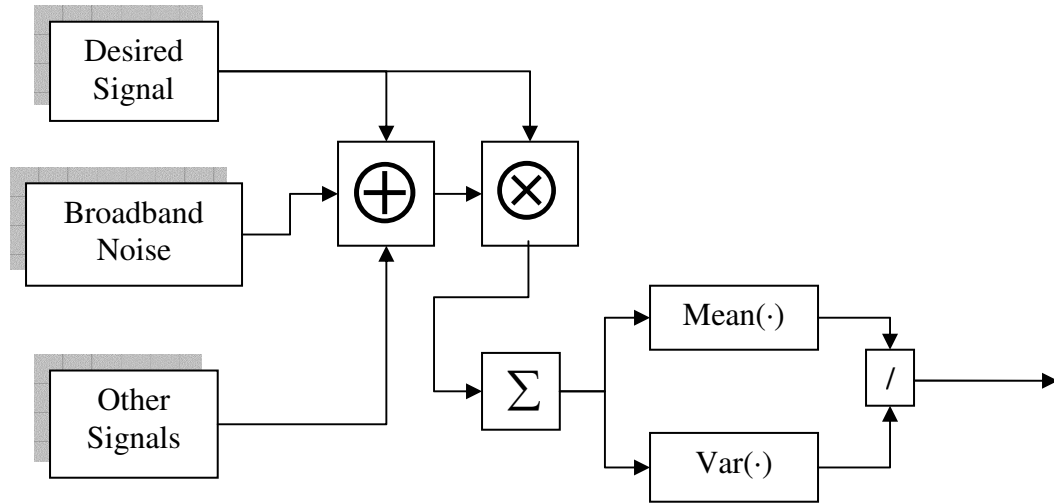


Figure 3.3: Simulation Scheme for Average SNR

According to the assumption in the theoretical evaluation, the incoming signal consists of the desired signal that is tracked accurately (or the local replica is an exact duplicate with no difference in code delay or phase offset), signals from other satellites as the sources of cross-correlation, and broadband random noise. The broadband noise is a Gaussian process uncorrelated in time, referred to as WGN. Since the local replica signal is supposed to precisely track the desired signal (in-phase channel of the desired satellite), the code delay and phase offset are set to zero for simplicity without loss of generality (Pursley 1977a). The desired signal component of the correlator output is its mean value upon the assumption $b_{2m-1,0} = +1$. Thus, the data symbol on the desired signal is assigned to +1 throughout the simulation. Due to their different transmission distances and clock errors, the code delay and phase offset of the signal from another space vehicle (SV) are

assumed to be independent random variables uniformly distributed in their own ranges, namely $[0, T_p]$ for code delay and $[0, 2\pi]$ for phase offset.

The block diagram shown in Figure 3.3 represents the whole simulation scheme. The IF signal is generated through addition of the desired signal, broadband noise or channel noise, and signals from other satellites. According to the assumption of accurate code and phase tracking, the local replica is replaced by a copy of the desired signal and enters the correlator that consists of a multiplier and a summation. The average SNR is calculated as the mean value of the correlator output divided by the variance.

3.2.2.2 Results and Analysis

This section presents the result of quantification represented by Equation (3.55) and its counterpart in simulation for the verification of the theory coupled with analyses. Theoretical curves are all in red while simulated ones in blue.

Figure 3.4 displays the correlator output SNR versus desired signal strength (broadband noise only). According to the interface control document ICD-GPS-705, the received minimum RF signal strength is -157.9 dBW for either the I5 or Q5 channel. Thus, the power of the compound signal, including both in-phase and quadrature, is -154.9 dBW for the line-of-sight case. The signal strength may be degraded significantly (up to 20 dB before complete signal loss) indoor due to the attenuation caused by building material. The simulation using 10,000 1-ms correlations matches the theory quite well, with a RMS error less than 0.03 dB. The SNR in dB increases linearly with the desired signal

power in dBW, because $SNR_{2m-1} = 10\log_{10}[P_m] + 10\log_{10}[T_p / N_0]$. $10\log_{10}[P_m]$ varies from -175 to -155 dBW.

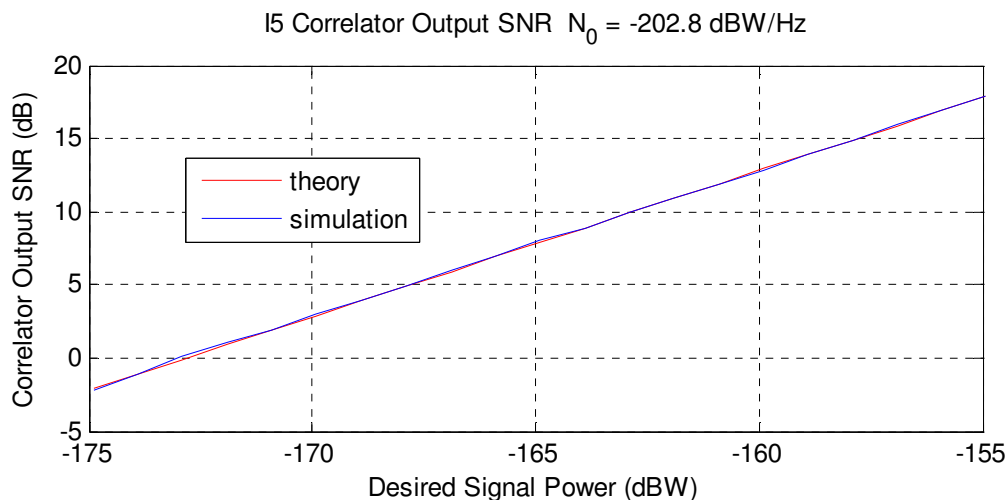


Figure 3.4: The Average SNR of the I5 Correlator Output under Broadband Noise

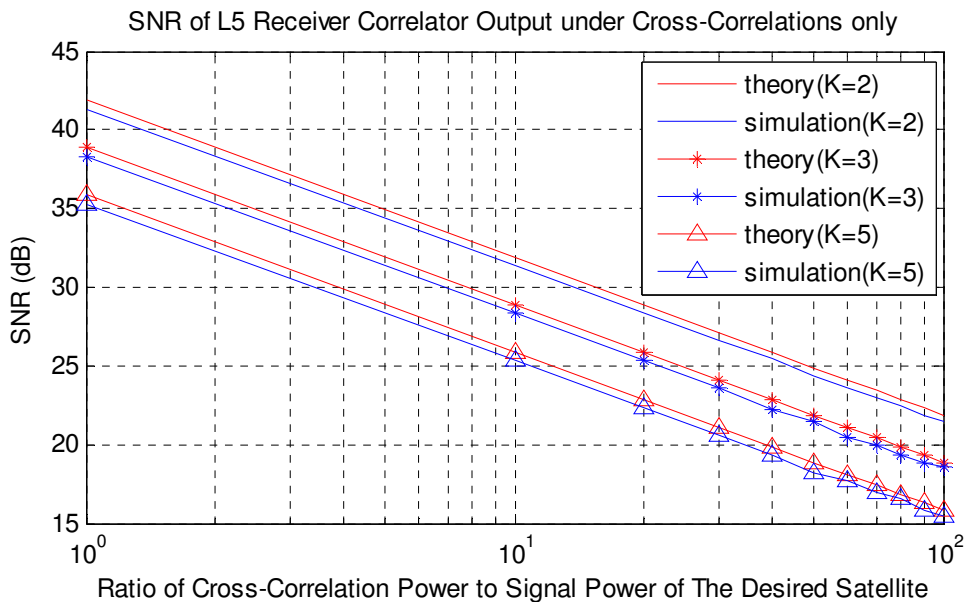


Figure 3.5: SNR of the I5 Correlator Output under Cross-Correlation Only

Figure 3.5 shows the variation of the correlator output SNR in accordance with an increase in the ratio of cross-correlation power to desired signal power. It is assumed that there are K satellites in view; namely, the desired signal is interfered with by signals from

the other $K-1$ satellites. Since broadband noise is not taken into consideration and the interferers are assumed to share the same power level or ratio of cross-correlation power to the signal power of the desired satellite ($\alpha_k = \alpha$), the SNR in dB, equation (3.55) can be simplified to

$$SNR_{2m-1} = 10 \log_{10} \left[\frac{\sum_{\substack{k=1 \\ k \neq m}}^K (r_{2k-1, 2m-1} + r_{2k, 2m-1})}{6N^3} \right]^{-1} - 10 \log_{10} \alpha \quad (3.57)$$

From this equation, it is obvious that the first element is a constant value if the desired satellite and other satellites visible are fixed. The SNR in dB depends linearly on the logarithm of the ratio of cross-correlation power to the signal power of the desired satellite, as shown in Equation (3.57) as well as in Figure 3.5. The RMS difference between simulation and theory is less than 0.5 dB. Both of them display linearity in the semi-logarithmic coordinate system.

Figure 3.6 depicts the combined effect of broadband noise and cross-correlation. The desired signal strength and the noise power are both kept at constant levels in this simulation. The sole parameter changed is the ratio of cross-correlation power to signal power. The simulation differs little from the theory, and they show approximately the same trend, namely that the correlation SNR decreases with strengthened cross-correlation. Their RMS difference is less than 0.2 dB. At the left end, the theory curve tends to approach that of the simulation, since broadband noise dominates the interference budget and the theory for broadband noise only is quite accurate as shown in

Figure 3.4. At the right end, the tendency is the opposite and theoretical curves diverge from the simulated ones. This divergence occurs more quickly and obviously when K rises – the number of cross-correlation sources increases so that the cross-correlation overwhelms the effect of broadband noise. However, this divergence is not unlimited since it is bounded by the error of the theoretical estimation for cross-correlation depicted in Figure 3.5. In brief, the fact that the theoretical estimation of combined interferences (broadband and cross-correlation) fails to maintain a constant accuracy results from the difference in estimation errors for broadband noise and cross-correlation, respectively, since the estimation accuracy degrades when the cross-correlation interference overwhelms the effect of broadband noise.

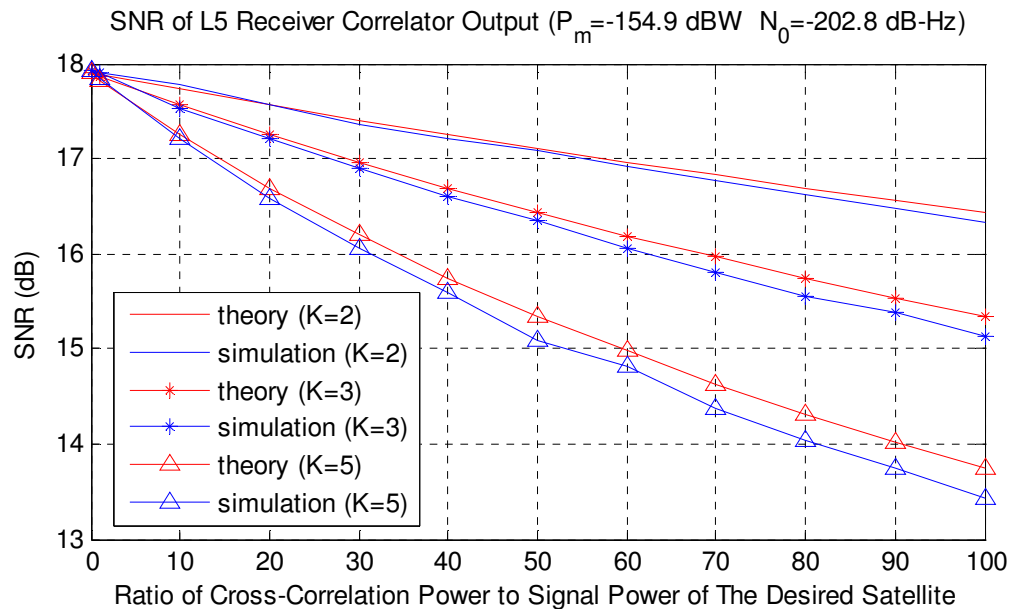


Figure 3.6: IS Correlation SNR under Broadband Noise and Cross-Correlation

The effect of large cross-correlation values arising for certain values of the delay parameters (worst case) could not be demonstrated by the average performance evaluation. Figure 3.7 displays a sample of the partial correlation function defined in

Equation (3.38). In the derivation of the average SNR, a statistical expectation is implemented on the partial correlation function between different signals. The maximum absolute value of this sample is 303; the mean value, 0.25; and the mean absolute, 55. Therefore, the worst case signal environment is more serious, and the performance of the receiver may be much poorer than this evaluation smoothed by averaging. Nevertheless, the average performance is more meaningful than the worst case (Pursley 1977a), since the worst case rarely occurs.

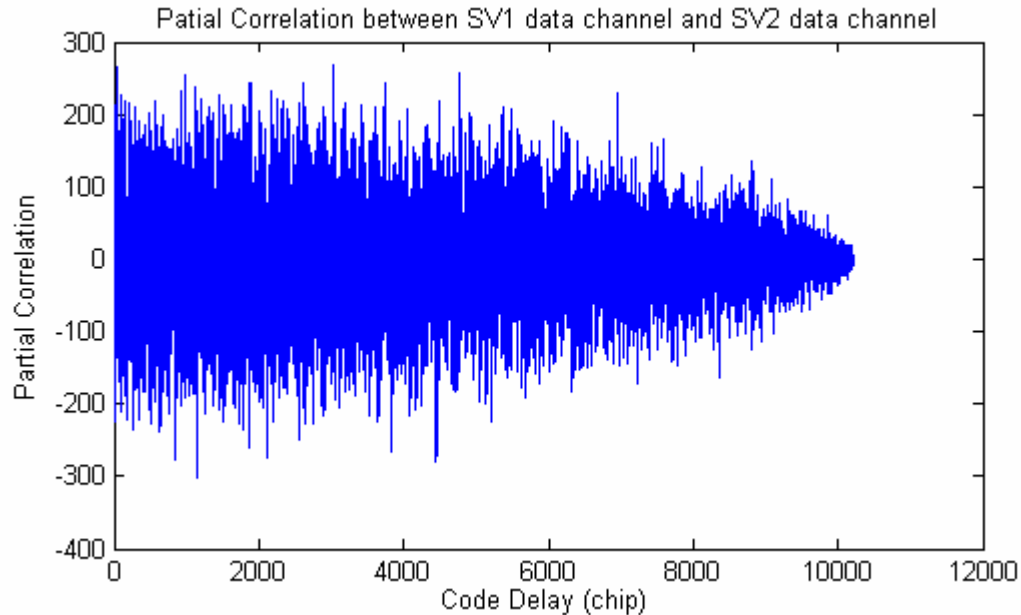


Figure 3.7: Partial Correlation between Satellite 1 Data Channel and Satellite 2 Data Channel

3.3 Conclusions

The interference impact on the L5 correlator provides an indication of the operational performance of GPS signal acquisition, code tracking loop, and phase tracking loop.

The simulation provides a direct and strong support of the validity of the theoretical quantification. As mentioned in the discussion of the results, the RMS error between simulation and theory is less than 0.5 dB. When these two interferences are investigated separately (Figure 3.4 and Figure 3.5), each pair of curves (simulated and theoretical) are parallel, with small gaps. Although they deviate from each other in Figure 3.6, as the combined effect consideration demonstrates, their overall trends are about the same because the RMS error is small. Furthermore, the appearance of the divergence does not indicate that the curves will diverge farther apart, since the cause of this phenomenon will bound the gap at large cross-correlation powers.

Both theory and simulation results display the predominant impact of broadband noise on the average SNR. The SNR value driven by four interference satellites at their full strength (Figure 3.5) is approximately equivalent to that of broadband interference only under normal (line-of-sight) conditions (Figure 3.4). From the perspective of the average effect, L5 cross-correlation is a minor interference on GPS receivers compared with broadband noise. However, the addition of cross-correlation in an indoor signal environment will certainly degrade the reception performance of L5 receivers, where the SNR value is already driven to a critically low level by the strong broadband noise.

The research on the average SNR is assessed on the basis of reception strategies with 1 ms coherent integration. However, the signal structure of L5 allows for long coherent integration schemes that improve the reception performance. For instance, 10 ms

coherent integration is an option for the L5 data channel, and 20 ms or longer coherent integration for the pilot channel. According to Equation (3.56), the average SNR of correlator output is directly proportional to the square root of the coherent integration time. The mitigation of broadband noise through long coherent integration is effective for indoor applications especially if combined with non-coherent integration to reduce the effect of data transition. However, this method is powerless if the signal coexists with strong cross-correlation (Jade Morton *et al* 2003). However, some special methodologies have been successively developed to deal with the near-far problem, for example, the successive interference cancellation (SIC) technique (Madhani *et al* 2003). As this thesis for the L5 signal and the research implemented by (Van Dierendonck *et al* 2002) on L1 demonstrate, broadband noise is the more serious challenge in the front end of GPS receivers than cross-correlation especially for indoor applications. Actually, the effect of cross-correlation in Van Dierendonck's bench testing can only be observed at high C/N_0 , since it is difficult to distinguish this effect from that of noise differences on the two runs. Therefore, the 10 ms coherent integration strategy can significantly improve the reception performance of L5 receivers compared with the 1 ms scheme, in the presence of broadband noise and cross-correlation associated with indoor environments.

Chapter Four: RFI IMPACT ON L5 TRACKING LOOPS

This chapter focuses on the phase tracking error caused by cross-correlation and broadband noise. The purpose is to quantify the RFI effect on the decision-directed PLL. Hence, the phase locked loop models, non-linear and linear, in the absence of and in the presence of noise are described first; then the impact is investigated from two perspectives, tracking RMS error and symbol estimation error rate.

4.1 Theory of PLL Tracking Loops

Phase locked loops (PLL) have been widely used in applications involving automatic control of phase or frequency (for example, communications) since 1932, when it was invented by a scientist in France named H. De Bellescize and termed “La Réception Synchrone” in *Onde Electrique, volume II*. The PLL is non-linear in nature and only a non-linear theory satisfactorily interprets its behaviour. However, the conventional linear theory is able to satisfy the analysis of and the guidance to the PLL applications (Gardner 1979) under certain conditions that will be described in the following section.

4.1.1 Elementary Tracking Theory

The function of tracking loops is to continuously track the variation in the code delay and carrier offset that have been coarsely estimated in the acquisition stage. Then precise pseudorange and carrier phase measurements are obtained upon data demodulation by bit and frame alignment (Bao & Tsui 2000).

The GPS signal is a phase modulated waveform, making it impossible for an operator to track the carrier without removing the spreading code, and vice versa. As a result, there are two phase-locked loops that govern the tracking of GPS signals. One loop is used to track the spreading code, called the delay locked loop (DLL); the other is employed to replicate and trace the carrier frequency. These two loops are closely coupled in their operation because a loss of lock occurring in either loop is bound to result in the loss of tracking by the other. The basic concepts of a phase locked loop (PLL) are described first, since they are applicable to both carrier and code tracking.

The phase-locked loop is composed of three main components (Viterbi 1966): a multiplier, a time-invariant linear filter, and a voltage controlled oscillator (VCO), all visualized in Figure 4.1.

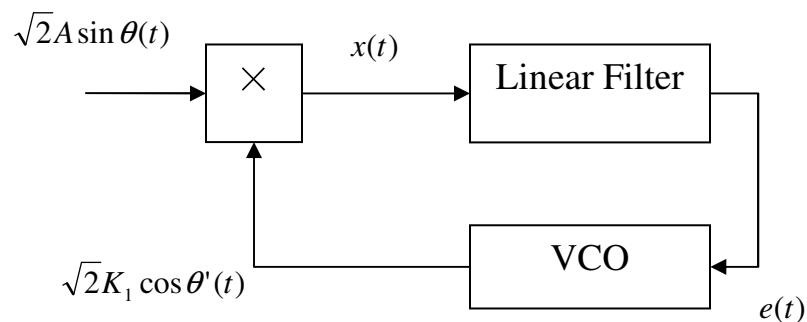


Figure 4.1: Phase-Locked Loop (Viterbi 1966)

The received signal and the VCO output signal are expressed as $\sqrt{2}A \sin \theta(t)$ and $\sqrt{2}K_1 \cos \theta'(t)$ respectively (Viterbi 1966), where K_1 is its root-mean-square amplitude. The oscillator generates a constant-frequency sinusoid if no control signal, $e(t)$, is fed to the input of VCO. This frequency is denoted as ω_0 and termed the quiescent frequency of

the VCO. The relationship between the phase angle of the VCO output and the control signal is

$$\frac{d\theta'(t)}{dt} = \omega_0 + K_2 e(t) \quad (4.1)$$

where K_2 is the proportionality constant.

The output of the multiplier is the product of the received signal and the VCO output signal and is written as

$$x(t) = AK_1 \{\sin[\theta(t) - \theta'(t)] + \sin[\theta(t) + \theta'(t)]\}. \quad (4.2)$$

The product enters the linear time-invariant filter and culminates in the control signal

$$e(t) = e_0(t) + \int_0^t x(t-u)f(u)du = e_0(t) + \int_0^t x(u)f(t-u)du, \quad (4.3)$$

where $e_0(t)$ is the filter response completely dependent on the initial conditions at $t=0$ when the input is applied, and $f(t)$ is the filter's impulse response. The transfer function of the filter is thus determined by the Laplace transform of $f(t)$ (Viterbi 1966) as

$$F(s) = \int_0^{\infty} f(t)e^{-st} dt \quad \text{Re}\{s\} \geq 0. \quad (4.4)$$

Upon the assumption that the filter suppresses high-frequency components of its input and has zero initial conditions, Equation (4.3) can be rewritten as

$$\frac{d\theta'(t)}{dt} = \omega_0 + K_2 \int_0^t f(t-u)AK_1 \sin[\theta(u) - \theta'(u)]du. \quad (4.5)$$

If the phase error is defined as

$$\phi(t) = \theta(t) - \theta'(t), \quad (4.6)$$

it follows that

$$\frac{d\phi(t)}{dt} = \frac{d\theta(t)}{dt} - \omega_0 - AK \int_0^t f(t-u) \sin[\phi(u)] du \quad (4.7)$$

where the loop gain $K = K_1 K_2$.

For the purpose of a simplified presentation of the PLL, the relative input phase and relative VCO phase are defined as

$$\begin{aligned} \theta_1(t) &= \theta(t) - \omega_0 t \\ \theta_2(t) &= \theta'(t) - \omega_0 t \end{aligned} \quad (4.8)$$

The non-linear model of the phase locked loop shown in Figure 4.2 is represented by the following equation (Viterbi 1966):

$$\frac{d\phi(t)}{dt} = \frac{d\theta_1(t)}{dt} - AK \int_0^t f(t-u) \sin[\phi(u)] du, \quad (4.9)$$

where

$$\phi(t) = \theta_1(t) - \theta_2(t). \quad (4.10)$$

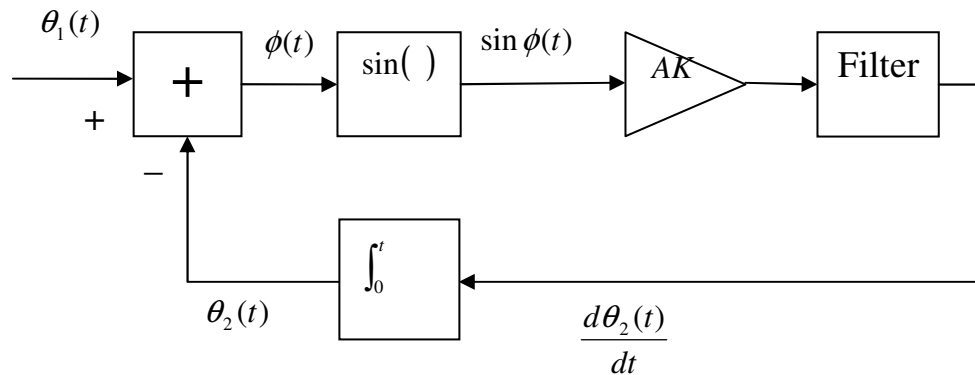


Figure 4.2: Non-linear Model of Phase-Locked Loop (Viterbi 1966)

The difference between Figure 4.2 and Figure 4.1 is that in Figure 4.2, a subtractor and a sinusoidal non-linearity take the place of the multiplier in Figure 4.1 and an integrator is substituted for the VCO. The phase of the VCO output is proportional not only to the loop gain but also to the amplitude of the received signal. The PLL is considered to be in phase lock when the phase error is zero. Practically, phase lock indicates that the phase error approaches zero or values considered negligible (compared with 1 rad). Under this circumstance, the sinusoidal nonlinearity of Figure 4.2 may be disregarded with the approximation

$$\sin \phi \approx \phi, \quad (4.11)$$

which introduces, at most, a 5% relative error for a ϕ value less than 30° . Henceforth, the non-linear model is reduced to a linear model represented by the following differential equation:

$$\frac{d\phi(t)}{dt} = \frac{d\theta_1(t)}{dt} - AK \int_0^t f(t-u)\phi(u)du. \quad (4.12)$$

Taking the Laplace transform of both sides of the equation, it follows that

$$s\tilde{\phi}(s) = s\tilde{\theta}_1(s) - AK\tilde{\phi}(s) \quad (4.13)$$

where

$$\begin{aligned} \tilde{\theta}_1(s) &= \int_0^\infty \theta_1(t)e^{-st} du & \operatorname{Re}\{s\} \geq 0 \\ \tilde{\phi}(s) &= \int_0^\infty \phi(t)e^{-st} du & \operatorname{Re}\{s\} \geq 0 \end{aligned} \quad (4.14)$$

Figure 4.3 illustrates the time domain configuration, and Figure 4.4 the S domain configuration. The following equations, which can be inferred from Figure 4.4, mathematically express the framework and behaviour of the PLL (Viterbi 1966):

$$\begin{aligned}\tilde{\phi}(s) &= \tilde{\theta}_1(s) - \tilde{\theta}_2(s) = \frac{1}{1 + AKF(s)/s} \tilde{\theta}_1(s) \\ \tilde{\theta}_1(s) &= \tilde{\theta}_2(s) \left(1 + \frac{s}{AKF(s)} \right).\end{aligned}\tag{4.15}$$

In terms of the definition of the closed-loop transfer function,

$$H(s) = \frac{\tilde{\theta}_2(s)}{\tilde{\theta}_1(s)} = \frac{AKF(s)/s}{1 + AKF(s)/s}\tag{4.16}$$

Equation (4.15) can be expressed as

$$\begin{aligned}\tilde{\phi}(s) &= [1 - H(s)]\tilde{\theta}_1(s) \\ \tilde{\theta}_1(s) &= H(s)\tilde{\theta}_2(s).\end{aligned}\tag{4.17}$$

The expression for the error transfer function, $H_e(s)$, is:

$$H_e(s) = \frac{\tilde{\theta}_1(s) - \tilde{\theta}_2(s)}{\tilde{\theta}_1(s)} = 1 - H(s) = \frac{1}{1 + AKF(s)/s}.\tag{4.18}$$

The equivalent noise bandwidth, B_n , is defined as:

$$B_n = \int_0^{\infty} |H(j\omega)|^2 df\tag{4.19}$$

where ω is the angular frequency.

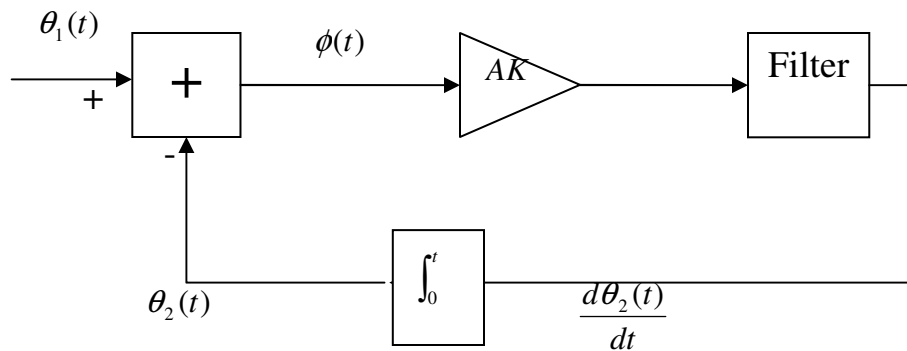


Figure 4.3: Linear Model of Phase-Locked Loop (Viterbi 1966)

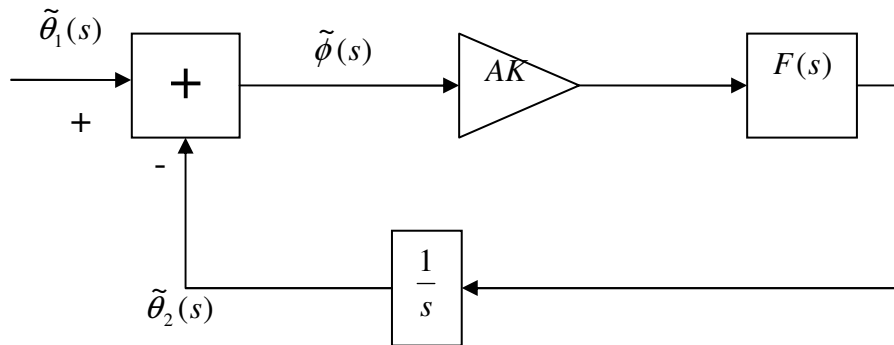


Figure 4.4: Linear Model (S Domain) of Phase-Locked Loop (Viterbi 1966)

4.1.2 The Effect of Additive Noise and Other Disturbances

Described as a zero-mean wideband Gaussian process with almost flat spectral density over the frequency range of the receiver, thermal noise acts as the most important and unavoidable disturbance in most radio communication systems. As described in Chapter 2, thermal noise is modeled by broadband random noise as:

$$n(t) = \sqrt{2}[n_1(t) \sin \omega_0 t + n_2(t) \cos \omega_0 t] \quad (4.20)$$

where $n_1(t)$ and $n_2(t)$ are sample functions of the stationary zero-mean Gaussian processes, whose spectral densities $S_1(\omega)$ and $S_2(\omega)$ are even functions with magnitude $N_0/2$ over a range of frequency covering the bandwidth of receivers.

In the presence of additive white Gaussian noise (AWGN), the received signal is

$$\sqrt{2}A \sin \theta(t) + n(t) = \sqrt{2}[A \sin[\omega_0 t + \theta_1(t)] + n_1(t) \sin \omega_0 t + n_2(t) \cos \omega_0 t]. \quad (4.21)$$

Although the VCO output assumes the same form as that in section 4.1.1, namely

$$\sqrt{2}K_1 \cos \theta'(t) = \sqrt{2}K_1 \cos[\omega_0 t + \theta_2(t)], \quad (4.22)$$

the phase $\theta'(t)$ is no longer uniquely determined by the signal modulation, but is influenced by the noise as well. The multiplier output is accordingly changed to

$$\begin{aligned} x(t) = & AK_1 \sin[\theta_1(t) - \theta_2(t)] - K_1 n_1(t) \sin \theta_2(t) + K_1 n_2(t) \cos \theta_2(t) \\ & + AK_1 \sin[2\omega_0 t + \theta_1(t) + \theta_2(t)] + K_1 n_1(t) \sin[2\omega_0 t + \theta_2(t)] \\ & + K_1 n_2(t) \cos[2\omega_0 t + \theta_2(t)] \end{aligned} \quad (4.23)$$

All high frequency terms centered on the frequency $2\omega_0$ may be neglected due to the limited passband of the filter that follows the multiplier. Thus, the input signal of the VCO driven by both the desired signal and thermal noise is

$$e(t) = K_1 \int_0^t [A \sin \phi(u) - n_1(u) \sin \theta_2(u) + n_2 \cos \theta_2(u)] f(t-u) du \quad (4.24)$$

where

$$\phi(t) = \theta(t) - \theta'(t) = \theta_1(t) - \theta_2(t). \quad (4.25)$$

Then, the model of the phase locked loop with additive noise illustrated in Figure 4.5 is represented by the differential equation

$$\frac{d\phi(t)}{dt} = \frac{d\theta_1(t)}{dt} - K \int_0^t [A \sin \phi(u) + n'(u)] f(t-u) \sin du, \quad (4.26)$$

where

$$\begin{aligned} n'(t) &= -n_1(t) \sin \theta_2(t) + n_2(t) \cos \theta_2(t) \\ K &= K_1 K_2 \end{aligned} \quad (4.27)$$

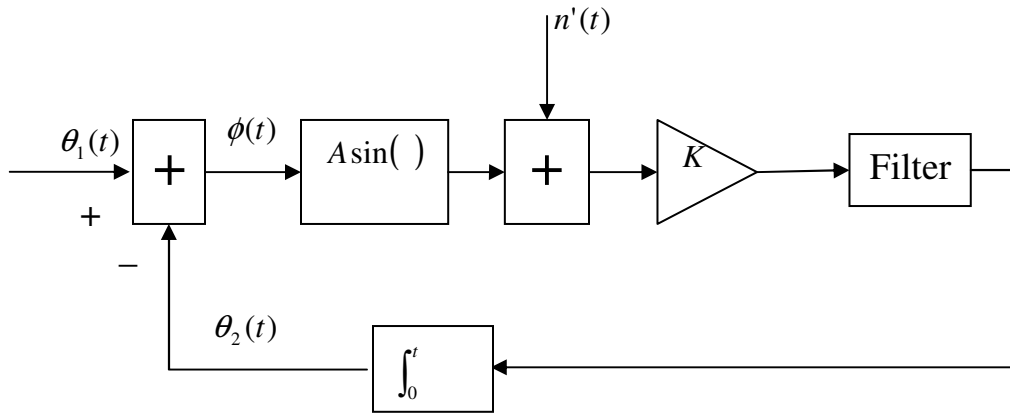


Figure 4.5: Non-linear Model of a Phase-Locked Loop with Additive Noise

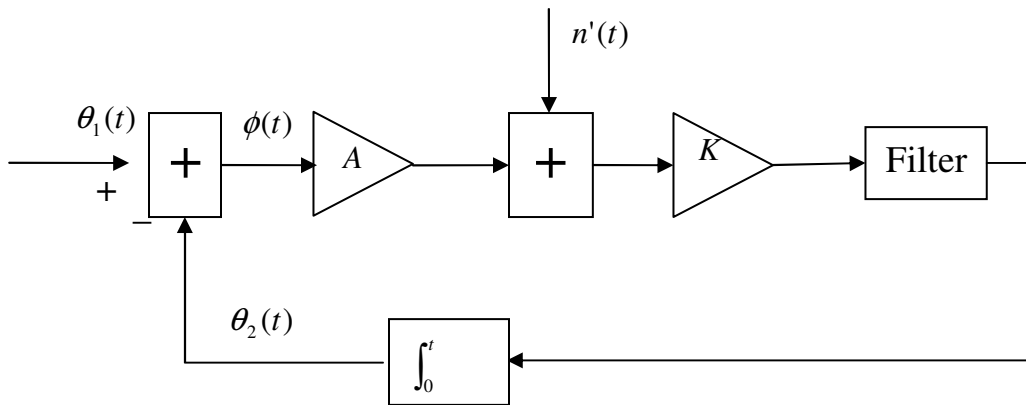


Figure 4.6: Linear Model of a Phase-Locked Loop with Additive Noise

When the phase error $\phi \ll 1$ rad, the approximation $\sin \phi \approx \phi$ produces the linear model of PLL with additive noise in Figure 4.6. The spectral density of the phase error in response to white noise is

$$S_\phi(\omega) = \left| \frac{KF(\omega)/i\omega}{1 + AKF(\omega)/i\omega} \right|^2 S_n(\omega) = \frac{N_0}{2A^2} |H(i\omega)|^2 \quad (4.28)$$

where the white noise is assumed to have a one-sided spectral density N_0 and consequently $S_n(\omega) = N_0/2$.

Therefore, the variance of the phase error introduced by the white noise is

$$\sigma_\phi^2 = \frac{N_0}{2A^2} \int_{-\infty}^{\infty} |H(i\omega)|^2 \frac{d\omega}{2\pi} = \frac{N_0}{A^2} \int_0^{\infty} |H(i\omega)|^2 \frac{d\omega}{2\pi} = \frac{N_0 B_n}{A^2}. \quad (4.29)$$

4.2 L5 Decision-Directed PLL Tracking Error in the Presence of Broadband Noise and Cross-Correlation

4.2.1 Theoretical Investigation

In general, PLL performance is degraded due to a variety of noise sources such as additive white Gaussian noise (AWGN) which is the model used for broadband random noise, phase noise, and interference originating from other GPS satellite signals or channels (cross-correlation). There are several loop types that can be used to track the carrier phase of the incoming signal. Normally, Costas loops are the only option for the data channel because a pure PLL can not tolerate data transitions. The distinguishing features of a Costas loop are its discriminator and phase adjusting ability. This is

necessary to avoid integrating across the data transition boundary. This research investigates a decision-directed PLL whose discriminator is described in the following section, by following the research of Huang *et al* (1998) on BPSK signals.

The locally generated code sequence of the expected signal (data component of satellite m) is expressed as (Huang *et al* 1998):

$$l_{2m-1,\alpha}(t) = a_{2m-1}(t - \tau_m) \cos[\omega_0 t + \phi(t) - p_\alpha \frac{\pi}{2}], \quad \alpha = I, Q \quad (4.30)$$

where

- $p_I (=0)$ and $p_Q (=1)$ denote the in-phase and quadrature-phase terms within the receiver digital channels;
- $\phi(t)$ is the carrier phase of the local oscillator;
- $a_{2m-1}(t - \tau_m)$ is the local spreading code signal with the estimated signal code delay.

The received IF signal after correlation over $[0, NT_C]$ and sampled at $t = T_p = NT_C$ can be represented by:

$$\begin{aligned} Z_{2m-1,\alpha} = & \sqrt{P_m/4} \{ b_{2m-1,0} T_p \cos[\theta_m(t) + p_\alpha \frac{\pi}{2}] + \sum_{\substack{k=1 \\ k \neq m}}^K \sqrt{\alpha_k} Y_{2k-1,2m-1}(\tau_k, 0) \cos[\theta_k(t) + p_\alpha \frac{\pi}{2}] \\ & + \sum_{\substack{k=1 \\ k \neq m}}^K \sqrt{\alpha_k} Y_{2k,2m-1}(\tau_k, 0) \sin[\theta_k(t) + p_\alpha \frac{\pi}{2}] + \int_0^{T_p} n(t) l_{2m-1,\alpha}(t) dt \end{aligned} \quad (4.31)$$

where $\theta_k(t)$ is the carrier phase difference between the phase of incoming satellite k and the local clock. θ_k is randomly and evenly distributed over the interval $[0, 2\pi]$, if $(k \neq m)$, and $\tau_k (k \neq m)$ conforms to an even distribution over $[0, T_p]$. The description of the signal and sampling is similar to that of Equations (3.30) and (3.34) in the section on SNR analysis. The term from the dataless component of satellite k in Equation (4.30) is neglected because of the preferable suppression of cross-correlation between two channels of the same satellite signal at the same signal power level.

Under the assumption $\tau_m = 0$, the resulting cross-correlations between the local signal and the signal from other satellites, $Y_{2k-1, 2m-1}$ in Equation (4.30), are integrated and sampled (Huang *et al* 1998) as:

$$\begin{aligned}
Y_{2k-1, 2m-1}(\tau_k, u) &= \int_{|u|}^{T_p+|u|} d_{2k-1}(t-\tau_k)NH_{10}(t-\tau_k)a_{2k-1}(t-\tau_k)a_{2m-1}(t)dt \\
&= B(|u|, \tau_k) \left[\int_{|u|}^{\tau_k} d_{2k-1}(t-\tau_k)NH_{10}(t-\tau_k)a_{2k-1}(t-\tau_k)a_{2m-1}(t)dt + \right. \\
&\quad \left. \int_{\tau_k}^{T_p+|u|} d_{2k-1}(t-\tau_k)NH_{10}(t-\tau_k)a_{2k-1}(t-\tau_k)a_{2m-1}(t)dt \right] + \\
&\quad B(\tau_k, |u|) \left[\int_{|u|}^{T_p+\tau_k} d_{2k-1}(t-\tau_k)NH_{10}(t-\tau_k)a_{2k-1}(t-\tau_k)a_{2m-1}(t)dt + \right. \\
&\quad \left. \int_{T_p+\tau_k}^{T_p+|u|} d_{2k-1}(t-\tau_k)NH_{10}(t-\tau_k)a_{2k-1}(t-\tau_k)a_{2m-1}(t)dt \right] \\
&= B(|u|, \tau_k) [d_{k,n}NH_{10,-1}Q_{2k-1, 2m-1}(|u|, \tau_k, \tau_k) + \\
&\quad d_{k,n'}NH_{10,0}Q_{2k-1, 2m-1}(\tau_k, T_p+|u|, \tau_k)] \\
&\quad + B(\tau_k, |u|) [d_{k,n'}NH_{10,0}Q_{2k-1, 2m-1}(|u|, T_p+\tau_k, \tau_k) \\
&\quad + d_{k,n''}NH_{10,1}Q_{2k-1, 2m-1}(T_p+\tau_k, T_p+|u|, \tau_k)] \\
&= B(|u|, \tau_k) [d_{k,n}NH_{10,-1}Q_{2k-1, 2m-1}(|u|, \tau_k, \tau_k) + d_{k,n'}NH_{10,0}Q_{2k-1, 2m-1}(\tau_k, T_p+|u|, \tau_k)] \\
&\quad + B(\tau_k, |u|) [d_{k,n'}NH_{10,0}Q_{2k-1, 2m-1}(|u|, T_p+\tau_k, \tau_k) + d_{k,n''}NH_{10,1}Q_{2k-1, 2m-1}(\tau_k, |u|, \tau_k)]
\end{aligned} \tag{4.32}$$

where $n \leq n' \leq n''$, $B(\alpha, \beta) = 1$ for $0 \leq \alpha \leq \beta$ and $B(\alpha, \beta) = 0$ otherwise. As defined in (Huang *et al* 1998),

$$Q_{n,j}(\alpha, \beta, \gamma) = \int_{\alpha}^{\beta} a_n(t - \gamma) a_j(t) dt. \quad (4.33)$$

In the same way,

$$\begin{aligned} Y_{2k,2m-1}(\tau_k, u) &= \int_{|u|}^{T_p+|u|} b_{2k}(t - \tau_k) a_{2k-1}(t - \tau_k) a_{2m-1}(t) dt \\ &= B(|u|, \tau_k) [NH_{20,-1} Q_{2k,2m-1}(|u|, \tau_k, \tau_k) + NH_{20,0} Q_{2k,2m-1}(\tau_k, T_p + |u|, \tau_k)] + \\ &\quad B(\tau_k, |u|) [NH_{20,0} Q_{2k,2m-1}(|u|, T_p + \tau_k, \tau_k) + NH_{20,1} Q_{2k,2m-1}(\tau_k, |u|, \tau_k)] \end{aligned} \quad (4.34)$$

At $u = 0$, the cross-correlation terms become:

$$\begin{aligned} Y_{2k-1,2m-1}(\tau_k, 0) &= B(0, \tau_k) [d_{k,n} NH_{10,-1} Q_{2k-1,2m-1}(0, \tau_k, \tau_k) + d_{k,n'} NH_{10,0} Q_{2k-1,2m-1}(\tau_k, T_p, \tau_k)] \\ &\quad + B(\tau_k, 0) [d_{k,n''} NH_{10,0} Q_{2k-1,2m-1}(0, T_p + \tau_k, \tau_k) + d_{k,n} NH_{10,1} Q_{2k-1,2m-1}(\tau_k, 0, \tau_k)] \\ &= d_{10,n} NH_{10,-1} R_{2k-1,2m-1}(\tau_k) + d_{10,n'} NH_{10,0} \hat{R}_{2k-1,2m-1}(\tau_k) \end{aligned} \quad (4.35)$$

Then,

$$Y_{2k,2m-1}(\tau_k, 0) = NH_{20,-1} R_{2k,2m-1}(\tau_k) + NH_{20,0} \hat{R}_{2k,2m-1}(\tau_k) \quad (4.36)$$

where $R_{j,i}(\tau_k)$ and $\hat{R}_{j,i}(\tau_k)$ are defined by Equations (3.38) and (3.39) as the continuous-time partial cross-correlation functions. The decision-directed PLL discriminator (Huang *et al* 1998) output is:

$$\Psi(\theta) = \hat{b}_{2m-1,0} Z_{2m-1,Q} = \text{sign}(Z_{2m-1,I}) Z_{2m-1,Q} \quad (4.37)$$

where $\hat{b}_{2m-1,0}$ or $\text{sign}(Z_{2m-1,l})$ is an estimate of the information data on the data channel of satellite m . By substituting Equation (4.31) into (4.37), the PLL discriminator becomes

$$\Psi(\theta) = \sqrt{\frac{P_m}{4}} \hat{b}_{2m-1,0} b_{2m-1} T_p \sin \theta_m + \Lambda_C(t) + \Lambda_G(t) \quad (4.38)$$

where $\Lambda_C(t)$ and $\Lambda_G(t)$ correspond to cross-correlation interference and AWGN, respectively. The cross-correlation and AWGN are expressed as:

$$\Lambda_C(t) = \sqrt{\frac{P_m}{4}} \hat{b}_{2m-1,0} \left[\sum_{\substack{k=1 \\ k \neq m}}^K \sqrt{\alpha_k} Y_{2k-1,2m-1}(\tau_k, 0) \sin \theta_k + \sum_{\substack{k=1 \\ k \neq m}}^K \sqrt{\alpha_k} Y_{2k,2m-1}(\tau_k, 0) \cos \theta_k \right] \quad (4.39)$$

$$\Lambda_G(t) = \hat{b}_{2m-1,0} \int_0^{T_p} l_{2m-1,\alpha}(\tau) n(\tau) dt. \quad (4.40)$$

The autocorrelation function of the combination of these two types of interference is:

$$\begin{aligned} R_{C+G}(u) &= E\{[\Lambda_C(t) + \Lambda_G(t)][\Lambda_C(t+u) + \Lambda_G(t+u)]\} \\ &= E[\Lambda_C(t)\Lambda_C(t+u)] + E[\Lambda_G(t)\Lambda_G(t+u)] \\ &= R_C(u) + R_G(u) \end{aligned} \quad (4.41)$$

since $\Lambda_C(t)$ and $\Lambda_G(t)$ are independent and have zero mean.

As these two noise components are white over the bandwidth of the loop filter, their autocorrelation functions are zero at $|u| \geq NT_C$. Their one-sided PSD can be derived from

(Huang *et al* 1998):

$$\mu_i = 2 \int_{-NT_C}^{NT_C} R_i(u) du \quad (i = C, G). \quad (4.42)$$

The autocorrelation of $\Lambda_G(t)$ is expressed as:

$$\begin{aligned}
R_G(u) &= E[\Lambda_G(t)\Lambda_G(t+u)] \\
&= E\left[\int_0^{NT_C} a_{2m-1}(s)\cos(\omega_0s+\phi_m)n(s)ds\int_{|u|}^{NT_C+|u|} a_{2m-1}(t)\cos(\omega_0t+\phi_m)n(t)dt\right] \\
&= \int_0^{NT_C} \int_{|u|}^{NT_C+|u|} a_{2m-1}(s)\cos(\omega_0s+\phi_m)a_{2m-1}(t)\cos(\omega_0t+\phi_m)\frac{N_0}{2}\delta(s-t)dtds \\
&= \frac{N_0}{2} \int_{|u|}^{NT_C} \cos^2(\omega_0t+\phi_m)dt = \frac{N_0}{4} \int_{|u|}^{NT_C} 1+\cos(2\omega_0t+2\phi_m)dt \\
&= \frac{N_0}{4} \left\{NT_C-|u|+\frac{1}{2\omega_0}[\sin(2\omega_0NT_C+2\phi_m)-\sin(2\omega_0|u|+2\phi_m)]\right\} \\
&\cong \frac{N_0}{4}(NT_C-|u|)
\end{aligned} \tag{4.43}$$

since $\omega_0NT_C \gg 1$.

Therefore, the PSD of the AWGN is:

$$\mu_G = 2\int_{-NT_C}^{NT_C} R_G(u)du = 2\int_{-NT_C}^{NT_C} \frac{N_0}{4}(NT_C-|u|)du = \frac{N_0}{2}(NT_C)^2. \tag{4.44}$$

The cross-correlation function, $R_C(u)$, is expressed by

$$\begin{aligned}
R_C(u) = E[\Lambda_C(t)\Lambda_C(t+u)] &= \frac{P_m}{8} \left[\sum_{\substack{k=1 \\ k \neq m}}^K \overline{\alpha_k Y_{2k-1,2m-1}(\tau_k,0)Y_{2k-1,2m-1}(\tau_k,u)} + \right. \\
&\quad \left. \sum_{k=1}^K \overline{\alpha_k Y_{2k,2m-1}(\tau_k,0)Y_{2k,2m-1}(\tau_k,u)} \right]
\end{aligned} \tag{4.45}$$

Due to a large number of random variables, the derivation is simplified by taking the statistical average of one variable at a time. The bar denotes the statistical expectation of the term underneath it. As before, the expectation values

$$\begin{aligned}
E(\sin \theta_k \cos \theta_k) &= E(\sin 2\theta_k)/2 = 0 & E(\sin \theta_k) &= 0 & E(\cos \theta_k) &= 0 \\
E(\sin^2 \theta_k) &= E(\cos^2 \theta_k) &= \frac{1}{2} & & &
\end{aligned} \tag{4.46}$$

help to reduce terms between different satellites and different channels (in-phase and quadrature)

$$E(b_{2k-1,i} b_{2k-1,j}) = E(d_{k,i}) E(d_{k,j}) E(NH_{10,i} NH_{10,j}) = 0 \quad (i \neq j) \tag{4.47}$$

which allows for further simplification of the autocorrelation function. The first summation term of Equation (4.45), representing the data channel, can then be expanded as follows:

$$\begin{aligned}
& \overline{Y_{2k-1,2m-1}(\tau_k, 0)Y_{2k-1,2m-1}(\tau_k, u)} \\
&= \overline{[d_{k,n}NH_{10,-1}R_{2k-1,2m-1}(\tau_k) + d_{k,n}NH_{10,0}\hat{R}_{2k-1,2m-1}(\tau_k)]\{B(|u|, \tau_k)[d_{k,n}NH_{10,-1} \times} \\
&\quad \overline{Q_{2k-1,2m-1}(|u|, \tau_k, \tau_k) + d_{k,n}NH_{10,0}Q_{2k-1,2m-1}(\tau_k, |u| + T_P, \tau_k)}\} + B(\tau_k, |u|) \times} \\
&\quad \overline{[d_{k,n}NH_{10,0}Q_{2k-1,2m-1}(|u|, \tau_k + T_P, \tau_k) + d_{k,n}NH_{10,1}Q_{2k-1,2m-1}(\tau_k, |u|, \tau_k)]\}} \\
&= B(|u|, \tau_k)R_{2k-1,2m-1}(\tau_k)Q_{2k-1,2m-1}(|u|, \tau_k, \tau_k) + \\
&\quad B(|u|, \tau_k)\hat{R}_{2k-1,2m-1}(\tau_k)Q_{2k-1,2m-1}(\tau_k, |u| + T_P, \tau_k) + \\
&\quad B(\tau_k, |u|)\hat{R}_{2k-1,2m-1}(\tau_k)Q_{2k-1,2m-1}(|u|, \tau_k + T_P, \tau_k) \\
&= B(|u|, \tau_k)R_{2k-1,2m-1}(\tau_k)Q_{2k-1,2m-1}(|u|, \tau_k, \tau_k) + \\
&\quad \hat{R}_{2k-1,2m-1}(\tau_k)B(|u|, \tau_k)[Q_{2k-1,2m-1}(0, T_P, \tau_k) - Q_{2k-1,2m-1}(|u|, \tau_k, \tau_k)] + \\
&\quad \hat{R}_{2k-1,2m-1}(\tau_k)B(\tau_k, |u|)[Q_{2k-1,2m-1}(0, T_P, \tau_k) - Q_{2k-1,2m-1}(\tau_k, |u|, \tau_k)] \\
&= B(|u|, \tau_k)R_{2k-1,2m-1}(\tau_k)Q_{2k-1,2m-1}(|u|, \tau_k, \tau_k) + \\
&\quad \hat{R}_{2k-1,2m-1}(\tau_k)[Q_{2k-1,2m-1}(0, T_P, \tau_k) - Q_{2k-1,2m-1}(\min\{|u|, \tau_k\}, \max\{|u|, \tau_k\}, \tau_k)] \\
&= B(|u|, \tau_k)R_{2k-1,2m-1}(\tau_k)Q_{2k-1,2m-1}(|u|, \tau_k, \tau_k) + \hat{R}_{2k-1,2m-1}(\tau_k)[R_{2k-1,2m-1}(\tau_k) \\
&\quad + \hat{R}_{2k-1,2m-1}(\tau_k) - Q_{2k-1,2m-1}(\min\{|u|, \tau_k\}, \max\{|u|, \tau_k\}, \tau_k)] \\
&= \hat{R}_{2k-1,2m-1}^2(\tau_k) + \hat{R}_{2k-1,2m-1}(\tau_k)R_{2k-1,2m-1}(\tau_k) + [B(|u|, \tau_k)R_{2k-1,2m-1}(\tau_k) \\
&\quad - \hat{R}_{2k-1,2m-1}(\tau_k)]Q_{2k-1,2m-1}(\min\{|u|, \tau_k\}, \max\{|u|, \tau_k\}, \tau_k)]
\end{aligned} \tag{4.48}$$

where τ_k is a random variable.

By the same token, the representation for the pilot channel is:

$$\begin{aligned}
& \overline{Y_{2k,2m-1}(\tau_k, 0)Y_{2k,2m-1}(\tau_k, u)} \\
&= B(|u|, \tau_k)R_{2k,2m-1}(\tau_k)Q_{2k-1,2m-1}(|u|, \tau_k, \tau_k) + \\
&\quad B(|u|, \tau_k)\hat{R}_{2k,2m-1}(\tau_k)Q_{2k-1,2m-1}(\tau_k, |u| + T_P, \tau_k) + \\
&\quad B(\tau_k, |u|)\hat{R}_{2k,2m-1}(\tau_k)Q_{2k-1,2m-1}(|u|, \tau_k + T_P, \tau_k)
\end{aligned} \tag{4.49}$$

since

$$E(b_{2k,i}b_{2k,j}) = E(NH_{20,i}NH_{20,j}) = 0 \quad 0 < |i - j| \leq 2. \tag{4.50}$$

Therefore the autocorrelation for the pilot channel is:

$$\begin{aligned} & \overline{Y_{2k,2m-1}(\boldsymbol{\tau}_k, 0)Y_{2k,2m-1}(\boldsymbol{\tau}_k, u)} \\ &= \hat{R}_{2k,2m-1}^2(\boldsymbol{\tau}_k) + \hat{R}_{2k,2m-1}(\boldsymbol{\tau}_k)R_{2k,2m-1}(\boldsymbol{\tau}_k) + [B(|u|, \boldsymbol{\tau}_k)R_{2k,2m-1}(\boldsymbol{\tau}_k) - \hat{R}_{2k,2m-1}(\boldsymbol{\tau}_k)]. \quad (4.51) \\ & \quad \times Q_{2k,2m-1}(\min\{|u|, \boldsymbol{\tau}_k\}, \max\{|u|, \boldsymbol{\tau}_k\}, \boldsymbol{\tau}_k)]. \end{aligned}$$

Finally, using Equations (4.47) and (4.50) cross-correlation function can be simplified as:

$$\begin{aligned} R_C(u) = E[\Lambda_C(t)\Lambda_C(t+u)] &= \frac{P_m}{8} \left\{ \sum_{\substack{k=1 \\ k \neq m}}^K \alpha_k E[\hat{R}_{2k-1,2m-1}^2(\boldsymbol{\tau}_k) + \hat{R}_{2k-1,2m-1}(\boldsymbol{\tau}_k)R_{2k-1,2m-1}(\boldsymbol{\tau}_k) + \right. \\ & (B(\boldsymbol{\tau}_k, |u|)R_{2k-1,2m-1}(\boldsymbol{\tau}_k) - \hat{R}_{2k-1,2m-1}(\boldsymbol{\tau}_k))Q_{2k-1,2m-1}(\min\{|u|, \boldsymbol{\tau}_k\}, \min\{|u|, \boldsymbol{\tau}_k\}, \boldsymbol{\tau}_k)] + \quad (4.52) \\ & \left. \sum_{\substack{k=1 \\ k \neq m}}^K \alpha_k E[\hat{R}_{2k,2m-1}^2(\boldsymbol{\tau}_k) + \hat{R}_{2k,2m-1}(\boldsymbol{\tau}_k)R_{2k,2m-1}(\boldsymbol{\tau}_k) + \right. \\ & \left. (B(\boldsymbol{\tau}_k, |u|)R_{2k,2m-1}(\boldsymbol{\tau}_k) - \hat{R}_{2k,2m-1}(\boldsymbol{\tau}_k))Q_{2k,2m-1}(\min\{|u|, \boldsymbol{\tau}_k\}, \min\{|u|, \boldsymbol{\tau}_k\}, \boldsymbol{\tau}_k)] \right\}. \end{aligned}$$

Next, since $\boldsymbol{\tau}_k$ is a random variable, the autocorrelation function is finally determined by the statistical average of $\boldsymbol{\tau}_k$. As shown in (Huang *et al* 1998), the one-sided PSD of the cross-correlation is expressed as:

$$\mu_C = 2 \int_{-T_p}^{T_p} R_S(u) du = \frac{P_m T_C^3}{8N} I_K \quad (4.53)$$

where (Huang *et al* 1998):

$$\begin{aligned}
I_K = & \frac{1}{3} \sum_{k=1}^K \alpha_k \sum_{\substack{l=0 \\ k \neq m}}^{N-1} \{ \Psi[2C_{2k-1,2m-1}(l), NC_{2k-1,2m-1}(l-N) - D_{2k-1,2m-1}(l)] + \\
& \Psi[2C_{2k-1,2m-1}(l), D_{2k-1,2m-1}(l)] + \Psi[2C_{2k-1,2m-1}(l-N), D_{2k-1,2m-1}(l-N)] + \\
& \Theta[C_{2k-1,2m-1}(l), C_{2k-1,2m-1}(l)] + \Theta[C_{2k-1,2m-1}(l-N), C_{2k-1,2m-1}(l-N)] - \\
& \Theta[C_{2k-1,2m-1}(l), C_{2k-1,2m-1}(l-N)] \} + \\
& \frac{1}{3} \sum_{k=1}^K \alpha_k \sum_{\substack{l=0 \\ k \neq m}}^{N-1} \{ \Psi[2C_{2k,2m-1}(l), NC_{2k,2m-1}(l-N) - D_{2k,2m-1}(l)] + \\
& \Psi[2C_{2k,2m-1}(l), D_{2k,2m-1}(l)] + \Psi[2C_{2k,2m-1}(l-N), D_{2k,2m-1}(l-N)] + \\
& \Theta[C_{2k,2m-1}(l), C_{2k,2m-1}(l)] + \Theta[C_{2k,2m-1}(l-N), C_{2k,2m-1}(l-N)] - \\
& \Theta[C_{2k,2m-1}(l), C_{2k,2m-1}(l-N)] \}
\end{aligned} \tag{4.54}$$

with

$$\Psi[A(l), B(l)] = A(l)B(l) + \frac{1}{2}A(l)B(l+1) + \frac{1}{2}A(l+1)B(l) + A(l+1)B(l+1) \tag{4.55}$$

$$\Theta[A(l), B(l)] = \frac{4}{5}A(l)B(l) + \frac{3}{4}A(l+1)B(l+1) + \frac{3}{4}A(l+1)B(l) + \frac{1}{4}A(l)B(l+1) \tag{4.56}$$

$$D_{k,i}(l) = \begin{cases} \sum_{j=0}^{N-1-l} (j+l)a_{k,j}a_{i,j+l}, & 0 \leq l \leq N-1 \\ \sum_{j=0}^{N-1+l} ja_{k,j-l}a_{i,j}, & 1-N \leq l \leq 0 \\ 0, & |l| \geq N \end{cases} \tag{4.57}$$

Based on the above equations, the phase error induced by white noise (cross-correlation and broadband noise) is expressed as:

$$\mu_\phi = \frac{(\mu_G + \mu_C) |H(j2\pi f)|^2}{T_P^2 P_m / 4} = \left(\frac{T_C}{2N^3} I_K + \frac{2N_0}{P_m} \right) |H(j2\pi f)|^2. \tag{4.58}$$

The corresponding PLL tracking error variance is:

$$\begin{aligned}
 \sigma_{\phi}^2 &= \int_0^{\infty} \mu_{\phi} df \\
 &= \left(\frac{T_C}{2N^3} I_K + \frac{2N_0}{P_m} \right) \int_0^{\infty} |H(j2\pi f)|^2 df \\
 &= \left(\frac{T_C}{2N^3} I_K + \frac{2N_0}{P_m} \right) B_n
 \end{aligned} \tag{4.59}$$

where

- T_C is the L5 PRN chip width;
- N denotes the period of the L5 PRN code in chips (10230);
- I_K is a factor of the one-sided cross-correlation PSD from K-1 satellites given in Equations (4.53) and (4.54);
- N_0 stands for the one-sided broadband noise PSD in the receiver (-202.8 dBW/Hz normally);
- P_m is the total signal strength of satellite m;
- B_n is defined as the loop-noise bandwidth.

The calculation of the PLL variance is based on the linear model noise theory (Viterbi 1966) and the fact that the two components of the decision-directed discriminator output are both white over the loop filter region of interest (Huang 1998). Therefore, most of the aforementioned derivation is concentrated on the one-sided PSD of these two independent noise components. Equations (4.39) and (4.40) express the noise

components in the discriminator output. Equation (4.43) gives the autocorrelation function of the white noise generated by the broadband noise, which is necessary for the calculation of its PSD by equation (4.44). Equations (4.45) to (4.52) implement the inference of the autocorrelation function of the white noise originating from the cross-correlations, and Equation (4.53) gives the estimation of its one-sided PSD. Finally, Equations (4.58) and (4.59) present the tracking error and its variance by using these two PSDs and the linear PLL model.

4.2.2 Numerical Evaluation

4.2.2.1 Simulation Scheme

The purpose of this section is to design a simulation for the validation of the results obtained theoretically. It is natural that the theoretical estimation be based on some idealized assumptions and the simulation may either follow or ignore these assumptions. In any GPS receiver, the code delay and carrier phase are tracked by two types of tracking loops, DLL and PLL, which are coupled with each other. Because this chapter focuses on PLL tracking performance, it is assumed that there is no code tracking error either in theory or in the simulation.

As the PLL is a closed loop system, the feedback is generated by the input signal and loop components before the second input can be processed. Because of the heavy computational load, the PLL tracking error simulation is implemented on the baseband signals. Then the task is naturally divided into two parts: the simulation of baseband

signals including the desired signal, signals from other satellites and broadband noise, and the simulation of the decision-directed PLL loop.

In terms of the assumption of accurate code tracking, it is convenient to assign zero to the code delay of the desired signal and assume a completely correct wipe-off of the L5 PRN code. The code delay of the interference signals from other satellites is generated randomly and is uniformly distributed within the range $[0, T_P]$, upon which the PRN code, NH code and navigation data are produced. The phase of the carrier for the satellite interference is considered a random variable with a uniform distribution over $[0, 2\pi]$. The incoming signal is then correlated with the local replica signal – the PRN code of the desired signal.

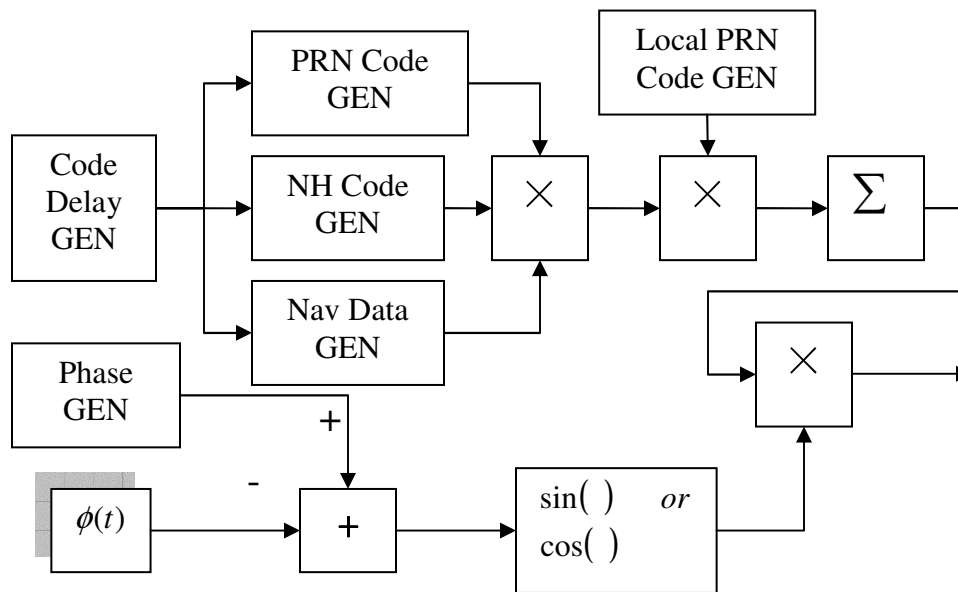


Figure 4.7: Baseband Satellite Signal Simulation

The block diagram in Figure 4.7 illustrates the generation of the desired baseband or cross-correlation signal. As mentioned already, the code delay is assumed to be zero for the desired signal for simplicity. As to the signal from another GPS satellite, the code

delay generator and phase generator produce random numbers according to uniform distributions in their own domains. The estimated or predicted phase $\phi(t)$, as discussed in terms of Equation (4.30), is the feedback of the decision-directed tracking loop shown in Figure 4.8. The difference between the desired signal's phase and this estimate represents the PLL tracking error, whose RMS value corresponds to and is utilized to verify the PLL tracking error variance presented by Equation (4.59). The sinusoid of this differential signal is the quadrature-phase term (Q) and the cosine, the in-phase term (I).

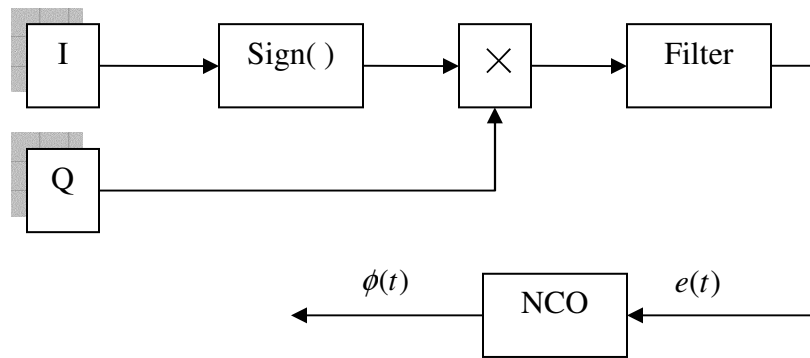


Figure 4.8: Decision-Directed PLL Simulation

Figure 4.8 illustrates the decision-directed phase tracking loop. Both the in-phase and quadrature-phase terms consist of the desired signal, cross-correlation and broadband noise. The desired signal component of the in-phase term denotes the estimation of data symbol $\hat{b}_{2m-1,0}$ in Equation (4.37). The product of the quadrature-phase channel and the sign of the in-phase channel passes through the loop filter in order to produce the control signal, $e(t)$, for the NCO. Finally, the NCO generates the feedback signal or predicted phase $\phi(t)$. The loop noise bandwidth is set to be 15 Hz for all simulation scenarios due to the dynamics of indoor applications.

4.2.2.2 Results and Analysis

Figure 4.9 illustrates the decision-directed PLL tracking errors due to broadband noise, from the theory and simulation as a function of C/N_0 . The simulation curve matches the theoretical one well if the C/N_0 is larger than 35 dB-Hz, in which case the PLL error is less than 6 degrees. With a decrease in C/N_0 , both theoretical and simulated tracking errors rise since the noise power increases compared with that of the signal. However, below a C/N_0 of 30 dB-Hz, the two curves diverge. The divergence indicates the degradation of the tracking error estimation in accordance with the rise of the phase error itself. The cause is that this error estimation is in theory based on the linear model while the phase error is actually transferred non-linearly inside the PLL tracking loop. The linear model assumes that the difference between the error and its sinusoid is negligible. When this difference is enlarged with the rise of the phase error, the linear model becomes gradually invalid.

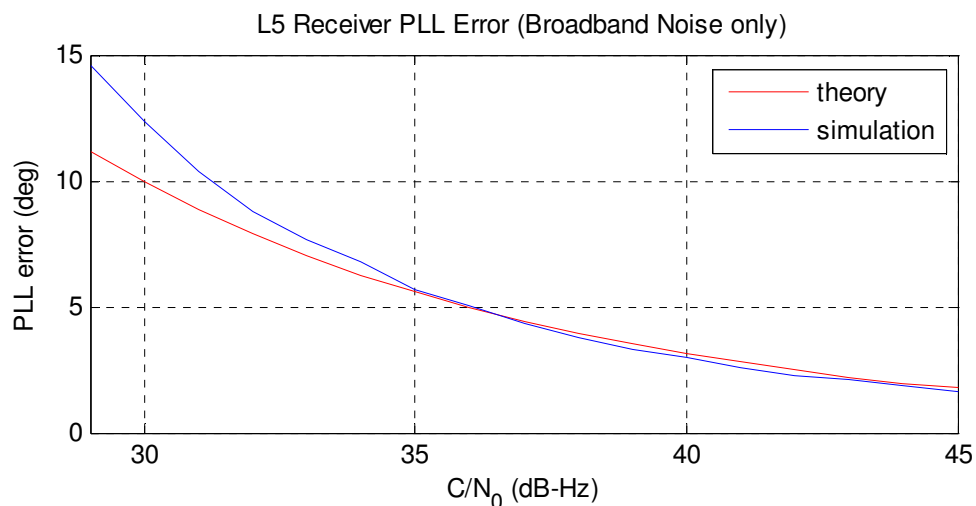


Figure 4.9: L5 Receiver PLL Error in the Presence of Broadband Noise only

As shown in Figure 4.10, the gap between the theoretical and simulated results broadens abruptly and becomes very large when the phase error approaches a value of 15° . The cause is the frequent occurrence of cycle slips in the simulations, resulting in very large phase errors (multiple of 2π). PLLs suffer from frequent cycle slips when the tracking error approaches 15° as discussed in (Humphreys *et al* 2005). “A conservative rule-of-thumb threshold for a PLL tracking loop is that the 3-sigma phase errors from all causes should not exceed 45° deg. Therefore, the 1-sigma rule-of-thumb PLL tracking threshold is 15° deg” (Kaplan 1996). The actual tracking error might be larger than that described in Figure 4.9 when the error variance is above $\frac{1}{4} \text{ rad}^2$ (Viterbi 1989), since the linear model employed in this analysis can no longer exactly model the PLL behaviour. The reason is that the linear model is established on the assumption that the phase error is small enough to substitute for its sinusoid ($\sin \phi \approx \phi$). Cycle slips produce a change in phase of $n \times 2\pi$ which breaks the prerequisite for the linear model mentioned above. The tracking loop enters the non-linear state frequently and makes the linear assumption invalid. When the simulated PLL error reaches 15° , the C/N_0 is approximately 28 dB-Hz. Such a C/N_0 value is equivalent to an input signal power of -174 dBW. From Figure 3.3 (15 Correlator Output SNR), one sees that, for a signal power of -174 dBW, the average SNR number is less than 0 dB, a fact which also explains why the loop loses lock.

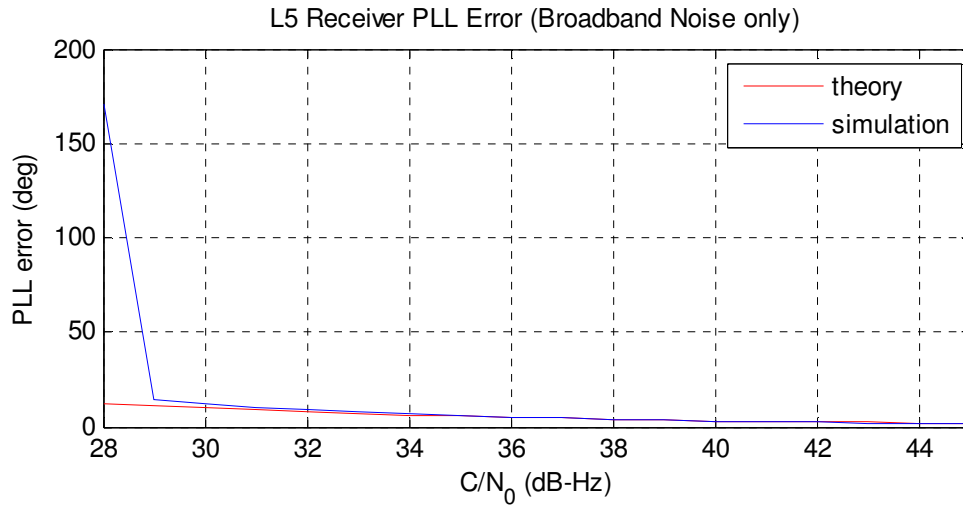


Figure 4.10: L5 Receiver PLL Error in the Presence of Broadband Noise only

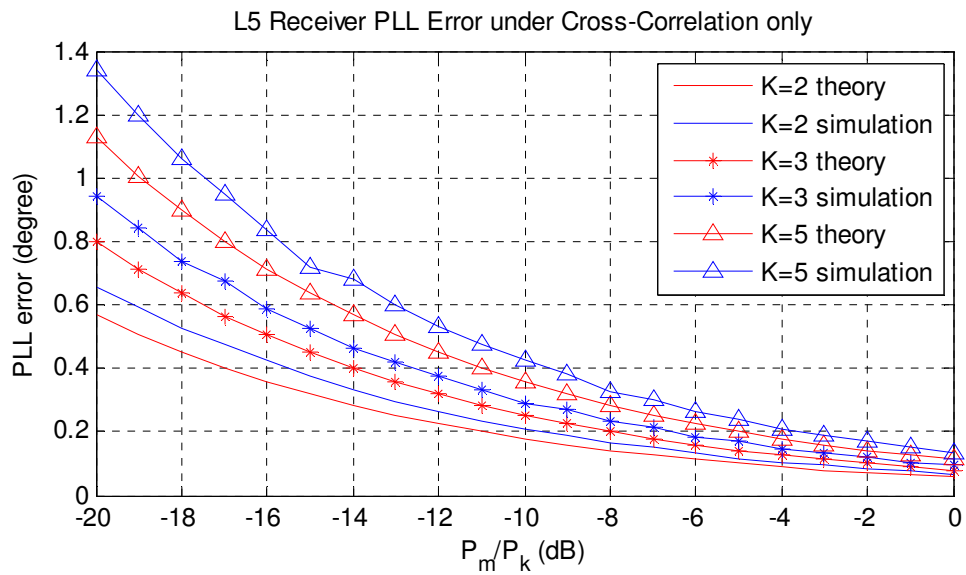


Figure 4.11: L5 PLL Error under Cross-Correlation only

Figure 4.11 displays the L5 PLL error under various cross-correlation conditions. The K value denotes the total number of satellites in view, and P_m/P_k stands for the ratio of the desired signal power to that of the signal from another satellite. This ratio is the inverse of α_k . For GPS applications under open sky conditions, the impact of low power cross-correlation is negligibly small, as the right end of these curves show (below 0.2°). In GPS

indoor environments, the magnitude of the cross-correlation interference may be an order of magnitude higher than that of the desired signal. As a result, the PLL tracking accuracy deteriorates to the degree level. The estimation error that indicates the gap between the theoretical phase error and the phase error measurement obtained from simulations presents a similar tendency to that of broadband noise – it becomes larger with the enlargement of the phase error itself. More specifically, the estimation error increases in size when P_m/P_k drops or the K value rises, since $K-1$ is the number of interference sources. The reason is that the accuracy of the linear model and any theoretical assessment based on this model is negatively proportional to the phase error that is positively associated with the interference strength.

Figure 4.12 displays the PLL tracking error at various cross-correlation strengths and a constant broadband noise level ($C/N_0=55$ dB-Hz). K indicates the number of satellites in view. The L5 signal strength is prescribed to be no less than -154.9 dBW, which is equivalent to 47.9 dB-Hz (C/N_0). However, the actual radiated power is normally slightly higher. The main purpose of this figure is to assess the accuracy and validity of the theoretical estimate of the PLL error (RMS) due to both broadband noise and cross-correlation interference. In this case, the effects of broadband noise and cross-correlation are comparable in strength. Figure 4.12 demonstrates that the phase errors are confined to the degree level, and the estimation error – the gap between the estimate and the simulation – to the sub-degree level. Although the absolute estimation error increases in accordance with P_m/P_k , the relative error is still below 16%.

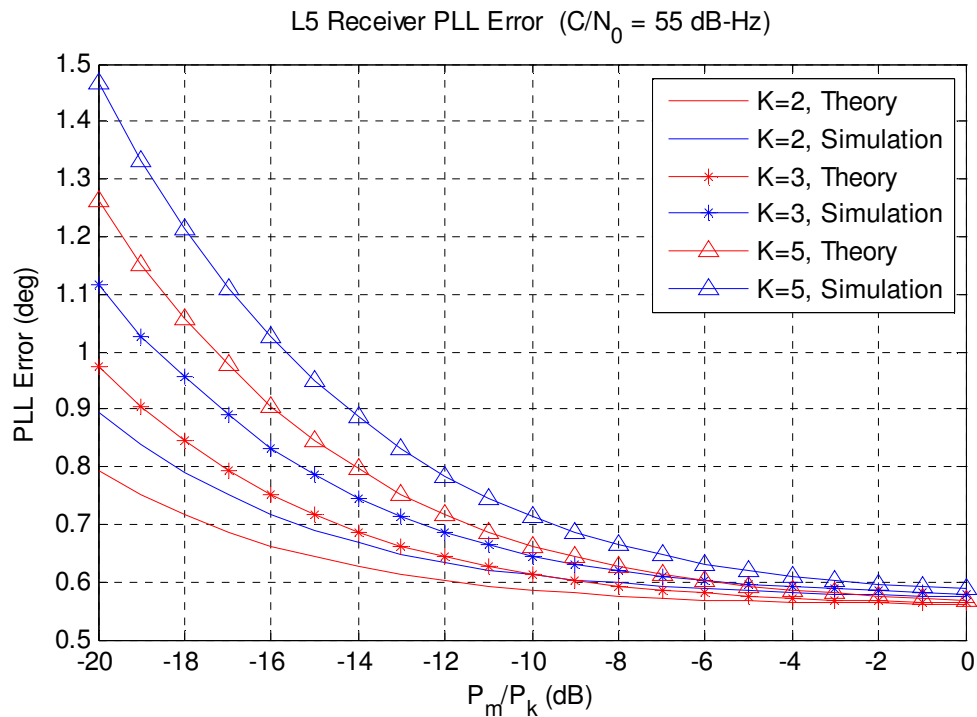


Figure 4.12: The PLL Tracking Error under Broadband Noise and Cross-Correlation

On the right part of Figure 4.12, all PLL phase error curves obtained from simulation rise above any theoretical curve. For instance, the phase error on the curve “K=2, Simulation”, which is the smallest for the simulations, is larger than the corresponding value on “K=5, Theory”, which is the largest for the theory, when P_m/P_k approaches zero. This phenomenon also occurs in Figure 4.13. Its cause is analysed below together with Figure 4.13.

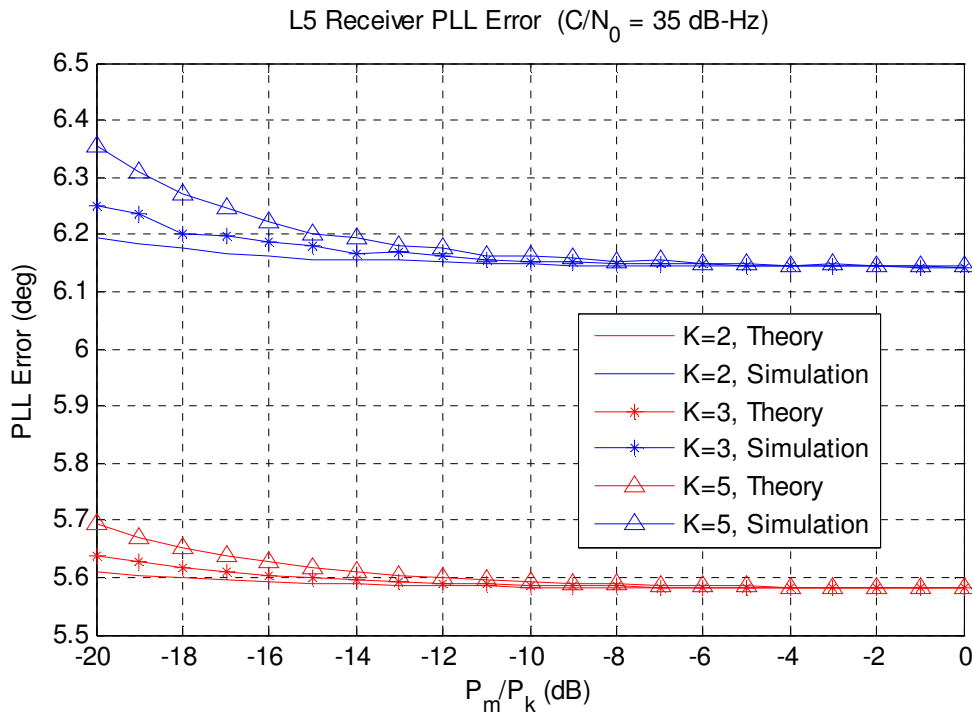


Figure 4.13: The PLL Tracking Error for an Indoor Scenario

Figure 4.13 shows the PLL tracking error under cross-correlation and a higher broadband noise level. In this case, the C/N_0 is 35 dB-Hz, which is 13 dB lower than the minimum C/N_0 expected under line-of-sight conditions. The average impact of the cross-correlation is comparatively small in the presence of powerful broadband noise, because these curves stand for RMS errors. The theoretical phase tracking error is elevated by 0.1° with the introduction of cross-correlation from four other satellites even if the cross-correlation achieves its full strength (-20 dB), while its simulation result is 0.2° .

Both absolute and relative estimation errors are small – less than 0.7° (absolute) and 12% (relative). However, all theory curves are located above the simulation, an occurrence similar to the aforementioned phenomenon on Figure 4.12. The common underlying cause is that the broadband noise power is overwhelmingly larger than that of cross-

correlation. The lower effect of broadband noise is obvious in Figure 4.13. At the right end of theoretical curve (K=5) in Figure 4.12, the total phase error, $\sigma_{\phi} = \sqrt{\sigma_{\phi B}^2 + \sigma_{\phi C}^2}$, is 0.57° , while the phase error associated with broadband noise, $\sigma_{\phi B}$, is 0.56° , as shown in Figure 4.11, while the phase error produced by the cross-correlation, $\sigma_{\phi C}$, is 0.11° .

The linear model employed in this theoretical estimation assumes that the phase error is small enough to use the approximation $\sin\phi \approx \phi$, providing an explanation of the increase in the estimation error difference between the theory and simulation with an increase in the interference power. As Figure 4.13 indicates, the simulation curve goes higher than the theoretical one. And the estimation error increases with the rise of the phase error itself that results from interference. If the broadband noise is much more powerful than cross-correlation, the estimation error resulting from powerful broadband noise may be greater than the additional theoretical tracking error from the cross-correlation. In other words, the tracking error in simulation solely introduced by broadband can exceed the phase error produced by cross-correlation and broadband in theory. This speculation can be verified by the fact that the simulated phase error at a C/N_0 value 35 dB-Hz (broadband noise only) is 5.7 degrees or so (shown in Figure 4.9), larger than any points on the theory curve of Figure 4.13 when K has a value of 2. By the same token, the simulation curve is located higher than the theoretical curve related to higher cross-correlation sources, as shown in Figure 4.13. In conclusion, it is the inherent drawback of the linear model that results in this phenomenon.

4.3 L5 Decision-Directed PLL Symbol Estimation Error in the Presence of Broadband Noise and Cross-Correlation

4.3.1 Theoretical Investigation

The estimation of the information data, $\hat{b}_{2m-1,0}$ or $\text{sign}(Z_{2m-1,l})$ is also susceptible to interference and noise, resulting in errors in the output of a decision-directed discriminator. This section will evaluate the error probability of this symbol estimation so as to provide a thorough understanding of the impact of interference on the PLL.

Upon the assumption that the phase tracking error is negligibly small, the in-phase L5 correlation output is

$$Z_{2m-1,l} = \sqrt{P_m / 4} \{ b_{2m-1,0} T_p + \sum_{\substack{k=1 \\ k \neq m}}^K \sqrt{\alpha_k} [b_{2k-1,-1} R_{2k-1,2m-1}(\tau_k) + b_{2k-1,0} \hat{R}_{2k-1,2m-1}(\tau_k)] \cos \phi_k \\ + \sum_{\substack{k=1 \\ k \neq m}}^K \sqrt{\alpha_k} [b_{2k,-1} R_{2k,2m-1}(\tau_k) + b_{2k,0} \hat{R}_{2k,2m-1}(\tau_k)] \sin \phi_k \} + \int_0^{T_p} n(t) a_m(t) \cos \omega_0 t dt \quad (4.60)$$

The symbol estimation error probability is defined as $P_r\{Z_{2m-1,l} > 0 | b_{2m-1,0} = -1\}$ and $P_r\{Z_{2m-1,l} < 0 | b_{2m-1,0} = 1\}$ for all τ_k , ϕ_k , $b_{2k-1,-1}$, $b_{2k-1,0}$, $b_{2k,-1}$ and $b_{2k,0}$ (Pursley 1977a).

In terms of the obvious symmetry of the set of parameters aforementioned for both probabilities, these two share the same maximum value $P_{\max}(2m-1)$. Therefore, the computation of one probability can be automatically applied to the other. The following discussion is based on the assumption that $b_{2m-1,0} = -1$.

According to Equation (4.60), $v_{j,i}(\tau_j)$ is defined by

$$v_{j,i}(\tau_j) = b_{j,-1} R_{j,i}(\tau_j) + b_{j,0} \hat{R}_{j,i}(\tau_j). \quad (4.61)$$

Taking equations (3.38) and (3.39) into account, it follows that

$$v_{j,i}(\tau_j) = b_{j,-1} \{C_{j,i}(l-N)T_C + [C_{j,i}(l+1-N) - C_{j,i}(l-N)](\tau - lT_C)\} \\ + b_{j,0} \{C_{j,i}(l)T_C + [C_{j,i}(l+1) - C_{j,i}(l)](\tau - lT_C)\} \quad (4.62)$$

The periodic cross-correlation function is defined by

$$\theta_{k,i}(l) = \sum_{j=0}^{N-1} a_{k,j} a_{i,j+l} \quad (4.63)$$

for any integer $0 \leq l < N$. This function can be expressed by an aperiodic cross-correlation as (Pursley 1977b)

$$\theta_{k,i}(l) = C_{k,i}(l) + C_{k,i}(l-N) \quad (4.64)$$

since

$$\theta_{k,i}(l) = \sum_{j=0}^{N-1} a_{k,j} a_{i,j+l} = \sum_{j=0}^{N-1-l} a_{k,j} a_{i,j+l} + \sum_{j=N-l}^{N-1} a_{k,j} a_{i,j+l} \\ = C_{k,i}(l) + \sum_{n=N}^{N-1+l} a_{k,n-l} a_{i,n} = C_{k,i}(l) + \sum_{n=0}^{l-1} a_{k,n-l} a_{i,n} \quad (4.65) \\ = C_{k,i}(l) + \sum_{n=0}^{N-1+(l-N)} a_{k,n-l} a_{i,n} = C_{k,i}(l) + C_{k,i}(l-N)$$

Noting that

$$\theta_{k,i}(l) = \theta_{k,i}(N-l), \quad (4.66)$$

an odd cross-correlation function was defined by Massey and Ufran (1975) as

$$\hat{\theta}_{k,i}(l) = C_{k,i}(l) - C_{k,i}(l-N), \quad (4.67)$$

because

$$\hat{\theta}_{k,i}(l) = -\hat{\theta}_{k,i}(N-l). \quad (4.68)$$

If $0 \leq l_j T_C \leq \tau_j \leq (l_j + 1)T_C \leq T_p$ for an integer l_j , then $v_{j,i}(\tau_j)$ can be rewritten as

$$v_{j,i}(\tau_j) = b_{j,0} \{ \theta_{j,i}(l_j) T_C + [\theta_{j,i}(l_j + 1) - \theta_{j,i}(l_j)] [\tau_j - l_j T_C] \} \quad (4.69)$$

under the assumption that $b_{j,0} = b_{j,-1}$, or that

$$v_{j,i}(\tau_j) = b_{j,0} \{ \hat{\theta}_{j,i}(l_j) T_C + [\hat{\theta}_{j,i}(l_j + 1) - \hat{\theta}_{j,i}(l_j)] [\tau_j - l_j T_C] \} \quad (4.70)$$

if $b_{j,0} = -b_{j,-1}$.

The correlation output can be expressed in terms of $v_{j,i}(\tau_j)$ as

$$\begin{aligned} Z_{2m-1} &= \sqrt{P_m / 4} \{ b_{2m-1,0} T_P + \sum_{\substack{k=1 \\ k \neq m}}^K \sqrt{\alpha_k} [v_{2k-1,2m-1}(\tau_k) \cos \phi_k + v_{2k,2m-1}(\tau_k) \sin \phi_k] \\ &\quad + \int_0^{T_P} n(t) a_m(t) \cos \omega_0 t dt \\ &= \sqrt{P_m / 4} \{ b_{2m-1,0} T_P + \sum_{\substack{k=1 \\ k \neq m}}^K \sqrt{\alpha_k} \sqrt{v_{2k-1,2m-1}^2(\tau_k) + v_{2k,2m-1}^2(\tau_k)} \sin(\phi_k + \varphi_k) \\ &\quad + \int_0^{T_P} n(t) a_m(t) \cos \omega_0 t dt \end{aligned} \quad (4.71)$$

where

$$\tan(\varphi_k) = \frac{v_{2k-1,2m-1}(\tau_k)}{v_{2k,2m-1}(\tau_k)}. \quad (4.72)$$

This correlator output conforms to a Gaussian distribution with the expectation value

$$E[Z_{2m-1}] = \sqrt{P_m / 4} \left\{ b_{2m-1,0} T_P + \sum_{\substack{k=1 \\ k \neq m}}^K \sqrt{\alpha_k} \sqrt{v_{2k-1,2m-1}^2(\tau_k) + v_{2k,2m-1}^2(\tau_k)} \sin(\phi_k + \varphi_k) \right\} \quad (4.73)$$

and variance

$$\text{Var}[Z_{2m-1}] = \frac{N_0 T_P}{4}. \quad (4.74)$$

From Equations (4.69) and (4.70), it is clear that for $0 \leq l_j T_C \leq \tau_j \leq (l_j + 1) T_C \leq T_P$

$$v_{j,i}(\tau_j) = v_{j,i}(l_j T_C) + [v_{j,i}((l_j + 1)T_C) - v_{j,i}(l_j T_C)] \left(\frac{\tau_j}{T_C} - l_j \right) \quad (4.75)$$

where

$$v_{j,i}(l_j T_C) = b_{j,0} \theta_{j,i}(l_j) T_C \quad v_{j,i}((l_j + 1)T_C) = b_{j,0} \theta_{j,i}(l_j + 1) T_C \quad (4.76)$$

if $b_{j,0} = b_{j,-1}$, or

$$v_{j,i}(l_j T_C) = b_{j,0} \hat{\theta}_{j,i}(l_j) T_C \quad v_{j,i}((l_j + 1)T_C) = b_{j,0} \hat{\theta}_{j,i}(l_j + 1) T_C \quad (4.77)$$

if $b_{j,0} = -b_{j,-1}$. This fact means that inside the two-dimension $\tau - v(\tau)$ plane, an arbitrary point $(\tau_j, v_{j,i}(\tau_j))$ ($0 \leq l_j T_C \leq \tau_j \leq (l_j + 1)T_C \leq T_p$) is located on the line between $(\tau_j, v_{j,i}(l_j T_C))$ and $(\tau_j, v_{j,i}((l_j + 1)T_C))$.

It follows that

$$\max \left(\sqrt{v_{2k-1,2m-1}^2(\tau_k) + v_{2k,2m-1}^2(\tau_k)} \right) = \max \left(\sqrt{v_{2k-1,2m-1}^2(l_k T_C) + v_{2k,2m-1}^2(l_k T_C)} \right) \quad (4.78)$$

where $0 \leq l_k < N$ is an integer.

Actually, the validity of Equation (4.78) can be ensured by

$$v_{2k-1,2m-1}^2(\tau) + v_{2k,2m-1}^2(\tau) \leq \max \left(\begin{array}{l} v_{2k-1,2m-1}^2(l T_C) + v_{2k,2m-1}^2(l T_C), v_{2k-1,2m-1}^2((l+1)T_C) \\ + v_{2k,2m-1}^2((l+1)T_C) \end{array} \right) \quad (4.79)$$

where τ is an arbitrary value ($0 \leq l T_C \leq \tau \leq (l+1)T_C \leq T_p$). Equation (4.79) converts the problem into an issue of analytical geometry, and the equation will be proven in the following section.

Assume an arbitrary τ_0 ($l T_C < \tau_0 < (l+1)T_C$); then the point $(\tau_0, v_{2k-1,2m-1}(\tau_0))$ must reside on the line whose ends are $(l T_C, v_{2k-1,2m-1}(l T_C))$ and $((l+1)T_C, v_{2k-1,2m-1}((l+1)T_C))$.

According to analytical geometry, any point $(\tau, v_{2k-1,2m-1}(\tau))$ on this line can be depicted as

$$v_{2k-1,2m-1}(\tau) = v_{2k-1,2m-1}(\tau_0) + K_1(\tau - \tau_0), \quad (4.80)$$

$$\text{where } K_1 = \frac{v_{2k-1,2m-1}((l+1)T_C) - v_{2k-1,2m-1}(lT_C)}{T_C}.$$

The same conclusion is also valid for the points $(\tau_0, v_{2k,2m-1}(\tau_0))$, $(lT_C, v_{2k,2m-1}(lT_C))$, $((l+1)T_C, v_{2k,2m-1}((l+1)T_C))$ and any point $(\tau, v_{2k,2m-1}(\tau))$ on their line

$$v_{2k,2m-1}(\tau) = v_{2k,2m-1}(\tau_0) + K_2(\tau - \tau_0), \quad (4.81)$$

$$\text{where } K_2 = \frac{v_{2k,2m-1}((l+1)T_C) - v_{2k,2m-1}(lT_C)}{T_C}.$$

It follows that

$$\begin{aligned} v_{2k-1,2m-1}^2(\tau) + v_{2k,2m-1}^2(\tau) &= (v_{2k-1,2m-1}(\tau_0) + K_1(\tau - \tau_0))^2 + (v_{2k,2m-1}(\tau_0) + K_2(\tau - \tau_0))^2 \\ &= v_{2k-1,2m-1}^2(\tau_0) + v_{2k,2m-1}^2(\tau_0) + 2(K_1 v_{2k-1,2m-1}(\tau_0) + K_2 v_{2k,2m-1}(\tau_0))(\tau - \tau_0) \\ &\quad + (K_1^2 + K_2^2)(\tau - \tau_0)^2. \end{aligned} \quad (4.82)$$

The last term $(K_1^2 + K_2^2)(\tau - \tau_0)^2$ is of course non-negative. The situation of the second term $2(K_1 v_{2k-1,2m-1}(\tau_0) + K_2 v_{2k,2m-1}(\tau_0))(\tau - \tau_0)$ is somewhat complicated, and needs to be clarified.

If $K_1 v_{2k-1,2m-1}(\tau_0) + K_2 v_{2k,2m-1}(\tau_0)$ is zero, then the second term is also zero. If $K_1 v_{2k-1,2m-1}(\tau_0) + K_2 v_{2k,2m-1}(\tau_0)$ is negative, then the term is positive for $\tau < \tau_0$, including $\tau = lT_C$. Otherwise, $K_1 v_{2k-1,2m-1}(\tau_0) + K_2 v_{2k,2m-1}(\tau_0)$ is positive, and consequently, the second term is positive for $\tau > \tau_0$, including $\tau = (l+1)T_C$. Therefore,

$v_{2k-1,2m-1}^2(\tau_0) + v_{2k,2m-1}^2(\tau_0)$ is no greater than at least either $v_{2k-1,2m-1}^2(lT_C) + v_{2k,2m-1}^2(lT_C)$ or $v_{2k-1,2m-1}^2((l+1)T_C) + v_{2k,2m-1}^2((l+1)T_C)$. Combined with the arbitrariness of τ_0 , Equation (4.79) has been proved.

Based on Equations (4.76) and (4.77), $v_{j,i}^2(l_j T_C) = \theta_{j,i}^2(l_j) T_C^2$ is valid when $b_{j,0} = b_{j,-1}$, or $v_{j,i}^2(l_j T_C) = \hat{\theta}_{j,i}^2(l_j) T_C^2$ if $b_{j,0} = -b_{j,-1}$. Thus, the maximum value of $P_{\max}(2m-1)$ is obtained when $\sqrt{v_{2k-1,2m-1}^2(\tau_k) + v_{2k,2m-1}^2(\tau_k)}$ approaches its maximum quantity $\lambda_{k,2m-1} T_C$ and when $\sin(\phi_k + \varphi_k) = 1$, under the assumption $b_{2m-1,0} = -1$, where

$$\lambda_{k,2m-1} = \max \left(\begin{array}{l} \sqrt{\theta_{2k-1,2m-1}^2(l_k) + \theta_{2k,2m-1}^2(l_k)}, \quad \sqrt{\theta_{2k-1,2m-1}^2(l_k) + \hat{\theta}_{2k,2m-1}^2(l_k)} \\ \sqrt{\hat{\theta}_{2k-1,2m-1}^2(l_k) + \theta_{2k,2m-1}^2(l_k)}, \quad \sqrt{\hat{\theta}_{2k-1,2m-1}^2(l_k) + \hat{\theta}_{2k,2m-1}^2(l_k)} \end{array} \right) \quad (4.83)$$

for the integer l_k ($0 \leq l_k < N$). In this worst-case condition, the expectation value becomes

$$E[Z_{2m-1}] = \sqrt{\frac{P_m}{4}} \left\{ -T_P + \sum_{\substack{k=1 \\ k \neq m}}^K \sqrt{\alpha_k} \lambda_{k,2m-1} T_C \right\}. \quad (4.84)$$

Since the threshold for estimating this correlation value as either -1 or +1 is zero, the maximum error probability is

$$\begin{aligned}
P_{\max}(2m-1) &= 1 - \Phi \left(\frac{\left\{ 0 - \sqrt{P_m/4} \left\{ -T_p + \sum_{\substack{k=1 \\ k \neq m}}^K \sqrt{\alpha_k} \lambda_{k,2m-1} T_C \right\} \right\}}{\sqrt{\frac{N_0 T_p}{4}}} \right) \\
&= 1 - \Phi \left(\sqrt{\frac{P_m T_p}{N_0}} \left\{ 1 - \frac{1}{N} \sum_{\substack{k=1 \\ k \neq m}}^K \sqrt{\alpha_k} \lambda_{k,2m-1} \right\} \right), \quad (4.85) \\
&= 1 - \Phi \left(\sqrt{\frac{E}{N_0}} \left\{ 1 - \frac{1}{N} \sum_{\substack{k=1 \\ k \neq m}}^K \sqrt{\alpha_k} \lambda_{k,2m-1} \right\} \right)
\end{aligned}$$

where

- Φ is the standard (zero mean and unit variance) Gaussian cumulative distribution function; and
- $E = P_m T_p = (P_{mI} + P_{mQ}) T_p = 2P_{mI} T_p = 2E_{mI} = 2E_{mQ}$ is the total L5 signal energy of the expected satellite m within period T_p , including both in-phase and quadrature channels.

If there is no cross-correlation from another satellite ($K=1$), this error probability reduces to

$$P_{\max}(1) = 1 - \Phi \left(\sqrt{\frac{2E_{mI}}{N_0}} \right), \quad (4.86)$$

a result also agreeing with the error probability for the coherent receiver (matched filter) under the condition of white Gaussian noise.

Simulations in the following section will verify the theory represented by Equation (4.85).

It is obvious that the maximum cross-correlation, represented by Equation (4.83), is an

important parameter for the final result. The condition under which the maximum cross-correlation is achieved is also of interest and listed in Table 4.1.

Table 4.1 the Maximum Cross-Correlation and Associated Combination of Parameters

		$\lambda_{k,1}$	τ_k (chips)	ϕ_k ($^\circ$)	A	B
k	2	425.52	7109	32.7	Yes	Yes
	3	438.99	6643	138.0	No	Yes
	4	454.69	4114	167.6	Yes	No
	5	450.28	3697	15.5	Yes	Yes

A: data transition on data channel

B: data transition on pilot channel

4.3.2 Numerical Evaluation

4.3.2.1 Simulation Scheme

As the definition of the decision-directed discriminator in Equation (4.37) shows, the decision-directed phase tracking loop is affected by the sign of the in-phase correlator output. The proper operation of the tracking loop depends on the correct retrieval of information data – its sign. But the information data is contaminated by broadband noise, which is unavoidable in any system, and by the cross-correlation if there is more than one satellite in view.

As in the previous simulations, the broadband noise is treated as a white Gaussian process. However, the impact of cross-correlation is no longer considered from the

perspective of the average effect – the worst-case situation is investigated here.

Therefore, the simulation produces the worst combination of cross-correlation in terms of code delay and phase offset as the first step, and the symbol estimation error rate is evaluated under the circumstance of these worst-case combinations and broadband random noise. Just as in the theoretical analysis, the simulation concentrates on only one probability, $P_r\{Z_{2m-1,l} > 0 | b_{2m-1,0} = -1\}$. As a result of the symmetry, the conclusions are valid for the other probability, $P_r\{Z_{2m-1,l} < 0 | b_{2m-1,0} = 1\}$. Since the correlation is a linear transform or a matched filter, the correlator output of the incoming signal is equivalent to the sum of the correlations of each component of the input signal with the local replica. Thus, the simulation consists of two comparatively independent parts.

In the first stage, the so-called worst-case cross-correlation is obtained through the simulation shown in Figure 4.14. More specifically, the objective is to find the maximum correlation which will be associated with a particular code delay, phase offset, and the absence or presence of data transition on the signals from unexpected satellites.

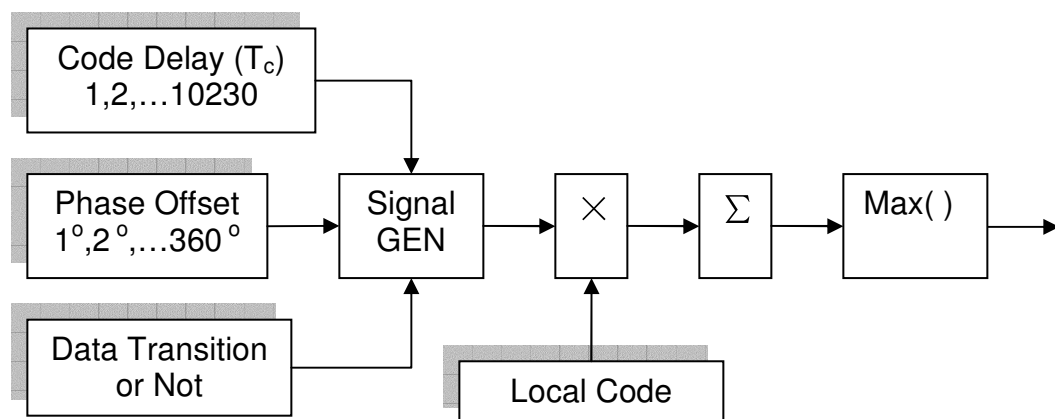


Figure 4.14: Search for the Maximum Cross-Correlation

Then, the in-phase L5 correlator output is formed as the maximum or worst-case cross-correlation plus the correlation of the desired signal and broadband noise with the local replica, as Figure 4.15 shows. The data symbol carried on the PRN code of the desired signal is set to -1 for the entire simulation. Thus, an error is identified when the output in Figure 4.15 exceeds the threshold of zero. The symbol estimation error rate is determined through a statistical approach with a set of simulations.

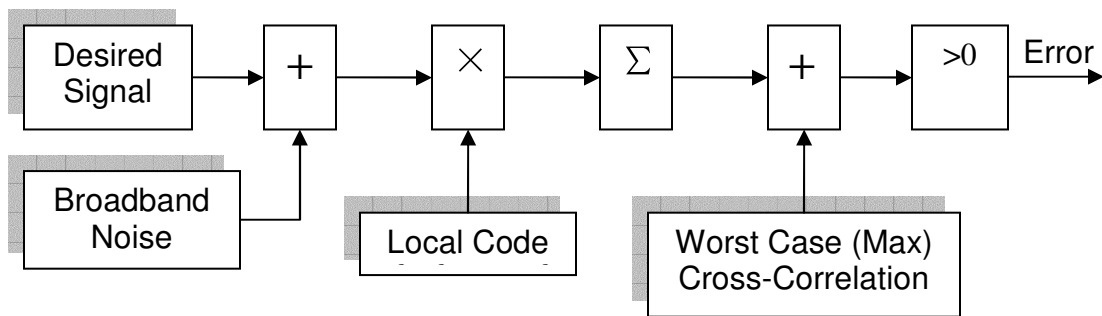


Figure 4.15: Symbol Estimation Error

4.3.2.2 Results and Analysis

Figure 4.16 depicts the symbol estimation error rate in the presence of broadband noise only. The theoretical and simulated curves demonstrate that an erroneous symbol estimate is a small probability event if the C/N_0 is above 35 dB-Hz. When the C/N_0 drops to approximately 30 dB-Hz, the symbol estimation error rate is no longer negligible and contributes to the large gap between the estimated and simulated PLL tracking errors, as Figure 4.9 shows. The reason is that the theoretical curve does not take the symbol estimation error into account. After the C/N_0 is lowered to 32 dB-Hz, the error rate approaches 0.1, a value that is considered to affect the PLL tracking error significantly (Huang *et al* 1998). As the symbol estimation error rate increases further, cycle slips

producing unacceptably large PLL errors become more frequent. Figure 4.10 demonstrates the effect on the PLL tracking error.

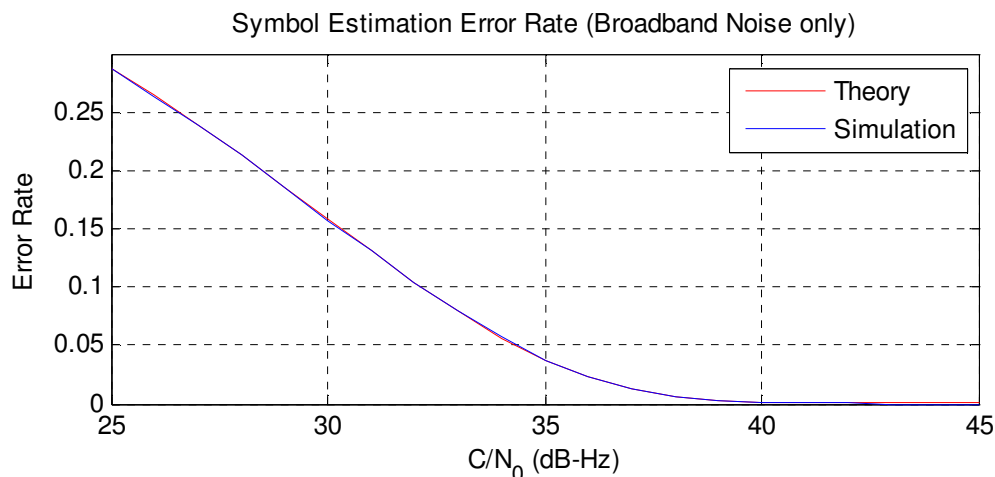


Figure 4.16: Symbol Estimation Error Rate for Broadband Noise only

Figure 4.17 presents the joint effect of both broadband noise and cross-correlations on symbol estimation. The figure shows that in the worst case, even a single cross-correlation satellite ($K=2$) can produce a relatively high symbol estimation error rate (over 0.16). With four interfering satellites having large SIR values, the performance of the symbol estimation inside the PLL discriminator degrades to an unacceptable level, as the $K=5$ curve displays. The poor quality of the symbol estimation is bound to increase the PLL error and cycle slip rate. The results of Figure 4.17 demonstrate for the first time how serious the impact of cross-correlation can be. Note that these results are for the worst case, while the SNR and tracking errors investigated previously, are both evaluated from an average viewpoint. The information indicates the worst case combination of code delay, phase offset and data transitions on two channels, as given in Table 4.1 the Maximum Cross-Correlation and Associated Combination of Parameters, Although this combination has a small probability of occurring and, if it does, has a short duration, it

does warn us of the possibility of the destructive power of cross-correlation in certain cases.

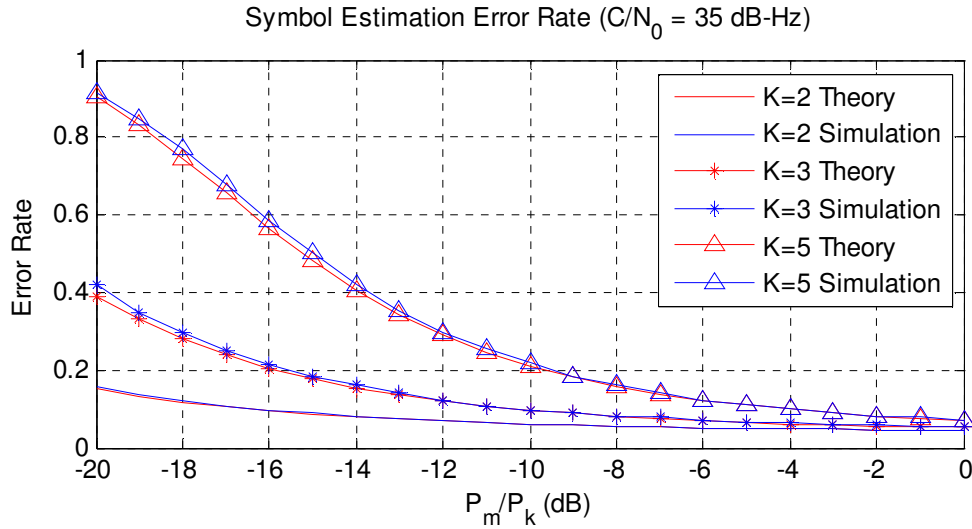


Figure 4.17: Symbol Estimation Error Rate under Broadband Noise and Cross-Correlations

4.4 Conclusions

This chapter investigates the RFI impact on the decision-directed phase tracking loop. The tracking error is estimated from the average point-of-view using a linear model and neglecting any symbol estimation error. The latter was studied separately to determine the maximum possible influence.

In the investigation of the RMS tracking error, both cross-correlation and broadband random noise are treated as white Gaussian noise because of the limited receiver passband. The most important parameter of a white Gaussian process is the power spectral density. The RMS error is obtained from the PSD and the closed-loop transfer function that describes the linear model. Thus, the theoretical deduction consists of the

calculation of the PSD of cross-correlation and broadband noise, respectively, and the tracking error. The computation of the tracking error depends upon the PSD and the linearization or approximation of the PLL, although PLL is in essence a non-linear system. The simulation results indicate that the theoretical estimate is adequate for assessing the RFI (cross-correlation and broadband noise) impact on the GPS L5 decision-directed PLL with acceptably small absolute and relative errors, especially for low interference power. Although the approximation and the ignored symbol estimation error actually introduce an additional tracking error which is seen in the simulation, the theory presents a relatively accurate indication of the behaviour of the phase tracking loop with a sub-degree estimation error level. When the C/N_0 decreases below 30 dB-Hz, the estimation error rate increases, due to the drawback of the linear approximation and the rise of the symbol estimation error rate. However, the estimate and measurement of the tracking error make no sense if the lower C/N_0 drives the PLL into a loss of track, because the control will be taken over by the frequency locked loop (FLL) or the receiver may have to search for the signal by returning to the stage of acquisition.

The average effect of cross-correlation is much smaller than that of broadband noise, since broadband noise is strong due to large signal attenuation after the long propagation distance between GPS satellites and the receiver. The RMS tracking error produced by cross-correlation is at the sub-degree level, and is not a serious problem under large C/N_0 circumstances. However, its impact is no longer negligible in an indoor environment where weak signal conditions have pushed reception performance to an already critical state.

The theoretical estimate of the symbol error rate is accurate because the model does not make use of the same kind of approximation as used in the tracking error estimate. The error rate estimate reveals another aspect of the cross-correlation interference – a short-term but destructive effect due to a particular combination of interference parameters. The symbol detection error makes little difference to the tracking error if its value is below 1% (Huang *et al* 1998), but its influence increases significantly with a rise in detection error. The outcome may be a loss of tracking, or an unreliable tracking state after a short period.

Chapter Five: CONCLUSIONS AND RECOMMENDATIONS

5.1 Conclusions

The objective of this thesis was to investigate and assess, from both the theoretical and the practical viewpoint, the effect of RF interference on the future GPS L5 signal with respect to the accuracy and reliability of acquisition and carrier tracking. This investigation was accomplished for the basic 1 ms coherent integration strategy on the in-phase component.

One purpose for the new signals of the GPS modernization scheme is to extend the positioning service to indoor applications, since GPS was originally designed for line-of-sight conditions. In indoor environments, receivers are susceptible to broadband noise and cross-correlation due to the large attenuation of signal power along the propagation path and the near-far problem. This thesis aims to present an appreciation of the impact of RF interference according to the major characteristics of the signal reception process, correlation, and carrier phase tracking.

The simulation results for average SNR and the worst-case symbol estimation error rate present strong support for the validity and accuracy of the theoretical quantification of these parameters. The average SNR values were obtained under the assumption that the code and carrier phase tracking of the desired signal were accurate. This assumption was used in the theoretical estimation as well as in the simulations. It should therefore be

referred to as the maximum average SNR at the correlator output, since the accuracy of code and carrier tracking is degraded with a rise in interference strength. The symbol estimation error rate was also analyzed under this assumption.

The theoretical L5 RMS tracking error accurately followed the simulation results (estimation error less than 0.3°) when the tracking error itself is below 5° . In the theoretical evaluation, the phase tracking loop was considered to be a linear system based on the approximation that the phase error can be substituted for its sinusoid. This approximation is valid in the case of small phase errors and, as a result, the linear model accurately describes and reflects the actual operation of the PLL.

The accuracy of the tracking error estimation degrades with an increase in interference power due to the breakdown of the linear model and the neglected symbol estimation error. Huang et al. (1998) investigated the difference in the decision-directed PLL tracking error with and without a detection error; they found that the tracking error increases significantly if the bit error rate is above 10%. BER is the ratio of the number of bits incorrectly received to the total number of bits during a specified time interval, while the symbol estimation error rate is the percentage of the number of symbols erroneously received to the total number of symbols transferred but it is assumed that the data transmitted is -1 rather than +1. Therefore, the investigation on BER gives some indication on the influence of symbol estimation error on the decision-directed tracking loop. Both theory and simulation reveal that broadband noise results in a symbol estimation error larger than 10% for low carrier-to-noise density ratios. Thus, the theoretical assessment based on the linear model, together with the omission of the

symbol estimation error, is unable to maintain a constant accuracy for different interference strengths.

From the perspective of average SNR and RMS tracking errors, cross-correlation is a minor interference compared with broadband noise. A GPS signal, whether it be the desired one or that of another satellite, is extremely weak near the earth's surface compared with sky noise and receiver thermal noise, both of which are modeled as broadband noise.

The worst-case error rate estimate reveals another aspect of cross-correlation interference: a short-term but destructive effect associated with certain combinations of interference parameters presented in Table 4.1 the Maximum Cross-Correlation and Associated Combination of Parameters. For the duration of these combinations of parameters, receiver performance may be degraded to the extent that positioning service may be disrupted because of the loss of track of incoming signals.

5.2 Recommendations for Future Research

The average SNR was obtained only from the data channel correlator output limited to 1 ms coherent integration. This integration period is the basic and simple strategy that matches the NH code width, such that no NH code wipe-off is necessary. A receiver may adjust and extend the coherent integration time for interference mitigation. The introduction of NH code wipe-off for longer correlation periods will make the theoretical analysis more complicated, with some differences in the underlying mathematical model. However, possible long coherent integration implementation is an important advantage of and motivation for the pilot channel that is added to L5 signal. Henceforth, it is necessary

to extend the average SNR analysis to various correlator schemes for the assessment of a L5 receiver.

Several discriminators may be used for the carrier phase tracking loop design besides the decision-directed loop upon which the tracking error is estimated. Furthermore, the dual channel signal structure presents more options on the tracking schemes for L5 with respect to different coherent times, tracking on either component, or combination strategies described and investigated by Hegarty (1999) and Julien et al. (2004). The research of RF interference impact on various tracking schemes will make possible a comprehensive understanding of future L5 receiver performance.

Due to time constraints and because the PLL is subject to much interference, code tracking performance was not discussed. As a CDMA system, code tracking (DLL) is as indispensable in a GPS receiver as the conventional phase tracking loop (PLL). The proper operation of either is the prerequisite for the stable functioning of the other. Therefore, an investigation of RF interference effects on the DLL, consistent with other discriminators and strategies, is required.

Finally, this thesis concentrates on the average effect based on statistical models. The averaged effect of cross-correlation was shown to be small compared with its impact in terms of certain code delays demonstrated by the worst-case analysis. It is expected that research on other methodologies beyond the statistical average will be proposed and executed to develop a fuller understanding of the influence of RF interference on the L5 signal acquisition and tracking.

REFERENCES

Anderson, D. R. and P. A. Wintz (1969) "Analysis of a spread-spectrum multiple-access system with a hard limiter," in *IEEE Transactions on Communication Technology*, vol COM-17, pp. 285-290

Akos, D. M. (1997) *A Software Radio Approach to Global Navigation Satellite System Receiver Design*, Ph.D. Dissertation, Ohio University, August 1997.

Bao, Jarnes and Yen Tsui (2000) "Tracking GPS Signals," in *Fundamentals of Global Positioning System Receivers: A Software Approach*, 2000, John Wiley & Sons, Inc., pp. 165-190

Bastide F., C. Macabiau, D. Akos and B. Roturier (2003a) "Assessment of L5 Receiver Performance in Presence of Interference Using a Realistic Receiver Simulator," in *Proceedings of ION GPS*, 9-12 September, OR, pp. 142-152

Bastide F., D. Akos, C. Macabiau and B. Roturier (2003b) "Automatic Gain Control (AGC) as an Interference Assessment Tool," in *Proceedings of ION GPS*, 9-12 September, OR, pp. 2042-2053

Bastide, F., O. Julien, C. Macabiau, and B. Roturier (2002) "Analysis of L5/E5 Acquisition, Tracking and Data Demodulation Thresholds," in *Proceedings of ION GPS*, 24-27 September, OR, pp. 2196-2207

Deshpande, Sameet Mangesh (2004) *Study of Interference Effects on GPS Signal Acquisition*, MSc Thesis, Department of Geomatics Engineering, University of Calgary, Canada (Available at <http://plan.geomatics.ucalgary.ca>)

Gardner, FM (1979) *Phaselock Techniques*, John Wiley & Sons, New York

Grabowski, Joseph and Christopher Hegarty (2002) "Characterization of L5 Receiver Performance Using Digital Pulse Blanking," in *Proceedings of ION GPS*, 24-27 September, Portland, OR, pp. 1630-1635

Gupta, Inder J. and Thomas D. Moore (2001) "Space-Frequency Adaptive Processing (SFAP) for Interference Suppression in GPS Receivers," in *Proceedings of ION NTM*, 22-24 January, Long Beach, CA, pp. 377-385

Hegarty C., A. J. VanDierendonck, D. Bobyn, M. Tran, T. Kim and J. Grabowski (2000) "Suppression of Pulsed Interference through Blanking," in *Proceedings of ION AM*, 26-28 June, San Diego, CA, pp. 399-408

Heppe S. and P. Ward (2003) *RFI & Jamming and its Effects on GPS Receivers, Based on communication theory*, Navtech seminars course 452, Dahlgren, VA

Holmes, J.K (1990) *Coherent Spread Spectrum Systems*, Krieger Pub Co.

Huang, W., and Ivan Andonovic (1998) "Code Tracking of DS-CDMA Systems in the Presence of Multiuser Interference and Additive Noise," in *Proceedings of IEEE 5th International Symposium on Spread Spectrum Techniques and Applications*, 2-4 Sept., Volume 3, Page(s):843 - 847

Huang, W., Ivan Andonovic, and Masao Nakagawa (1998) "PLL Performance of DS-CDMA Systems in the Presence of Phase Noise, Multiuser Interference, and Additive Gaussian Noise," in *IEEE Trans. Communications*, Volume 46, NO. 11, pp. 1507-1515

Humphreys T. E., Mark L. Psiaki and Paul M. Kintner (2005) "GPS Carrier Tracking Loop Performance in the Presence of Ionospheric Scintillations," in *Proceedings of ION GPS/GNSS*, Long Beach, CA, pp. 156-167

Jade Morton, Y. T., James B. Y. Tsui, David M. Lin, Liyeh. L. Liou, Mikel M. Miller, Qihou Zhou, Marcus P. French and John Schamus (2003) "Assessment and Handling of CA Code Self-Interference during Weak GPS Signal Acquisition," *ION GPS/GNSS*, 9-12 September, Portland, OR

Julien, O, G. Lachapelle, and M.E. Cannon (2004) “A New Multipath and Noise Mitigation Technique Using Data/Dataless Navigation Signals,” in *Proceedings of GNSS*, Long Beach, CA, 21-24 September, The Institute of Navigation, Fairfax, VA

Kaplan E. D. (1996) *Understanding GPS: Principles and Applications*, Artech House Inc., Norwood, MA.

Kay, Steven M. (1998) *Fundamentals of Statistical Signal Processing, Volume 2: Detection Theory*, Prentice Hall

Ma, Changlin (2005) *Implementation of a Pure Software Post-mission L1 C/A Code GPS Receiver*, The Design Document For The Software GPS Receiver Developed in PLAN Group

Macabiau, Christophe, Lionel Ries, Frederic Bastide and Jean-Luc Issler (2003) “GPS L5 Receiver Implementation Issues,” in *Proceedings of ION GPS/GNSS*, Portland, OR, pp. 153-164

Madhani, P. H., Axelrad, P., Krumvieda, K., and Thomas, J. (2003) “Application of Successive Interference Cancellation to the GPS Pseudolite Near-far Problem,” in *IEEE Trans on Aerospace and Electronic systems*, April, V. 39, No. 2, pp481-488

Massey, J. L. and J. J. Uhran (1975) "Sub-baud coding," in *Proceedings of the Thirteenth Annual Allerton Conference on Circuit and System Theory*, October, pp. 539-547.

Psiaki, M. L (2001) "Block acquisition of weak GPS signals in a software receiver," in *Proceedings of ION GPS*, 11-14 Sept., Salt Lake City, UT, pp. 2838-2850

Pursley, Michael B. (1977a) "Performance Evaluation for Phase-Coded Spread-Spectrum Multiple-Access Communication – Part I: System Analysis," in *IEEE Trans. Communications*, Volume 25, NO. 8, August, pp. 795-799

Pursley, Michael B. (1977b) "Performance Evaluation for Phase-Coded Spread-Spectrum Multiple-Access Communication – Part II: Code Sequence Analysis," in *IEEE Trans. Communications*, Volume 25, NO. 8, August, pp. 800-803

Ray, J. K. (2005) *Advanced GPS Receiver Technology*, ENGO 699.73 Course Notes, Department of Geomatics Engineering, University of Calgary, Canada, , pp. 36

RTCA Special Committee 159 (2000) "Ultra-Wideband Technology Radio Frequency Interference Effects to GPS and Interference Scenario Development" in *First Interim Report to Department of Transportation*

Spilker, J. J. Jr. (1978) "GPS Signal Structure and Performance Characteristics," *Journal of Navigation*, Vol. 25, No. 2, pp 121-146

Spilker, J. (1996) "Fundamentals of Signal Tracking Theory," in *Global Positioning System: Theory and Applications*, Vol. I, Parkinson, B.W. and Spilker, J.J. Jr., eds., American Institute of Aeronautics and Astronautics, Washington, 1996, pp. 245-327

Spilker, J. and F. D. Natali (1996) "Interference Effects and Mitigation Techniques," in *Global Positioning System: Theory and Applications*, Vol. I, Parkinson, B.W. and Spilker, J.J. Jr., eds., American Institute of Aeronautics and Astronautics, Washington, 1996, pp. 717-771

Spilker, J. and Van Dierendonck (1999) "Proposed New L5 Civil GPS Signal at 1176.45 MHz," in *Proceedings of ION GPS*, Cambridge, MA, pp. 761-770

Tsui Y. and J. Bao (2000), *Fundamentals of Global Positioning System Receivers: A Software Approach*, John Wiley & Sons Inc., New York, NY.

Van Dierendonck, A. J., Erlandson, R., McGraw, G. and Coker, R. (2002) "Determination of C/A code self-Interference Using Cross-Correlation Simulations and Receiver Bench Tests," in *Proceedings of ION GPS*, September, Portland, OR, pp. 630-642

Van Nee, R. D. J. (1992) "GPS Multipath and Satellite Interference," in *Proceedings of the 48th Annual Meeting*, June 29-July 1, Washington, DC, Institute of Navigation

Viterbi, Andrew J. (1966) *Principles of Coherent Communication*, McGraw-Hill, Inc.

Viterbi, Andrew J. (1963) "Phase-locked loop dynamics in the presence of noise by Fokker-Planck techniques," in *Proceedings of the IEEE*, Volume 51, Issue 12, Dec. 1963
Page(s):1737-1753

Ward, Phillip (1996a) "Effects of RF Interference on GPS Satellite Signal Receiver Tracking," in *Understanding GPS: Principles and Applications*, Elliott D Kaplan, Artech House, pp. 209-236

Ward, P. (1996b) "Satellite Signal Acquisition and Tracking," in *Understanding GPS Principles and Applications*, Kaplan, E. D., Norwood, MA, pp. 119-208.

Weik, M. (1989) *Communications Standard Dictionary*, 2nd ed., Van Nostrand Reinhold Co., New York, NY